

**STUDYING THE FUSION CUTTING MECHANISM IN CO2  
LASER BLANKING OF STAINLESS STEEL-304 SQUARE  
SAMPLES**

**ABU MOHAMMED SIFULLAH**

**FACULTY OF ENGINEERING  
UNIVERSITY OF MALAYA  
KUALA LUMPUR**

**2017**

**STUDYING THE FUSION CUTTING MECHANISM IN  
CO<sub>2</sub> LASER BLANKING OF STAINLESS STEEL-304  
SQUARE SAMPLES**

**ABU MOHAMMED SIFULLAH**

**DESSERTATION SUBMITTED IN FULFILMENT OF  
THE REQUIREMENTS FOR THE DEGREE OF MASTER  
OF ENGINEERING SCIENCE**

**FACULTY OF ENGINEERING  
UNIVERSITY OF MALAYA  
KUALA LUMPUR**

**2017**

**UNIVERSITY OF MALAYA**  
**ORIGINAL LITERARY WORK DECLARATION**

Name of Candidate: Abu Mohammed Sifullah

Registration/Matric No: KGA 130093

Name of Degree: Masters of Engineering Science

Title of Dissertation: **Studying the fusion cutting mechanism in CO2 laser blanking of stainless steel-304 square samples.**

Field of Study: Manufacturing Processes

I do solemnly and sincerely declare that:

- (1) I am the sole author/writer of this Work;
- (2) This Work is original;
- (3) Any use of any work in which copyright exists was done by way of fair dealing and for permitted purposes and any excerpt or extract from, or reference to or reproduction of any copyright work has been disclosed expressly and sufficiently and the title of the Work and its authorship have been acknowledged in this Work;
- (4) I do not have any actual knowledge nor do I ought reasonably to know that the making of this work constitutes an infringement of any copyright work;
- (5) I hereby assign all and every rights in the copyright to this Work to the University of Malaya ("UM"), who henceforth shall be owner of the copyright in this Work and that any reproduction or use in any form or by any means whatsoever is prohibited without the written consent of UM having been first had and obtained;
- (6) I am fully aware that if in the course of making this Work I have infringed any copyright whether intentionally or otherwise, I may be subject to legal action or any other action as may be determined by UM.

*sifullah*

Candidate's Signature

Date: 25 April' 2017

Subscribed and solemnly declared before,

Witness's Signature Date:

Name:

Designation:

## ABSTRACT

Stainless steel-304 is an austenitic steel bearing some unique characteristics like high melting point (1450°C), corrosion resistance, weldability, excellent toughness, deep drawing quality etc. These special characteristics widened its application in manufacturing industry. But cutting of stainless steel-304 into desired shape with high accuracy is a great challenge. To confront this challenge of non-conventional cutting process like fusion laser cutting is introduced. It is a thermal process where highly concentrated laser beam is used as heat source to melt or vaporize the material and assist gas is used to blown away the molten material from the workpiece. Consequently desired cutting with narrow-kerf has taken place. But melting and re-solidification associated with laser cutting introduce grain refinement, carbide or sulphide formation and thermal stress near the cutting edge, which cause unwanted heat affected zone (HAZ) and surface cracks. Those unwanted effects of laser cutting need to be identify and must be explain properly by numerical simulation. But comprehensive simulation of fusion laser cutting process of stainless steel-304 sheets is so complex since it is a thermo-mechanical problem. Thus, in this study a coupled thermo-mechanical finite element model was introduced using ANSYS in order to explain the fusion laser cutting mechanism in CO<sub>2</sub> laser blanking of square samples. Stainless steel-304 sheet of different thicknesses were cut into 10mm x 10mm square blank under different laser power and speed. The proposed simulation model was able to explain thermal distribution, kerf width, width of heat affected zone (HAZ) and thermal stress. It was assumed that the irradiated laser beam was Gaussian and formulated by using ANSYS parametric design language. Element death methodology was employed for material removal. The thermal stress was calculated from structural analysis where the model was considered as elasto-plastic. The proposed numerical model was validated by experiment. Optical microscope was used to measure the kerf-width and width of HAZ.

In addition, scanning electron microscope (SEM) was used to examine the morphological and metallurgical changes along the cut surface. Results of the simulation were validated by experimental and statistical analysis. It justifies that the proposed numerical model shows good agreement with experimental outcomes. In kerf-width analysis the value of  $R^2$  is 0.96 with goodness fitting of 0.9630. Likewise, for width of HAZ the value of  $R^2$  is 0.95 with goodness fitting of 0.923. The parametric study indicated that the laser power, cutting speed and material thickness have effect on kerf-width and width of HAZ. However from ANOVA results, it is suggested that laser power is the most significant parameter in laser blanking with 52.44% contribution to kerf width and 72.43% to width of HAZ for material thickness of 1mm. Similarly, 74.67% contribution to kerf width and 64.21% to width of HAZ are observed for material thickness of 3mm. Moreover, higher stress is developed along the cutting edges and maximum at the corner. Thus cracks and surface defects along the cutting edges are observed by SEM, which is more pronounced at the corner. The findings of current study have great implication in laser machining industry. It suggests that higher speed and lower laser power is ideal for square blanks and special concern needs to apply at the corner to reduce surface defects.

## ABSTRAK

Keluli tahan karat 304 ialah keluli austenitic Cr-Ni yang banyak digunakan di industri perkilangan moden. Memotong keluli tahan karat 304 oleh pemotongan laser ialah satu cabaran besar. Ianya adalah proses thermo-mechanical kompleks dikaitkan dengan pemanasan, peleburan, penyingkiran bahan yang dicairkan dan pemejalan semula sepanjang kerf. Akibat penghalusan bijian itu, karbida atau pembentukan sulfida dan pembangunan tegasan haba telah wujud. Akibatnya, beberapa kawasan tidak menyenangkan selepas kesan seperti kawasan yang terjejas oleh kepanasan (HAZ) dan rekahan permukaan maju. Maka, ia penting untuk menjumlahkan dan menganalisis kesan selepas laser memotong di keluli tahan karat 304. Dalam kajian ini, model elemen terhad thermo-mechanical ganding telah diperkenalkan dengan menggunakan ANSYS, supaya penyiasatan kualiti laser lakuran memotong mekanisme oleh laser CO<sub>2</sub>. Siasatan ini ditumpukan dengan penilaian pengagihan terma, kerf-width, kelebaran kawasan yang terjejas oleh kepanasan (HAZ) dan tegasan haba oleh parameter input yang berbeza (kuasa, kelajuan, ketebalan). Bagaimanapun, memikul taburan Gauss keamatan pancaran laser telah dirumuskan menggunakan ANSYS dengan bahasa reka bentuk (APDL) berparameter. Proses penyingkiran bahan disimulasikan dengan mengambil kaedah kematian unsur. Tegasan haba dinilai berdasarkan analisis struktur dan mempertimbangkan model sebagai elasto-plastic. Cadangan model berangka akan disahkan oleh hasil percubaan. Mikroskop optik digunakan untuk mengukur kerf-width dan kelebaran HAZ. Bagaimanapun, mikroskop elektron penskanan (SEM) digunakan untuk memeriksa perubahan morfologi dan pelogaman sepanjang proses memotong permukaan. Keputusan analisis berangka oleh ANSYS dengan hasil percubaan. Dalam analisis kerf-width nilai R<sup>2</sup> ialah 0.96 dan kebagusan penyuaian ialah 0.9630. Begitu juga, untuk kelebaran HAZ nilai R<sup>2</sup> ialah 0.95 dan kebagusan penyuaian ialah 0.923. Kajian-kajian berparameter ditunjukkan dengan kuasa laser, kelajuan memotong, kerf-

width dan kelebaran HAZ. Sebagai tambahan, keputusan analisis varians (ANOVA) menunjukkan kuasa laser ialah parameter yang paling penting dengan sumbangan 52.44 % kepada kelebaran kerf dan 72.43 % untuk kelebaran HAZ untuk keluli ketebalan 1 mm. Begitu juga, 74.67 sumbangan % kepada kelebaran kerf dan 64.21 % untuk kelebaran HAZ diperhatikan menggunakan keluli ketebalan 3 mm. Tambahan pula, bahagian sudut ditetapkan dan dikaitkan dengan suhu tinggi. Maka, tekanan tinggi dibangunkan sepanjang bahagian sudut, yang mempunyai kadar maksimum di sudut kosong bersegi. Rekahan permukaan dan kecacatan berlaku sepanjang bahagian sudut. Di bahagian rekahan, SEM telah digunakan untuk mencerap sepanjang bahagian sudut. Penemuan kajian ini mempunyai implikasi besar di industri pemotongan laser dan menunjukkan lebih tinggi kelajuan dan lebih rendah kuasa laser ialah keunggulan untuk pemotongan laser keluli tahan karat 304. Sementara itu, memotong sudut kosong serta bersegi memerlukan perhatian khas di bahagian sudut itu untuk menghapuskan atau mengurangkan kecacatan permukaan.

## **ACKNOWLEDGEMENTS**

At first I am saying alhamdulillah to Allah Subhanatawala for giving me this opportunity for completing this work. I would like to express my deepest thanks to my supervisor's Dr. Nukman Bin Yusoff, Dr. Mohsen Abdul Naeim Hassan Mohamed and Dr. Altab Hossain for their effective guidelines and cooperation in my research. I want to dedicate this work to my beloved parents, family, lab partners and friends. Special thanks to my wife Azizun Nessa for her understanding and supporting me all the way.

## TABLE OF CONTENTS

<b>Abstract</b> .....	<b>iii</b>
<b>Abstrak</b> .....	<b>v</b>
<b>Acknowledgements</b> .....	<b>vii</b>
<b>Table of Contents</b> .....	<b>viii</b>
<b>List of Figures</b> .....	<b>xiii</b>
<b>List of Tables</b> .....	<b>xviii</b>
<b>List of Symbols and Abbreviations</b> .....	<b>xix</b>
<b>List of Appendices</b> .....	<b>xxii</b>
<b>CHAPTER 1: INTRODUCTION</b> .....	<b>1</b>
1.1 Introduction.....	1
1.2 Problem statement .....	3
1.3 Research gap.....	3
1.4 Objectives of research.....	4
1.5 Outline of dissertation.....	4
<b>CHAPTER 2: LITERATURE REVIEW</b> .....	<b>6</b>
2.1 Introduction.....	6
2.2 Laser.....	6
2.2.1 Principle of laser construction and operation .....	6
2.2.2 Spontaneous and stimulated emission.....	7
2.2.3 Population inversion.....	9
2.2.4 The resonator .....	10
2.3 Properties of laser light.....	10
2.3.1 Monochromaticity .....	11

2.3.2	Collimation.....	11
2.3.3	Beam Coherence.....	12
2.3.4	Brightness or Radiance.....	12
2.4	Laser components .....	13
2.5	Types of Laser .....	13
2.5.1	Gas laser .....	13
2.5.1.1	CO <sub>2</sub> laser.....	14
2.5.2	Solid state laser.....	17
2.5.3	Excimer Laser.....	18
2.5.4	Dye laser.....	19
2.5.5	Semiconductor lasers.....	19
2.5.6	Free electron laser .....	20
2.6	Laser materials interaction.....	20
2.6.1	Absorption .....	21
2.6.2	Reflection .....	21
2.6.3	Heat transfer .....	22
2.6.4	Stress development.....	23
2.7	Laser in manufacturing industry .....	24
2.7.1	Laser Assisted Machining (LAM).....	24
2.7.2	Laser beam machining.....	26
2.8	Laser cutting .....	26
2.8.1	Principle of laser cutting.....	27
2.8.2	Quality aspects of laser cutting.....	28
2.8.2.1	Striations.....	28
2.8.2.2	Dross	29
2.8.2.3	Heat Affected Zone (HAZ) .....	30

2.8.3	Types of Laser Cutting .....	30
2.8.3.1	Vaporization Cutting .....	30
2.8.3.2	Fusion Cutting – Melt and Blow .....	31
2.8.3.3	Reactive Fusion Cutting .....	34
2.8.3.4	Controlled Fracture .....	35
2.8.4	Laser cutting parameters .....	36
2.8.5	Effect of laser cutting parameters.....	36
2.8.5.1	Effect of laser power .....	36
2.8.5.2	Effect of cutting speed.....	38
2.8.5.3	Effect of assist gas and pressure.....	38
2.8.6	Advantages of laser beam machining.....	40
2.8.6.1	Associated with quality .....	40
2.8.6.2	Associated with cutting process .....	41
2.9	Modeling techniques of laser cutting.....	41
2.9.1	Theoretical models .....	42
2.9.1.1	Analytical modelling .....	42
2.9.1.2	Numerical modeling of laser cutting .....	44
2.9.2	Artificial intelligence (AI) based modelling .....	49
2.10	Summary.....	50
<b>CHAPTER 3: RESEARCH METHODOLOGY .....</b>		<b>51</b>
3.1	Introduction.....	51
3.2	Model description and design of experiment: .....	51
3.3	Numerical Analysis .....	53
3.3.1	Model development and element selection .....	54
3.3.2	Thermal analysis.....	56
3.3.2.1	Material removal .....	57

3.3.2.2	Heat affected zone (HAZ) .....	58
3.3.2.3	Kerf width .....	58
3.3.3	Thermal stress analysis.....	59
3.4	Experimental work.....	60
3.4.1	Laser cutting machine .....	60
3.4.2	K-type thermo couple.....	61
3.4.3	Morphological and metallurgical analysis .....	61
3.4.4	Kerf width analysis.....	61
3.5	Analysis of variance (ANOVA) study.....	62
3.6	Material.....	64
 <b>CHAPTER 4: FEM ANALYSIS OF FUSION LASER CUTTING .....</b>		<b>66</b>
4.1	Introduction.....	66
4.2	Physical description of model.....	66
4.3	Model development for FEM analysis .....	67
4.3.1	Element selection .....	67
4.3.2	Material property.....	68
4.3.3	Meshing .....	69
4.3.4	Mesh density analysis.....	69
4.4	Mathematical description and boundary condition.....	72
4.4.1	Thermal analysis.....	72
4.4.2	Stress analysis.....	74
4.5	Heat flux input.....	77
4.6	Simulation of material removal .....	78
 <b>CHAPTER 5: RESULTS AND DISCUSSION .....</b>		<b>80</b>
5.1	Introduction.....	80

5.2	Thermal analysis.....	80
5.2.1	Thermal distribution .....	81
5.3	Heat affected zone (HAZ) analysis.....	85
5.3.1	Comparison of simulation and experimental results .....	86
5.3.2	Parametric study of width of HAZ .....	87
5.4	Kerf width results .....	89
5.4.1	Comparison of simulation and experimental results .....	89
5.4.2	Parametric study of kerf-width.....	90
5.5	Model validation for thermal analysis .....	92
5.6	Analysis of variance .....	94
5.6.1	Significant parameter for width of HAZ .....	94
5.6.2	Significant parameter for kerf width .....	94
5.7	Thermal stress analysis .....	95
<b>CHAPTER 6: CONCLUSIONS AND RECOMENDATION .....</b>		<b>99</b>
6.1	Conclusions .....	99
6.2	Recommendation for future work.....	100
<b>References .....</b>		<b>101</b>
<b>List of Publications and Papers Presented .....</b>		<b>107</b>

## LIST OF FIGURES

Figure 2.1 : The Bohr atom and energy level diagram (Herd et al., 1997).....	6
Figure 2.2 : Stimulated emission (Petru et al., 2013).....	8
Figure 2.3 : Amplification by stimulated emission (Herd et al., 1997). ....	8
Figure 2.4 : Population inversion and four level laser pumping system (Herd et al., 1997). ....	10
Figure 2.5 : Optical arrangement of reverse telescope for better collimation (Ready, 1997). ....	12
Figure 2.6 : Schematic diagram of a typical laser, showing the three basic components (Steen W. M. et al., 2003). ....	13
Figure 2.7 : Typical diagram of gas laser system (argon ion laser) (Singh et al., 2012).	14
Figure 2.8 : Vibration modes of CO <sub>2</sub> molecules. ....	15
Figure 2.9 : Energy level diagram of CO <sub>2</sub> laser (Steen W. M. et al., 2003). ....	16
Figure 2.10 : Energy level of excimer laser emission (Steen W. M. et al., 2003). ....	18
Figure 2.11 : Basic construction of dye laser (Steen W. M. et al., 2003). ....	19
Figure 2.12 : Schematic representation of possible laser materials interaction phenomena. ....	20
Figure 2.13 : Temperature gradient mechanism (Mercelis & Kruth, 2006). ....	24
Figure 2.14 : Schematic diagram and mechanism of LAM . ....	25
Figure 2.15 : Comparison of tool live between conventional and LBM of high chromium white irons (Ding & Shin, 2010). ....	25
Figure 2.16 : Total cost comparison of conventional and LAM; Material removed 150,000mm <sup>3</sup> from austenitic stainless steel (Anderson & Shin, 2006).....	26
Figure 2.17: Illustration of laser-cutting (melt and blow) mechanism. ....	27
Figure 2.18 : Typical pattern of striations formed during the laser cutting (J Powell, 1998). ....	28

Figure 2.19 : Process map showing the range of maximum cutting speeds and gas pressures for achieving the dross free acceptable quality cuts during oxygen assisted laser cutting of 3mm thick mild steel (Chen, 1999).....	29
Figure 2.20 : Heat affected zone (HAZ) laser-cut titanium alloy (Shanjin & Yang, 2006). .....	30
Figure 2.21 : Schematic of vaporisation cutting/drilling (Steen W. M. et al., 2003).....	31
Figure 2.22 : Schematic of the fusion cutting– Melt and Blow (Steen W. M. et al., 2003). .....	31
Figure 2.23 : Model geometry for laser cutting in a control volume (Steen W. M. et al., 2003). .....	32
Figure 2.24 : Basic operating mechanism of reactive laser cutting (Steen W. M. et al., 2003). .....	34
Figure 2.25 : Experimental setup for controlled fracture laser cutting technique (Steen W. M. et al., 2003). .....	35
Figure 2.26 : Effect of laser power on the (a) kerf width and (b) surface roughness for three different cutting speeds :CW Nd:YAG laser& 1.2mm thick austenitic stainless steel (Ghany & Newishy, 2005).....	37
Figure 2.27 : Determination of optimum laser power and cutting speed for laser cutting of steel having thickness less than 1mm (Lamikiz et al., 2005). .....	37
Figure 2.28 : Effect of laser cutting speed on sheet thickness (John Powell, 1993).....	38
Figure 2.29 : Cutting speed for a 2kW CO2 laser. Oxygen is used as cutting gas for mild steel and Nitrogen (20 bar) is used for stainless steel (Wandera, 2006).....	40
Figure 3.1 : Activities involved in research work. ....	51
Figure 3.2 : Schematic diagram of experimental set-up. ....	52
Figure 3.3 : Process flow diagram of thermo-mechanical analysis. ....	53
Figure 3.4 : Dimension of the model. ....	55
Figure 3.5 : Non uniform mesh generation. ....	55
Figure 3.6 : Gaussian heat flux distribution. ....	56
Figure 3.7 : HAZ and kerf width form during fusion laser cutting simulation.....	58
Figure 3.8 : Element death and live methodology for kerf width measurement.....	59

Figure 3.9 : Working flow of thermal stress analysis in ANSYS.....	59
Figure 3.10 : (a) CO2 Laser machine (b) Workpiece mounted on the table.....	60
Figure 3.11 : Procedure of kerf width measurement.....	61
Figure 4.1 : Physical description of model.....	67
Figure 4.2 : FEM model.....	69
Figure 4.3 : Mesh convergence parametric study for 1mm thickness (a) at cutting speed 20mm/s, (b) at laser power 2160watt.....	70
Figure 4.4 : Mesh convergence parametric study for 3mm thickness (a) at cutting speed 20mm/s, (b) at laser power 2160watt.....	70
Figure 4.5 : FEM model development and mesh management considering half of laser beam.....	71
Figure 4.6 : Maximum temperature along the cutting edge; comparison of results of full beam and half beam. ....	71
Figure 4.7 : Kinematic and isotropic hardening rule.....	76
Figure 4.8 : (a) Heat flux position & (b) Local co-ordinate system.....	77
Figure 4.9 : (a) Cylinder with diameter $d$ . (b) model to determine cutting speed $v$ (Nyon et al., 2012).....	78
Figure 5.1 : Significant points and location in proposed model. ....	80
Figure 5.2 : Temperature profile at different time (a) at 0.50s, (b) 1.00s , (c) 1.50s, (d) 2.00s ; laser power 1440watt, speed 20mm/s, thickness of workpiece 1mm.....	82
Figure 5.3 : Temperature profile at different time (a) at 0.25 s, (b) 0.75 s , (c) 1.25 s, (d) 1.75s ; laser power 1440watt, speed 20mm/s, thickness of workpiece 1mm.....	82
Figure 5.4 : Time dependent temperature graph at different point along the cutting edge; laser power 2160watt; thickness 1mm. ....	83
Figure 5.5 : Time dependent temperature graph at different point along the cutting edge; laser power 2160watt; thickness 3mm. ....	84
Figure 5.6: (a) Temperature distribution along X-axis ; heat source at point E and A, (b) Temperature distribution along Y-axis ; heat source at point G and C; Laser power 2160watt, thickness 1mm.....	85

Figure 5.7 : (a) Temperature distribution along X-axis ; heat source at point E and A, (b) Temperature distribution along Y-axis ; heat source at point G and C; Laser power 2160watt, thickness 3mm.....	85
Figure 5.8 : Comparison of width HAZ in experiment and simulation; Laser power 2160watt, cutting speed 10mm/sec, thickness 3mm. ....	86
Figure 5.9 : Width of HAZ for 1mm thick stainless steel-304 sheet. ....	87
Figure 5.10 : Width of HAZ for 3mm thick stainless steel-304 sheet. ....	87
Figure 5.11 : Effect of laser power on width of HAZ; (a) for 1mm thickness, (b) for 3mm thickness.....	88
Figure 5.12 : Effect of cutting speed on width of HAZ; (a) for 1mm thickness, (b) for 3mm thickness.....	88
Figure 5.13 : Kerf-width for 1mm thick stainless steel 304 sheet. ....	90
Figure 5.14 : Kerf-width for 3mm thick stainless steel-304 sheet. ....	90
Figure 5.15 : Effect of laser power on kerf-width ; (a) for 1mm thickness, (b) for 3mm thickness.....	91
Figure 5.16: Effect of cutting speed on kerf-width ; (a) for 1mm thickness, (b) for 3mm thickness.....	91
Figure 5.17 : Temperature at different location of thermocouple with time: comparison between the experimental and simulation outcomes.....	92
Figure 5.18 : Correlation between experimental and simulation kerf width.....	93
Figure 5.19 : Correlation between experimental and simulation width of HAZ. ....	93
Figure 5.20 : Von mises stress profile at different time (a) at 0.50s, (b) 1.00s, (c) 1.50s, (d) 2.00s ; laser power 2160W, speed 20mm/s, thickness of workpiece 3mm. ....	95
Figure 5.21 : Temperature distribution along the upper circumference of square blanks (near the cutting edge) ; laser power 2160W, cutting speed 20mm/s, thickness 3mm. ..	96
Figure 5.22 : Von-mises stress distribution along the upper circumference of square blanks (near the cutting edge) ; laser power 2160W, cutting speed 20mm/sec, thickness 3mm. ....	96
Figure 5.23 : Temporal variation of Von-mises stress at different speed; laser power 2160W, thickness 3mm.....	97

Figure 5.24 : Temporal variation of Von-mises stress at different speed; laser power 2160W, thickness 1mm.....	97
Figure 5.25 : SEM analysis at cutting edge.....	98
Figure B.6.1: SOLID70 3-D Thermal Solid.....	112
Figure B.6.2: SOLID185 3-D Structural Solid .....	114

## LIST OF TABLES

Table 2.1 : Performance characteristics of different types of solid state lasers (Steen W. M. et al., 2003). .....	17
Table 2.2 : Mixer of gas with wavelength in excimer laser .....	18
Table 2.3 : Complex refractive index and coefficient of reflection for different materials at 1.06 $\mu\text{m}$ wavelength (Higgins, 1994).....	22
Table 2.4 : Chemical composition in ejected droplets during reactive fusion cutting by 900W CO <sub>2</sub> laser (Ivarson et al., 1991) .....	35
Table 3.1 : Experimental parameters .....	52
Table 3.2 : Chemical composition of Stainless Steel-304 (Radu & Cristea, 2013).....	64
Table 4.1: Thermal properties of stainless steel 304 (Lee & Chen, 2011).....	68
Table 4.2: Mechanical properties of stainless steel 304 (Shiue et al., 2004). .....	68
Table 5.1 : Required time for laser beam to reach at specific point.....	81
Table 5.2 : ANOVA table for width of HAZ (workpiece thickness 1mm).....	94
Table 5.3 : ANOVA table for width of HAZ (workpiece thickness 3mm).....	94
Table 5.4 : ANOVA table for kerf-width (workpiece thickness 1mm) .....	94
Table 5.5 : ANOVA table for kerf-width (workpiece thickness 3mm) .....	95
Table 5.6 : Residual stress at point C,D,E .....	98
Table B.6.1 : SOLID 70 input Summery .....	112
Table B.6.2 : SOLID70 element output definitions .....	113
Table B.6.3 : SOLID185 Input Summary .....	115
Table B.4 : SOLID185 element output definitions .....	115

## LIST OF SYMBOLS AND ABBREVIATIONS

LASER	:	Light Amplification by Stimulated Emission of Radiation
HAZ	:	Heat Affected Zone
FEM	:	Finite Element Method
BEM	:	Boundary Element Method
FDM	:	Finite Difference Method
APDL	:	ANSYS Parametric Design Language
LBM	:	Laser Beam Machining
LAM	:	Laser Assisted Machining
LMZ	:	Laser Melted Zone
CW	:	Continuous Wave
AI	:	Artificial Intelligent
ANN	:	Artificial Neural Network
FES	:	FUZZY Expert Systems
GA	:	Genetic Algorithm
$E$	:	Photon Energy
$h$	:	Planck's constant
$f$	:	Frequency
$c$	:	Speed of light
$\lambda$	:	Wave length
$N_1$ & $N_2$	:	Population number of lower and upper energy level
$T$	:	Equilibrium temperature
$T_a$	:	Atmospheric Temperature
$T_s$	:	Surface Temperature
$h_{forceconv}$	:	Force heat transfer coefficient

$h_{freeconv}$	:	Heat transfer coefficient at atmospheric condition
$k_B$	:	Boltzmann's constant
$w_o$	:	Beam waist
$\theta$	:	Degree of collimation
$I_o$	:	Laser intensity
$\delta$	:	Absorption co-efficient
$A$	:	Absorptivity
$\alpha$	:	Thermal diffusivity
$v$	:	Cutting Speed
$v_m$	:	Melt flow speed
$F_o$	:	Static pressure force
$F_n$	:	Normal component of dynamic gas force
$F_t$	:	Tangential component
$F_a$	:	Ambient pressure force
$F_{st}$	:	Surface tension force
$F_d$	:	Dynamic force
$F_m$	:	Frictional force
$r$	:	Beam radius
$t_h$	:	Thickness of workpiece
$v_m$	:	Melt flow speed
$w_k$	:	Kerf width
$\rho_g$	:	Gas density
$\mu_g$	:	Gas dynamic viscosity

$p_a$	:	Atmospheric pressure
$\sigma$	:	Surface Tension
$T_p$	:	Time step
$D\_step$	:	Distance advances the laser beam at each time step
$TL\_step$	:	Total number of load step
$4 \times L_p$	:	Total length the laser travel during the cutting
$SS_F$	:	Sum of square mean
$SS_T$	:	Total sum of square
$SS_{Er}$	:	Sum of square error
N	:	Number of experiment
$\varepsilon$	:	Relative error
$\eta$	:	Goodness of fit
$\{\varepsilon\}$	:	Total strain vector
$\{\varepsilon^{el}\}$	:	Elastic strain vector
$\{\varepsilon^{th}\}$	:	Thermal strain vector
$\{\varepsilon^{pl}\}$	:	Plastic strain vector
$\{\sigma\}$	:	Stress vector
$E$	:	Young's modulus
$[D]$	:	Elastic stiffness matrix
$\nu$	:	Poisson's ratio
$T_{ref}$	:	Reference Temperature
$\Delta T$	:	Thermal difference
$\sigma_1, \sigma_2, \sigma_3$	:	Principal stresses

## LIST OF APPENDICES

Appendix A: ANSYS code « « « « « « « « « « « « « « « « « «	106
Appendix B ( O H P H Q W W \ S H G H \ F U L S W L R Q « «	110
Appendix C List of experimental and simulation results « « « « «	114
Appendix C ANOVA D Q D O \ V L V « « « « « « « « « « « « « « « « « «	115

## CHAPTER 1: INTRODUCTION

### 1.1 Introduction

Cutting of different materials into required shape by using appropriate process is one of the biggest challenges in the field of manufacturing industry. In general, the selection of cutting process depending on the material properties of workpiece (thermal, physical, chemical), parameters of cutting tool, parameters of operation (i.e cutting speed, depth of feed, feed rate, cooling media etc), cost of cut and desired design accuracy. Sometimes conventional cutting techniques such as milling, lathe, saw etc are failed to fulfill the requirement of modern manufacturing industry. Because in conventional cutting process, cutting tool makes contact with the workpiece and cutting or material removal has taken place by shear deformation in terms of chips formation. These generates huge amount of heat and residual stress. These may cause poor product and surface quality. Moreover, emergence of modern engineering materials and requirement of machining irregular dimensions with high design accuracy limits the application of conventional machining processes. To confront these issues non-conventional cutting process such as laser beam machining, electrochemical discharge grinding, electrochemical machining, photochemical machining etc are introduced.

Laser beam machining (LBM) is a non-conventional machining process uses laser beam as a heat source. In this process the workpiece is heated up to melting or vaporising temperature and unwanted material is removed by melting and blow or evaporation process. Compare to conventional machining, laser beam machining is much precise, accurate and less time consuming. Besides in LBM, the chance of material contamination is from cutting tool is zero due to absence of physical contact between workpiece and cutting tool.

Different kind of laser cutting processes such as fusion cutting (melt and blow), vaporisation cutting/drilling, reactive fusion cutting, controlled fracture, scribing etc are common. Among them fusion laser cutting is the most popular in the field of manufacturing industry to cut metal. In this method, highly concentrated laser beam is focused on the surface of workpiece and as a result of that the workpiece is heated up to melting temperature. Subsequently highly pressurised assist gas is used to blown away the molten material from the workpiece surface. If the assist gas is oxygen then exothermic reaction takes place which gives additional heating in to the system. These characteristics make fusion laser cutting suitable for stainless steel-304. Because, it is corrosion free austenitic steel alloy having high melting temperature (1450°C) and contain significant proportion of carbon (0.055%), manganese (1.00%), phosphorus (0.029%), sulphur (0.005%), silicon (0.6%), chromium(18.28%), nickel (8.48%) (Zhou et al., 2016).

On the other hand heating and rapid cooling associated with fusion laser cutting of stainless steel-304 may causes not only grain refinement but also carbide, sulphide and phosphate formation within a temperature range of 400°C to 800°C. In addition, the austenite to ferrite phase transformation also may takes place (Jamshidi Aval et al., 2009; Masumoto et al., 1990; P. S. Sheng & Joshi, 1995). Which may cause grain refinement and heat affected zone (HAZ), that need to identify. Because, the presence of HAZ in stainless steel introduces some undesirable effects such as reduction of weldability, decrease in corrosion and fatigue resistance, etc. Simultaneously, heating and cooling associated with fusion laser cutting results temporal variation and thermal stresses. When stresses exceed the strength of the material causes surface defects in the form as fractures and cracks. Many internal and external parameters influence the HAZ and stress concentration (Hossain et al., 2015; Nukman et al., 2013). Among them the most significant parameters are laser power and cutting speed, directly associated with

the heat generation. Thus it is necessary to analyse the effects of laser parameters on HAZ, kerfwidth and stress concentration to co-relate them with each other during fusion laser cutting of stainless steel-304.

## **1.2 Problem statement**

Laser cutting is one of the most advanced non-conventional technology which can be used to cut almost all types of material and any shape of cutting can be formed. Stainless steel 304 is a corrosion free austenitic steel alloy having high melting temperature (1450<sup>0</sup>C). Thus CO<sub>2</sub> fusion laser cutting is used to cut stainless steel 304; where the irradiated laser energy is used to heat the material up to desired level of temperature (melting temperature) and allows assist gas to remove the molten material layer from the workpiece. Heating and rapid cooling involved in fusion laser cutting of stainless steel 304 may cause some undesirable effects like grain refinement, HAZ formation and stress development; these need to identify and minimize. On the other hand simulation of CO<sub>2</sub> fusion laser cutting of stainless steel-304 is a complex problem since it is a thermo-mechanical process. Thus, application of advanced modelling technique is needed to treat the non-linear geometry and boundary conditions in fusion laser cutting.

## **1.3 Research gap**

Various studies from interdisciplinary areas of laser machining processes is found from the literature survey, which describe the machining process as well as parameters optimization and modelling of cutting process by using mathematical, statistical, numerical, artificial intelligent methods to cut metal and non-metal workpieces. Despite lots of studies on laser beam machining, there are still few gaps for research which are listed as follows:

- i. Most of the developed models are representing straight cutting. Very few models are developed which can simulate the complete process of cutting. But temperature

profile during laser cutting is changing through the process. Hence, a complete cut of square blanks from stainless steel 304 sheet need to be developed.

ii. Stainless steel 304 is a commercially important engineering material. During fusion laser cutting of stainless steel metallurgical and morphological changes happens. Hence, thermo-mechanical changes of stainless steel-304 during fusion laser cutting of square blanks need to be analyzed.

iii. Few research works has been done to analyse the effects of laser cutting parameters (power, speed) on HAZ, kerf width, thermal stress in stainless steel 304 sheet during fusion laser cutting. In this study the effect of laser parameters on HAZ, kerf width, thermal stress development are analysed.

#### **1.4 Objectives of research**

i. To develop a finite element simulation model for CO<sub>2</sub> fusion laser cutting of square shape from stainless steel-304 sheet by using ANSYS Software.

ii. To develop an ANSYS subroutine for examine the non-linear geometrical model and thermal analysis.

iii. To validate finite element simulation model with experimental data for kerf width and heat affected zone (HAZ).

iv. To determine the effect of laser parameters on kerf width, HAZ and thermal stress from simulation and experimental data.

#### **1.5 Outline of dissertation**

This dissertation is comprises with six chapters. Brief introduction of the chapter's content are presented as follows:

*In Chapter 1* main focused area is on background of laser cutting. This chapter also covers the objectives, scope and limitation of the study.

*In Chapter 2*, a brief discussion on the review of relevant literature is presented. Under the umbrella of this chapter, laser principle, application, laser cutting mechanism, processing constraints, different modelling technique etc are discussed.

Chapter 3 discusses about the methodology of research work. It focused on the methods and material used for numerical and experimental analysis, numerical model development, experimental set-up, design of experiment, result collection and analysis procedure etc.

*Chapter 4* focuses on coupled field FEM analysis technique. In this chapter details procedure of numerical simulation of fusion laser cutting process is discussed.

*Chapter 5* discusses the results of experimentally validated thermo-mechanical simulation of fusion laser cutting of square blanks. In this chapter the effect of laser parameters (laser power, cutting speed) on cutting quality (HAZ, kerf-width) are analysed. Besides stress concentration is determined and its effect is analysed.

*Chapter 6* summarizes the results and key research contributions. Recommendation for future work also mentioned in this chapter.

## CHAPTER 2: LITERATURE REVIEW

### 2.1 Introduction

Laser beam machining is one of the most advanced machining techniques. Plenty of research work has been done to develop this technique and make it efficient. Different kinds of statistical, analytical, numerical models have been developed to describe the nature of laser cutting. In this chapter we will discuss about laser, its working principle and previous research work on laser beam machining specially on laser cutting.

### 2.2 Laser

Laser is a piece of equipment that emits light through a process of optical amplification based on the stimulated emission of electromagnetic radiation. The expression “LASER” originated as an acronym of “light amplification by stimulated emission of radiation, it was first used by Gordon Gould in 1959 (Chryssolouris, 1991; Gould, 1959).

#### 2.2.1 Principle of laser construction and operation

According to Bohr’s model presented in 1915, the atom is a positively charged nucleus surrounded by electrons that travel in circular paths around the nucleus as shown in Figure 2.1. In an ideal condition the electron of ground state can be excited by absorbing electromagnetic radiation and jump to a higher state. Similarly the electron of higher state can fall to a lower state by emitting energy as electromagnetic radiation.

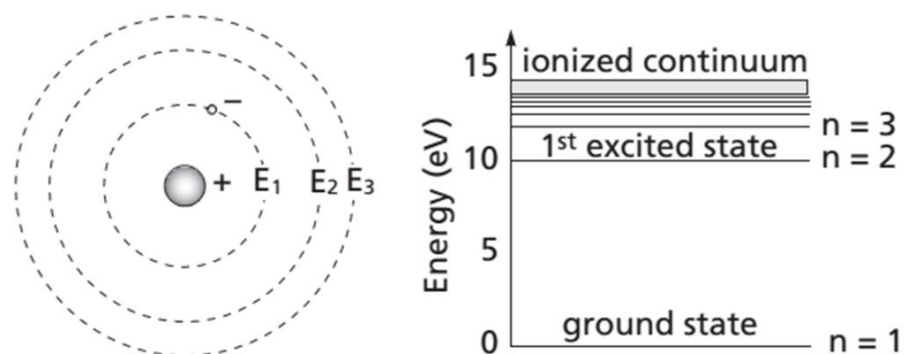


Figure 2.1 : The Bohr atom and energy level diagram (Herd et al., 1997).

In the beginning of 20<sup>th</sup> century researchers were able to explain the nature of light. They found that light is a combination of “photons” which bearing both wave-like and particle-like properties. The individual energy of photon can be expressed by following equation.

$$E = hf \tag{2.1}$$

where  $h$  is Planck’s constant and  $f$  is frequency, which can be represented in the form of wavelength by Equation 2.2

$$f = \frac{c}{\lambda} \tag{2.2}$$

where  $c$  is speed of light (300 million meters per second) and  $\lambda$  is wave length.

### **2.2.2 Spontaneous and stimulated emission**

In general electrons are unstable at upper level. Thus, electrons are trying to come down from upper energy level (excited state) to lower energy level by giving off some energy in terms of radiation of photon. This phenomenon is known as “spontaneous emission”, where photons are emitted in an arbitrary phase and direction. The average time duration for spontaneous emission is treated as spontaneous time.

Albert Einstein, founder of laser theory postulate that atom having excess energy is able to release photons arbitrarily (Majumdar & Manna, 2003). However, if any stray photon with accurate frequency travels through an excited atom will be stimulated to release photon. Interestingly the newly released photon is identical to stray photon in terms of frequency and phase. This process is treated as “stimulated emission”(Majumdar & Manna, 2003). Figure 2.2 describes the process of stimulated emission, where the single incident photon turns into two photons identical to incident photon.

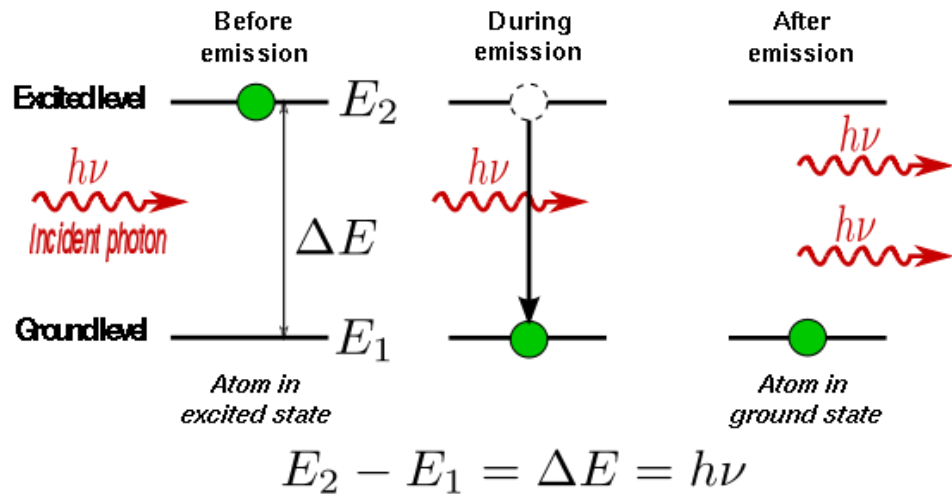


**Figure 2.2 : Stimulated emission (Petru et al., 2013).**

Figure 2.3 illustrated the situation while a group of atoms are stimulated. Here it shows that due to interaction between first atom and incoming (stimulating) photon a coherent photon generates. Later these two photons interact with following two atoms and generate four coherent photons. At the end of the process, many identical coherent photons are generated and travelling in the same direction. Thus numbers of photons amplification has taken place (Petru et al., 2013).

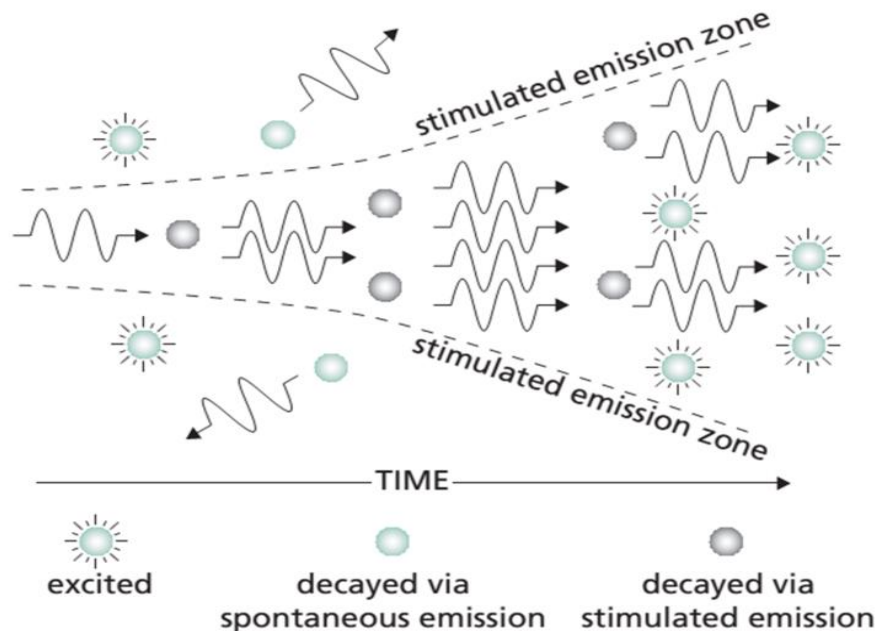


**Figure 2.3 : Amplification by stimulated emission (Herd et al., 1997).**

According to Boltzmann's principle the relative population of any two energy levels is calculated by Equation 2.3

$$\frac{N_2}{N_1} = \exp\left(-\frac{E_2 - E_1}{k_B T}\right) \quad (2.3)$$

where  $N_1$  and  $N_2$  are the population number of lower and upper energy level respectively,  $T$  is equilibrium temperature and  $k_B$  is Boltzmann's constant. At thermal equilibrium state more atoms are stayed in inferior energy levels than superior ones. As well as the probability of absorption is equal to probability of emission. Thus finally no amplification will be possible. Because the real atoms will neither be an absorber nor be an emitter. To overcome this problem population inversion technique is impose.

### 2.2.3 Population inversion

In real condition many energy levels are exist in atoms, which have different individual decay time for spontaneous emission. Thus population inversion is occurred naturally. It is mentionable that with the decay time constant for spontaneous emission is inversely related with energy level. Figure 2.4 shows four energy level diagram. It assumes that the electron is pumped (excited) from ground level  $E_1$  to higher level  $E_4$  by some pumping process. Due to spontaneous emission the electron falls from level  $E_4$  to  $E_3$ , then  $E_3$  to  $E_2$  and at end return to ground level  $E_1$ . As electrons are pumped from the ground level  $E_1$  to  $E_4$  continuously and spontaneous decay time of level  $E_4 \rightarrow$  level  $E_3 <$  level  $E_3 \rightarrow$  level  $E_2 <$  level  $E_4 \rightarrow$  level  $E_3$ . Thus population inversion is taken place in between level  $E_3$  and level  $E_2$ ; when a photon entering in this population, results coherent amplification.

Figure 2.4 : Population inversion and four level laser pumping system (Herd et al., 1997)

#### 2.2.4 The resonator

The process of laser generation is very complex. Though with a population inversion, amplification by stimulated emission has taken place, the overall gain of amplification is very small. To confront this issue a positive feedback system, known as optical resonator is employed. That circulating the photons multiple times in a close path by to and fro motion. Thus maximum participation of atom is ensured and gain of amplification is achieved. The optical close loop is created setting two mirrors at both ends. One of them is highly reflector 5% while remaining one allows partial transmission ( $R > 95\%$ ) of photons.

#### 2.3 Properties of laser light

The LASER has its own unique properties which differs from other forms of light. The combination and adjustment of these properties create different application of LASER. Some major laser properties are discussed as follows.

### 2.3.1 Monochromaticity

The term monochromaticity indicates the purity of emitted frequency or wavelength of laser light. In ideal condition it is assumed that the laser light is fully monochromatic as emission is generated from same energy level. But in real situation laser light is not fully monochromatic due to Doppler effect of progressing molecules or atoms from origin. In laser the degree of monochromaticity is quantitatively described by wavelength or frequency and it can be improved by using special method. In general the narrower is the line width, higher degree of the monochromaticity the laser has achieved. However this also relates with laser type. For better monochromaticity, single mode can be achieved by restricting laser to oscillate on a single transverse (TEM<sub>00</sub>) and longitudinal mode.

### 2.3.2 Collimation

The term collimation is used to explain the directional accuracy of irradiated laser beam. Well directional beams can be explained as collimated, that has ability to focus on a tiny area from a long distance. Thus energy can be focused on a tiny area apparently without losing beam intensity. The degree of collimation is explained by the angle of beam divergence expressed by Equation (Duley, 2012)

(2.4)

where  $w_0$  is the beam waist calculated by Equation 2.5.

(2.5)

For ideal situation  $\theta = 0$ , that produces maximum level of collimation. But due to physical limitation diffraction in real condition  $\theta = 0$  is impossible. Most of the cases the

limits of beam divergence angles lie in between  $0.2$  to  $10$  mrad. Different techniques are used to improve the results of laser collimation. Among them reverse telescope is the most popular as shown in Figure 2.5. By using the eyepiece and additional lenses having focal lengths  $f_1$  and  $f_2$ , the beam divergence is reduced by the factor  $f_1/f_2$  and the beam width is increased by the factor  $f_2/f_1$ .

Figure 2.5 : Optical arrangement of reverse telescope for better collimation (Ready, 1997)

### 2.3.3 Beam Coherence

In quantum physics the term coherence is used while two or more waves are identical in terms of phase difference and frequency. In laser it is expressed as a function and measure of the correlation between the light waves at two points at various times. The absolute value of  $\gamma$  lies between 0 and 1, equivalent to a purely incoherent beam and coherent beam, respectively. (Ready, 1997)

### 2.3.4 Brightness or Radiance

Brightness or radiance has great importance in the field of material processing. It indicates the amount of power emission of laser beam per unit area per unit solid angle i.e. the intensity or energy density of laser beam is expressed by it. High brightness is a desire in laser beam machining, which can be achieved by using Gaussian mode with least divergence angle and elevated output. (Ready, 1997)

## 2.4 Laser components

According to previous discussion it is evident that each laser is associated with following three basic components as shown in Figure 2.6.

- (i) Lasing material
- (ii) Pump source
- (iii) Optical resonator

Figure 2.6 : Schematic diagram of a typical laser, showing the three basic components (Steen W. M. et al., 2003)

## 2.5 Types of Laser

Generally lasers are classified and named according to lasing medium that used for lasing operation. There are six different types of lasing mediums are used in laser operation. Thus lasers can be divided in six categories such as: gas laser, excimer laser, solid state laser, dye laser, semiconductor laser and free electron laser.

### 2.5.1 Gas laser

Gas lasers are popular and extensively used in manufacturing industry due to their broad range of power output (Mw to W) and wavelength (UV-IR). Moreover, these kinds of lasers can be worked in pulsed and continuous modes, that make them unparallel and efficient compare to other lasers. In 1960 laser was first introduced

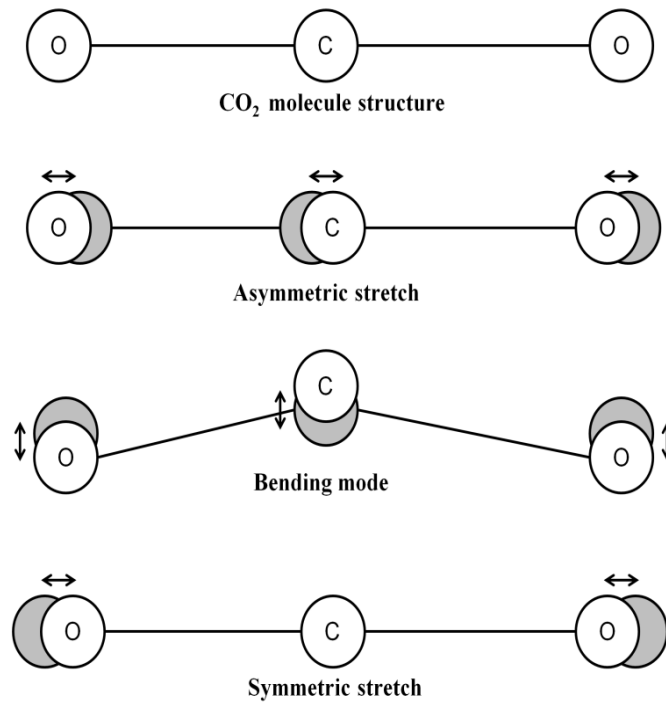
by Bennett Jr and Ali Javan by inventing He-Ne laser. After that due to rapid development and intensive research work, now various kinds of gas lasers are available. In gas laser three kinds of active mediums are used. Based on those active mediums gas lasers can be categorized as: molecular (CO laser, CO<sub>2</sub> laser, N<sub>2</sub> laser), atomic (He-Ne laser) and ionic (Argon ion laser). The operation of gas laser is closely associated with electrical energy. Where, electrical field is used to discharge / pump electrons inside the discharge tube. While atoms, ions, or molecules in the active medium collide with those electrons, stimulated emissions take place due to population inversion. Figure 2.7 illustrates the typical diagram of gas laser system.

Figure 2.7 : Typical diagram of gas laser system (Argon ion laser) (Singh et al., 2012)

#### 2.5.1.1 CO<sub>2</sub> laser

Carbon dioxide is one of the most competitive and oldest molecular typed gas lasers having up to 30% of operational efficiency. It was invented by Kumar Patel in 1964 (Patel, 1964). A mixture of CO<sub>2</sub>, N<sub>2</sub> & He at a ratio of 1: 1: 4.67 are used as a lasing medium and electrical field is employed to discharge the electron. It operates at infrared wavelength and generates laser power from 1 W to more than 10 KW. This CO<sub>2</sub> is widely used in various manufacturing processes like cutting, welding, drilling and so on.

The working principle of CO<sub>2</sub> laser is associated with vibrational and rotational modes of CO<sub>2</sub> molecules combining with electric energy field. Due to tri-atomic structure of CO<sub>2</sub> molecule two O<sub>2</sub> atoms are bonded covalently with one C atom and it has two stretching vibrational modes (V<sub>1</sub>& V<sub>3</sub>) as well as single bending mode (V<sub>2</sub>) as shown in Figure 2.8.



**Figure 2.8 : Vibration modes of CO<sub>2</sub> molecules.**

Individual atoms of CO<sub>2</sub> molecules are connected by a central force and due to lack of fixed orientations among the molecules molecular vibration has taken place. Moreover, rotation and spin may take place. These may cause photon emission in the infrared (due to alterations between vibrational modes) and microwave region (due to transition between rotational states). CO<sub>2</sub> laser's energy level diagram is illustrated in Figure 2.9.

Figure 2.9 : Energy level diagram of CO<sub>2</sub> laser (Steen W. M. et al., 2003)

In brief the important steps associated with CO<sub>2</sub> laser operation are as follows:

- (i) Excitation of N<sub>2</sub> vibration by electron impact
- (ii) Movement of energy from N<sub>2</sub> atom to nearest CO<sub>2</sub> atom which is in vibrational mode (V<sub>3</sub>).
- (iii) Alteration of laser energy from V<sub>3</sub> to V<sub>1</sub> mode.
- (iv) Population sharing between V<sub>1</sub> and two V<sub>2</sub> modes and relaxation within the V<sub>1</sub> manifold.
- (v) Due to presence of He collisions the vibrational energy in the V<sub>1</sub> manifold turned into translational energy. In CO<sub>2</sub>, even values of V<sub>2</sub> and V<sub>3</sub> along with I = 0, are symmetric. Asymmetric vibrations are happen when V<sub>2</sub> is odd, V<sub>3</sub> is even, and I = 0. So, the state 001 (written as, V<sub>2</sub>, V<sub>3</sub>) is associated with odd-spin members only. On the other hand states 100 and 020 are composed with even-spin members. It is assumed that the energy levels sorted out by Boltzmann statistics are in thermal equilibrium and associated with equal vibrational state members. Collision of electron with N<sub>2</sub> excites those molecules to their lowest state while potential difference across the plasma

18,000 V. The energy of this state is about 001 and 002 levels in  $\text{CO}$  (the  $n=1$  state of  $\text{N}_2$  excites the 001 state of  $\text{CO}$  and the  $n=2$  state of  $\text{CO}$  excites the 002 state of  $\text{CO}_2$ ). Sequentially, this energy is shifted to the  $\text{CO}$  molecules and finally populating their upper levels. It happens due to the constant returning force of  $\text{N}_2$  atoms about to identical to the  $\text{CO}$  molecule. However, presence of He in the mixture ensures the plasma discharge continuation and lower energy level development. As shown in Figure 2.9, the most significant energy levels transition are 100 and 001 to 020 where the emitted frequencies are  $6\ \mu\text{m}$  and  $9.4\ \mu\text{m}$  respectively. According to previous discussion the presence of He not only ensures the plasma but also initiates the population inversion. Thus duplication of energy levels between 100 and 020 has taken place within a short time interval.

## 2.5.2 Solid state laser

Solid state lasers have host materials as amorphous glass or dielectric crystal to which neodymium, chromium, erbium or other ions are doped. The performance characteristics of different types of solid state lasers are listed in Table 2.1.

Table 2.1 : Performance characteristics of different types of solid state lasers (Steen W. M. et al., 2003)

Property	Solid-state Lasers					
	Ruby	Nd:glass	Nd:YAG (CW)	Nd:YAG (pulsed)	Yb:fibre	Er:fibre
Wavelength ( $\mu\text{m}$ )	0.69	1.06	1.06	1.06	1.03-1.10	1.50-1.60
Average power output (watt)	10-20		0.04-800	0.04-400	0.01-20000	0.01-500
Output stability (%variation)	1-5	1-5	1-5	1-5	1-2	1-2
Pulse energy (J/pulse)	0.3-100	0.15-100		0.01-100		
Repetition rate (pulse/sec)	0.01-4	0.1-4		0.05-300	$10^{10}$	
Beam divergence (mrad)	0.2-10	3-10	2-8	0.3-10		
Efficiency (%)	0.10-0.50	1.0-5.0	0.10-2.00	0.10-2.00	12.50	

Solid state lasers are mainly industrial laser used in cutting, welding, drilling, cladding part marking alloying, micro-soldering surface hardening, surface cleaning etc.

### 2.5.3 Excimer Laser

An excimer laser uses a mixer of several noble and reactive gases as shown in Table 2.2.

Table 2.2 : Mixer of gas with wavelength in excimer laser

Mixture of gas	Wavelength (nm)
F	158
KrCl	222
XeCl	308
KrF	248
XeF	354
ArF	193

Under controlled condition the mixer of gases  $(F_2, Ne \& He)$  at high pressure ( $4.05E5 Pa$ ) formed an excited dimmer  $Kr^+F^-$  with a duration of  $510ns$  as shown in Figure 2.10. Then it passes through the stimulated emission process and creates short pulse ( $20 ns$ ) ultraviolet photons with high pulse energy ( $7 J$ ) at every discharge

Figure 2.10 : Energy level of excimer laser emission (Steen W. M. et al., 2003)

Excimer lasers are well suited for precision micromachining of organic materials, surgery, photolithography machine, scientific research etc.

#### 2.5.4 Dye laser

Among all types of lasers dye lasers are exceptionally efficient. It uses an organic dye (example: Oligophenylenes, Coumarins, Xanthenes, Merocyanines, Cyanines) which is usually a liquid chemical solution and a broad range of wavelengths are emitted under the influence of pumping laser (*e.g.*, a green copper vapour laser). The basic construction of dye laser is illustrated in Figure 2.11. Dye lasers are used for isotope separation, photodynamic therapy, laser cooling, LIDAR, optical trapping etc.

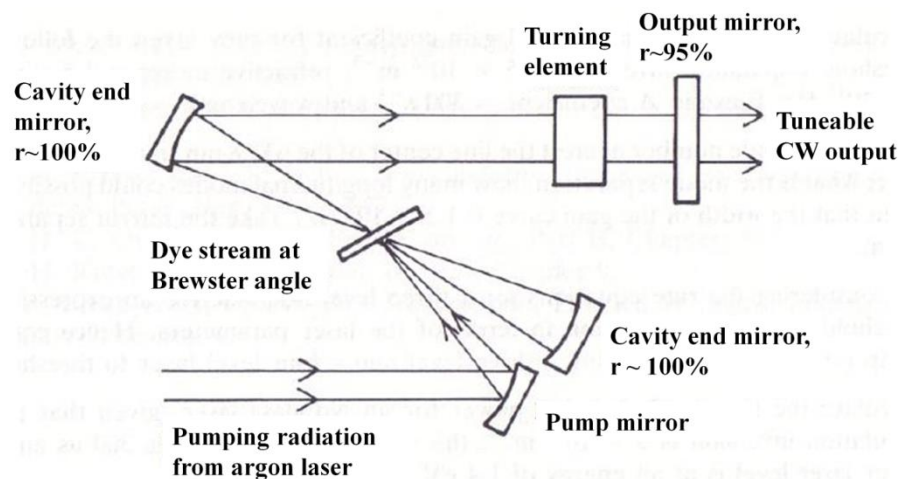


Figure 2.11 : Basic construction of dye laser (Steen W. M. et al., 2003).

#### 2.5.5 Semiconductor lasers

At present semiconductor lasers are the most competent lasers that convert electrical energy to optical energy. In semiconductor laser electrons are in the conduction band stay at energized condition. In an active area of semiconductor material p-n junction is formed while electrons and holes come together. Due to current flow induced electrons move from the conduction band to the valence band and sacrifice the energy difference between these two levels as photons. These photons are interacted with more electrons producing more photons. This repetitive exchange of electrons into departing photons is equivalent to the process of stimulated emission. Semiconductor lasers are small in size,

portable and efficient with rapid modulation reaction and consistency. These characteristics make it useful in the sector of telecommunication, measuring devices, barcode readers, printers, laser pointers, printers etc.

### 2.5.6 Free electron laser

Free electron lasers (FEL) use very high speed electron as lasing medium, which travels without stinting throughout a magnetic structure (Huang & Kim, 2007). It is tunable in a broad range of frequency, varying in wavelength from microwaves, all the way through [terahertz radiation](#) and [infrared](#), to the [visible spectrum](#), [ultraviolet](#), and [X-ray](#). Free electrons lasers are special type, it has application in the field of surgery, fat removal, military, biology etc.

## 2.6 Laser materials interaction

Laser beam interaction with workpiece is associated with different incidents such as reflection, refraction, absorption, scattering and transmission as shown in Figure 2.12. Among them absorption is the most important and significant incident. Because, most of the laser beam machining processes are started with material heating, melting, vaporization, plasma formation etc, which happen due to absorption of laser radiation (Steen W. M., 1991).

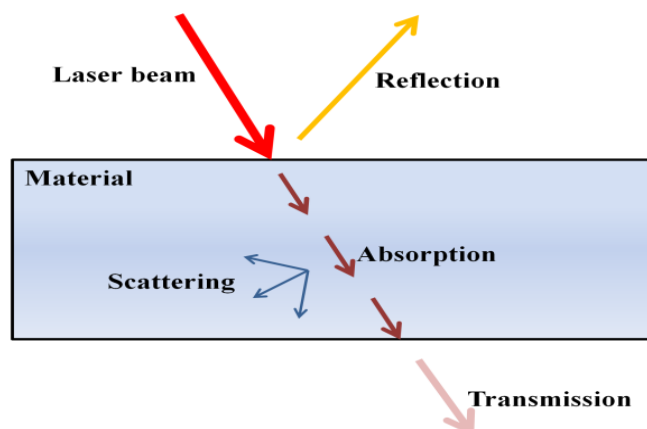


**Figure 2.12 : Schematic representation of possible laser materials interaction phenomena.**

### 2.6.1 Absorption

Laser is a light of electromagnetic radiation having high frequency. Absorption of laser light imposes additional force on the electrons of material. That can be expressed in terms of electric (E) and magnetic (H) field vectors as shown in Equation 2.6.

$$(2.6)$$

where  $v$  is the electron velocity and  $c$  is the light speed.

Considering negligible effect of magnetic energy compare to electric energy Equation 2.6 can be expressed by using This additional force causes kinetic energy of free electrons, excitation energy of bound electrons etc. Finally generation of heat has taken place due to excited electron transformation in different energy levels. Using Beer Lambert law the amount of absorption energy of laser radiation along the depth (z) can be calculated by using Equation 2.7.

$$(2.7)$$

where  $I$  is laser intensity and  $\alpha$  is absorption coefficient.

### 2.6.2 Reflection

Reflectivity is another significant parameter in laser material interaction. Based on material type the relationship among reflectivity, absorptivity and transmissivity be expressed as follows:

For opaque material: Reflectivity (R) = Absorptivity (A)

For transparent material: Reflectivity (R) = Absorptivity (A) - Transmissivity (T)

Reflectivity of material can be expressed in terms of optical constant by Equation 2.8.

$$(2.8)$$

where,  $n$  is refractive index and  $k$  is extinction coefficient. Some values of these constants are given Table 2.3.

Table 2.3 : Complex refractive index and coefficient of reflection for different materials at 1.06 $\mu$ m wavelength(Higgins, 1994)

Material	K	n	R
Al	8.50	1.75	0.91
Cu	6.93	0.15	0.99
Fe	4.44	3.81	0.64
Mo	3.55	3.83	0.57
Ni	5.26	2.62	0.74
Pb	5.40	1.41	0.84
Sn	1.60	4.70	0.46
Ti	4.00	3.80	0.63
Glass	0.00	1.50	0.04

### 2.6.3 Heat transfer

Laser beam strikes on the surface of workpiece and generates heat due to energy absorption as shown in Equation 2.7. Later the heat spread in all direction inside the workpiece due to heat transfer as shown in Equation

$$(2.9)$$

where  $A$  is absorptivity,  $I$  is laser intensity  $\alpha$  is absorption coefficient and  $r$  is laser beam profile distribution. For Gaussian beam distribution with beam radius  $r$  the Equation 2.9 can be written as follows

$$(2.10)$$

In order to understand the basic heat transfer phenomenon in laser heating it is assumed that no heat generation and phase change has taken place. As well as heat loss due to convection and radiation is omitted. Then the simplest form of partial differential equation for 3-D heat conduction in laser heating can be written as

$$\frac{\partial^2 T}{\partial x^2} + \frac{\partial^2 T}{\partial y^2} + \frac{\partial^2 T}{\partial z^2} = \frac{1}{\alpha} \frac{\partial T}{\partial t} \quad (2.11)$$

where  $T$  is temperature,  $t$  is time,  $\alpha$  is the thermal diffusivity.

In laser cutting the laser beam or heat source moves a constant velocity  $v$ . Thus steady temperature field is expressed as

$$\frac{\partial T}{\partial t} = \frac{\partial T}{\partial x} \frac{\partial x}{\partial t} = -v \frac{\partial T}{\partial x} \quad (2.12)$$

Thus combining Equation 2.11 & 2.12 the 3D heat conduction equation can be expressed by Equation 2.13

$$\frac{\partial^2 T}{\partial x^2} + \frac{\partial^2 T}{\partial y^2} + \frac{\partial^2 T}{\partial z^2} = -\frac{v}{\alpha} \frac{\partial T}{\partial x} \quad (2.13)$$

#### 2.6.4 Stress development

Thermal expansion and contraction are two significant physical properties of material. The term thermal expansion can be explained as the tendency of material to change (increase) its shape, area or volume subject to applying thermal load. In lasers material interaction rapid heating and cooling has taken place, which cause thermal expansion and contraction as shown in Figure 2.13.

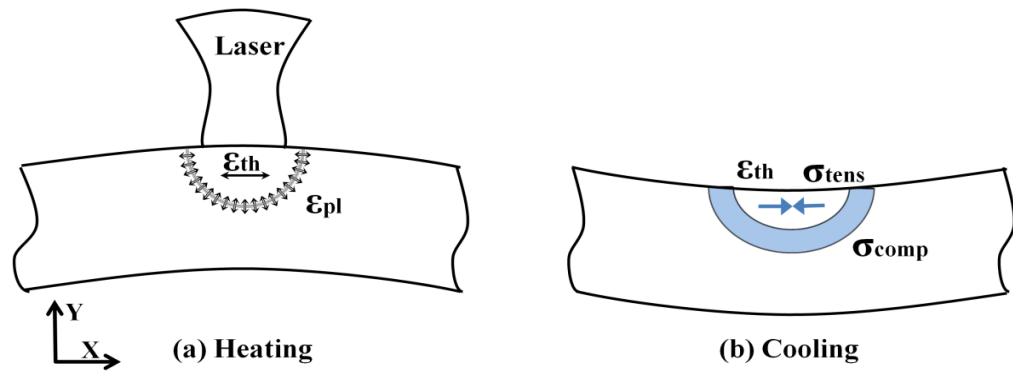


**Figure 2.13 : Temperature gradient mechanism (Merzelis & Kruth, 2006).**

## 2.7 Laser in manufacturing industry

In modern manufacturing industry different laser machining processes have been developed. Based on using approach of lasers it can be divided in two sections such as laser assisted machining (LAM) and laser beam machining (LBM).

### 2.7.1 Laser Assisted Machining (LAM)

Laser Assisted Machining (LAM) is a process of material machining where laser beam merges with the conventional machining process such as turning, milling, grinding etc. to expedite the machining process. In LAM process, a laser beam stands before the cutting tool and heating the surface of material, resulting shear strength reduction in a localized area. The heated material is then removed from the surface of the workpiece in the form of chip by conventional cutting tool as shown in Figure 2.14. Thus LAM allows difficult-to-cut materials to be machined by conventional cutting tools with greater ease. The most suitable LAM workpiece materials are hardened steels, titanium and nickel based alloys and ceramics.

Figure 2.14: Schematic diagram and mechanism of LAM .

Benefits of the LAM are: reduction of cutting forces, high material removal rates, machining without lubrication and reduction of processing cost etc. Figure 2.15 & 2.16 show the comparison between conventional machining and LAM.

Figure 2.15: Comparison of tool life between conventional and LBM of high chromium white irons (Ding & Shin, 2010)

Figure 2.16: Total cost comparison of conventional and LAM; Material removed 150,000mm<sup>3</sup> from austenitic stainless steel (Anderson & Shin, 2006)

### 2.7.2 Laser beam machining

Laser beam machining (LBM) is an advanced machining process where laser beam is used as a cutting tool like conventional machining processes and there is no direct contact with the workpiece. In LBM, laser acts as source of thermal energy, from the earlier discussion we come to know that during lasers material interaction it generates heat at the focused area of the workpiece. This heat resulting melting or vaporization of material and material removal is taken place without (vaporization) or with (melting) assist gas. Thus, LBM is able to shape nearly all kinds of engineering materials such as metals, nonmetals, polymers, composite, wood etc. Available and popular LBM processes are laser cutting, laser drilling, laser forming, laser welding, surface hardening, alloying, laser cladding, micromachining etc.

### 2.8 Laser cutting

Among different kinds of laser beam machining (LBM) processes laser cutting is one of the most significant process in modern manufacturing industry. It is a two

dimensional semi-automated machining process in which thermal heating is used to remove unwanted material from the workpiece. The basic mechanism of laser cutting is associated with laser beam, assist gas and control system. Where, highly concentrated laser beam generates heat in the focused area of the workpiece and subsequently melting / vaporizing throughout the depth of the workpiece has taken place that creates a cutting front. At the same time assist gas from the nozzle is impinged on the surface of the workpiece that eject the molten material from the workpiece. The control system is employed to control the movement of laser beam and workpiece. One of the initial industrial applications of laser cutting was to cut slots in die boards by using 200 W laser (Ready, 1997). Now laser cutting is well advanced and able to cut a broad range of metallic, non-metallic and alloy material.

### 2.8.1 Principle of laser cutting

Laser cutting is a non-traditional thermo-mechanical cutting process. Considering the nature of laser beam interaction with workpiece and the role of assist gas in cutting process, lasers can be applied in various ways to remove material. The main four approaches of material removal by laser are vaporization laser cutting, fusion cutting, reactive fusion cutting and controlled fracture technique. The basic mechanism of laser cutting process is illustrated in Figure 2.17.

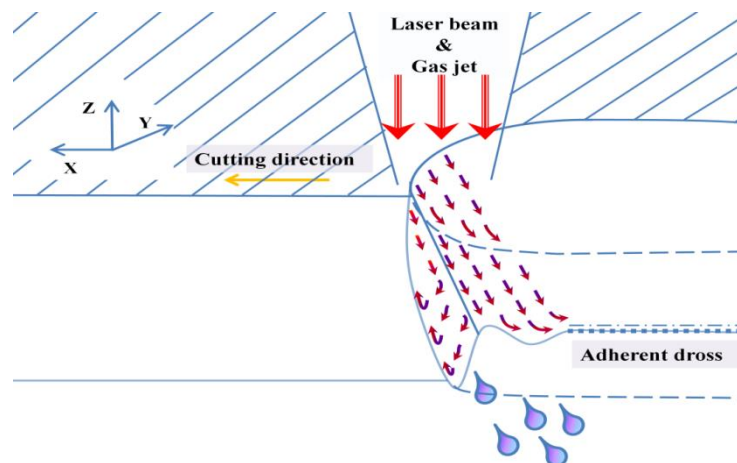


**Figure 2.17: Illustration of laser-cutting (melt and blow) mechanism.**

## 2.8.2 Quality aspects of laser cutting

Compare to other cutting technique available in manufacturing industry, laser cutting has some additional advantages in terms of quality such as narrow cut width, smooth cut surfaces, minimal thermal damage, non-adherent dross formation etc. Some of the major quality aspects associated with laser cutting are discussed bellow.

### 2.8.2.1 Striations

Striation formation is one of the most significant aspects of laser cutting. The presence of striations is undesirable because it may cause unexpected stress formation and removal of striations needs additional surface finishing. The typical pattern of striations is shown in Figure 2.18.

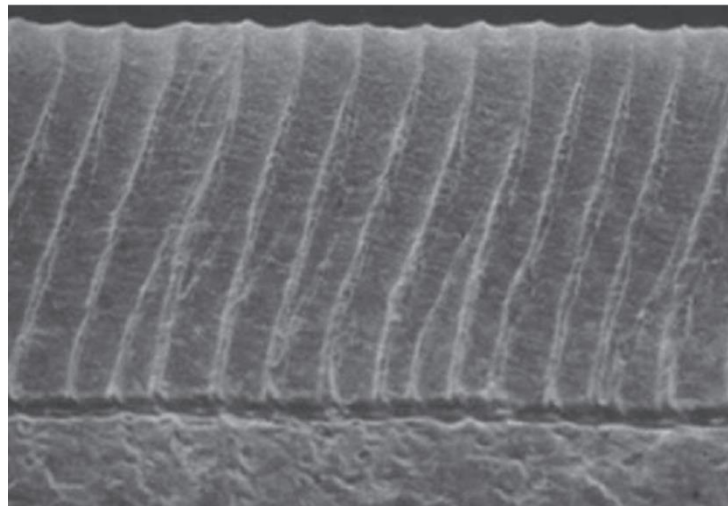


**Figure 2.18 : Typical pattern of striations formed during the laser cutting (J Powell, 1998).**

Even though extensive research works have taken place, the mechanism of striation formation is yet to reveal completely. Many justifications have been presented regarding periodic striations formation. Among them two possible justifications based on the pulsation in the molten layer and the side way burning are well accepted. The first justification was presented by Schuocker and Muller. According to them the dynamic nature of laser cutting causes fluctuations and oscillations of the liquid layer which

induce agitation on the cutting edges due to the movement of the liquid layer with the cutting front. The agitated liquid layer then solidifies into typical striation pattern (Schuocker & Muller, 1987). On the other hand, sideways burning justifies that at the cutting speed less than the speed of the reaction front caused by oxidation, sideways burning occur resulting in periodic striations (J Powell, 1998).

#### 2.8.2.2 Dross

Dross is associated with the partial ejection of molten material from the bottom of the kerf. It happens due to high surface tension and low viscosity of molten material, that is highly dependent on cutting speed. Figure 2.19 shows the effect of cutting speed and gas pressure on dross formation during oxygen-assisted laser cutting of 3mm thick mild steel. It can be eliminated by using an additional gas jet directed from the underside of the workpiece during the cutting process. Alternatively, it can be removed mechanically after cutting.

Figure 2.19: Process map showing the range of minimum cutting speeds and gas pressures for achieving the dross-free acceptable quality cuts during oxygen assisted laser cutting of 3mm thick mild steel (Chen, 1999)

### 2.8.2.3 Heat Affected Zone (HAZ)

The process of laser cutting is thermal in nature. The thermal effect associated with laser cutting cause changes of micro-structure and/or mechanical properties of material along the cut kerf. This causes distinct heat affected zone along the edge of cut as shown in Figure 2.20.

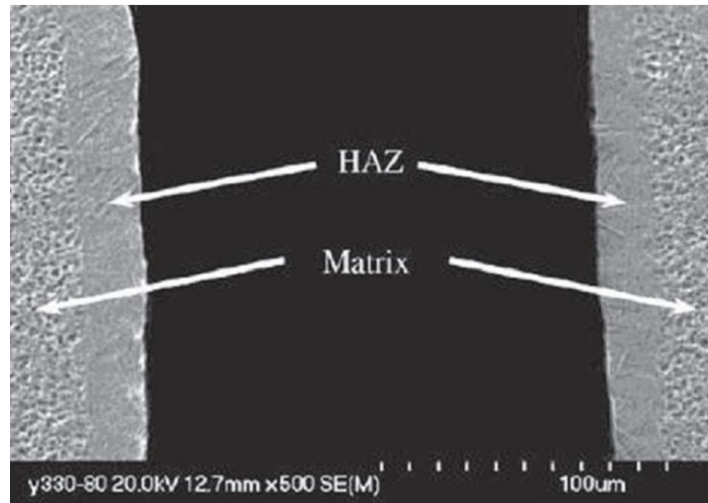


**Figure 2.20 : Heat affected zone (HAZ) laser-cut titanium alloy (Shanjin & Yang, 2006).**

### 2.8.3 Types of Laser Cutting

Laser cutting can be classified on the basis of laser type and method of using in cutting operation.

#### 2.8.3.1 Vaporization Cutting

In vaporization laser cutting the unwanted material of the workpiece is heated upto its vaporization point and ablates in to vapour. Without any melting stage, in this cutting process solid to vapour phase transformation has taken place directly. Thus extremely high quality cutting edge is possible to generate. Though the energy requirement for vaporization laser cutting is more, it is appropriate for materials those have low thermal conductivity and low latent heat of vaporization such as polymers, wood, paper, cloth, organic materials etc. (Mahrle et al., 2010).

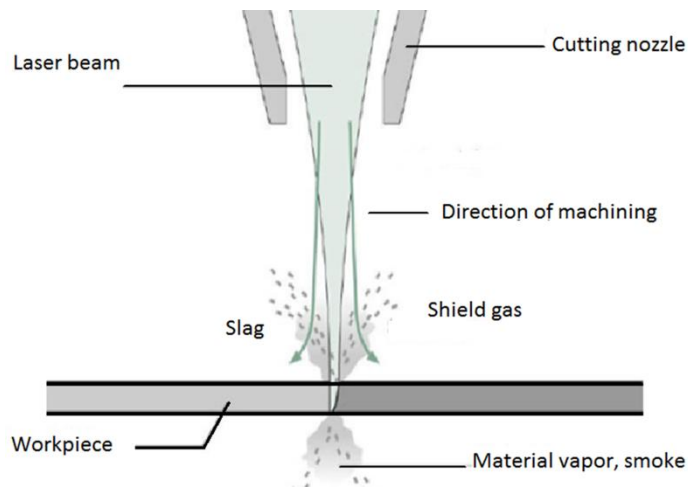


**Figure 2.21 : Schematic of vaporisation cutting/drilling (Steen W. M. et al., 2003).**

### 2.8.3.2 Fusion Cutting – Melt and Blow

In fusion laser cutting energy from the irradiated laser beam generates heat in material upto melting temperature and high pressure assist gas is used to remove the molten material from the workpiece. Hence, in fusion laser cutting the phase transformation of material is solid to liquid. For through cut, the cutting front is formed by high-intensity laser beam through the thickness of workpiece. Thus the material under the focused laser beam right through the thickness of the workpiece is melted and removed from the workpiece as shown in Figure 2.22.

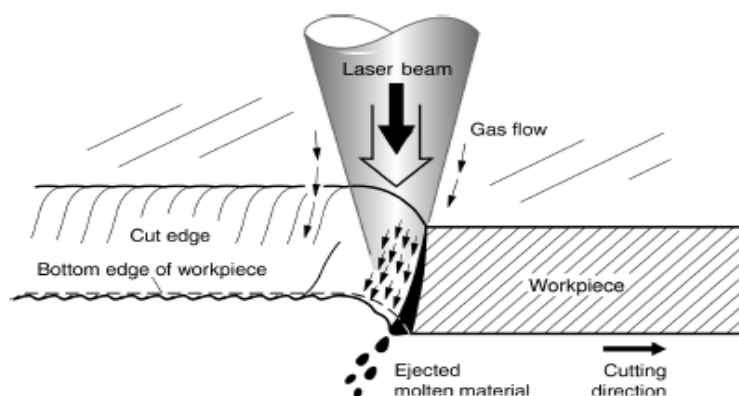


**Figure 2.22 : Schematic of the fusion cutting– Melt and Blow (Steen W. M. et al., 2003).**

Generally, non-reactive gases i.e.  $N_2$ , Ar are impinged at a high pressure from the conical nozzle as assist gas. As a result of that momentum in molten film is created and

while it crosses the surface tension material removal from the lower surface in the form of droplets has taken place.

(a) **Modeling procedure of fusion laser cutting**

The modelling procedure of fusion laser cutting is associated with heat transfer, fluid flow and gas dynamics. An analytical model of fusion laser cutting was proposed by Kaplan. In his proposed model he considered the mass, momentum, and energy balance equations in a controlled volume enclosed by cutting front and melting front as shown in Figure 2.23 (Kaplan, 1996).

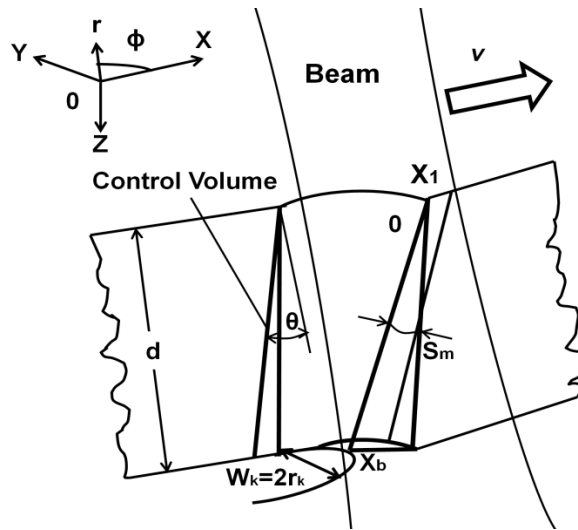


**Figure 2.23 : Model geometry for laser cutting in a control volume (Steen W. M. et al., 2003).**

The absorbed heat flux is expressed by Equation 2.14

$$q_{cms} = \alpha \tan(\theta)I \quad (2.14)$$

where  $q_{cms}$  is cylindrical moving heat source,  $\alpha$  is thermal diffusivity and  $\theta$  is angle of inclination.

From the mass balance equation the film thickness ( $S_m$ ) can be calculated as follows:

$$S_m = \frac{vt_h}{v_m} \quad (2.15)$$

where  $v$  is cutting speed,  $t_h$  is thickness of workpiece and  $v_m$  is melt flow speed.

From moment balance equation different forces associated with fusion laser cutting can be balanced as follows:

$$F_0 + F_n + F_t = F_a + F_{st} + F_d + F_m \quad (2.16)$$

$$\text{Static pressure force, } F_o = w_k t_h \frac{\pi}{2} p_g \quad (2.17)$$

$$\text{Normal component of dynamic gas force, } F_n = w_k t_h \frac{\pi}{2} p_g v_g^2 \tan(\theta) \quad (2.18)$$

$$\text{Tangential component, } F_t = w_k t_h \frac{\pi}{2} \sqrt{p_g \mu_g} \int_0^d \left( \frac{v_g}{z} \right)^{3/2} dz = \sqrt{d} w_k \frac{\pi}{2} \sqrt{p_g \mu_g} 2v_g^{3/2} \quad (2.19)$$

$$\text{Ambient pressure force, } F_a = w_k s_m p_a \quad (2.20)$$

$$\text{Surface tension force, } F_{st} = w_k t_h \frac{\pi}{2} \frac{2\sigma}{w_k} \quad (2.21)$$

$$\text{Dynamic force, } F_d = w_k t_h \frac{\pi}{2} \rho_g \frac{v_m^2}{3} \frac{s_m}{t_h} \quad (2.22)$$

$$\text{Frictional force, } F_m = w_k t_h \frac{\pi}{2} \mu \frac{v_m}{s_m} \quad (2.23)$$

where  $w_k$  is kerf width,  $\rho_g$  is gas density,  $\mu_g$  is gas dynamic viscosity,  $p_a$  is atmospheric pressure and  $\sigma$  is surface tension.

### 2.8.3.3 Reactive Fusion Cutting

The basic difference of reactive fusion cutting with fusion cutting is use of reactive gas i.e O<sub>2</sub> as an assist gas. This initiates exothermic reaction and additional heat energy. As a result of that more energy associated with reactive cutting causes vaporization from the molten layer at the cutting front as well as material removal by molten layer ejection from the bottom surface as shown in Figure 2.24.

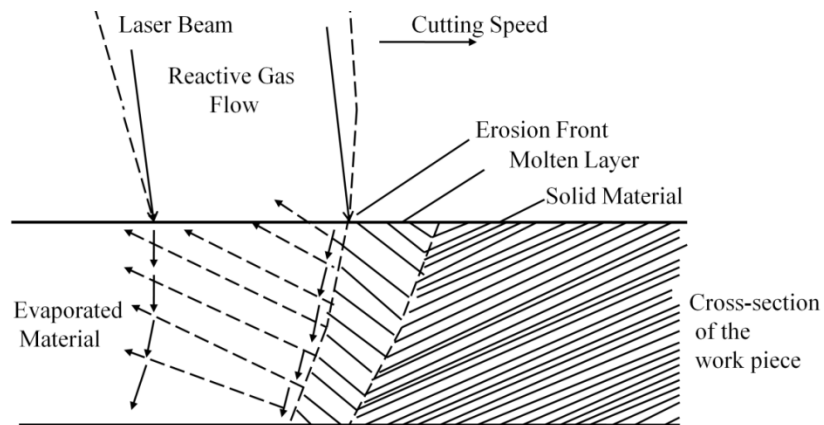
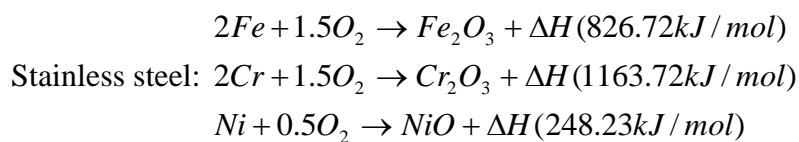
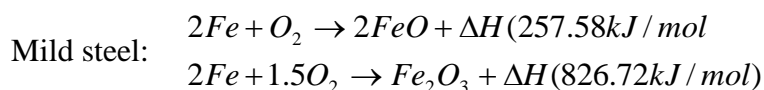


**Figure 2.24 : Basic operating mechanism of reactive laser cutting (Steen W. M. et al., 2003).**

During reactive fusion cutting of mild steel and stainless steel heat generation by exothermic reaction can be calculated by following chemical reaction:



The contribution of oxidation in oxygen assisted laser cutting can be estimated by analyzing the presence of chemical component in the ejected material. Table 2.4 shows percentage of different chemical composition in ejected droplet while the 900W CO<sub>2</sub> laser was used to cut 1-4mm thick workpiece.

Table 2.4 : Chemical composition in ejected droplets during reactive fusion cutting by 900W CO<sub>2</sub> laser(Ivarson et al., 1991)

Material	Free Fe (wt. %)	Oxidized Fe (wt. %)	Free Ni (wt. %)	Oxidized Ni (wt. %)	Total Cr (wt. %)	Total O (wt. %)
Mild Steel	43.10	44.70	-	-	-	13.10
Stainless Stee	43.00	19.50	10.90	0.67	15.20	10.70

#### 2.8.3.4 Controlled Fracture

In controlled fracture technique, mechanical crack is formed by laser energy in a localized area of the workpiece. The crack is then progress along the laser path in a controllable manner to complete material separation. In 1969, Lumley first proposed and applied this technique successfully to cut brittle material such as glass and alumina ceramic(Lumley, 1969) Tsai in cooperation with Liou and Chen describe it in detail. They used both CO<sub>2</sub> and Nd:YAG laser during experiment. CO<sub>2</sub> was used in a continuous mode to generate thermal stress on the surface to develop the crack whereas Nd:YAG laser was used to make the crack and deepen through the thickness(Tsai & Liou, 2001; C. Tsai & Chen, 2003) Experimental setup of controlled fracture technique is shown in Figure 2.25.

Figure 2.25 : Experimental setup for controlled fracture laser cutting technique (Steen W. M. et al., 2003)

#### 2.8.4 Laser cutting parameters

The process of laser cutting is associated with different parameters. Based on their influence in cutting operation these parameters can be divided in following groups (Ghany & Newishy, 2005)

(i) Parameters associated with system laser power, beam diameter of focused laser beam, system efficiency and beam frequency.

(ii) Parameters associated with optics spot diameter of induced laser beam, beam diameter, focal length, optical efficiency and depth of focus.

(iii) Parameters related to the operation cutting speed, striking position of laser beam with respect to upper surface of workpiece, diameter of nozzle tip, standoff distance, assist gas type, assist gas pressure, pulse frequency, duty percentage and laser peak

#### 2.8.5 Effect of laser cutting parameters

The quality of laser cut mainly depends on the laser power, pulse frequency, cutting speed and focus position (Ghany & Newishy, 2005). In this section effect of laser parameters are discussed.

##### 2.8.5.1 Effect of laser power

Laser power is one of the most significant laser parameters directly related to input energy of laser cutting process. It has significant effect on quality and efficiency of laser cut. Ghany & Newishy analysed the effect of laser by experimental analysis. They considered CW Nd:YAG laser with different laser power varying from 660 watt to 1980 watt. They used 1.2mm thick stainless steel and cutting was performed with three different cutting speeds (2 m/min, 4 m/min and 8 m/min). The experimental outcomes are illustrated in Figure 2.26. It is evident that better surface roughness and narrower

kerf- width is obtained at lower power and higher cutting speed (Ghany & Newishy, 2005)

Figure 2.26 : Effect of laser power on the (a) kerf width and (b) surface roughness for three different cutting speeds: CW Nd:YAG laser & 1.2mm thick austenitic stainless steel (Ghany & Newishy, 2005)

Laser power also determines the highest cutting speed which is termed as the lowest speed at which through cut is formed. The laser power-speed combination is illustrated at Figure 2.27 during CW CO<sub>2</sub> laser of 0.7mm to 0.8mm thick high steel sheets. It is found that the optimum combination of laser power and speed are 300 watt and 7,000mm/min respectively.

Figure 2.27 : Determination of optimum laser power and cutting speed for laser cutting of steel having thickness less than 1mm (Lamikiz et al., 2005)

### 2.8.5.2 Effect of cutting speed

Laser cutting can be conducted in a wide range of cutting speeds, which strongly depends on laser power, material property of the workpiece and its thickness. From previous study it is found that for a definite laser power, the maximum cutting speed is decreases with workpiece thickness (Poprawe & König, 2001).

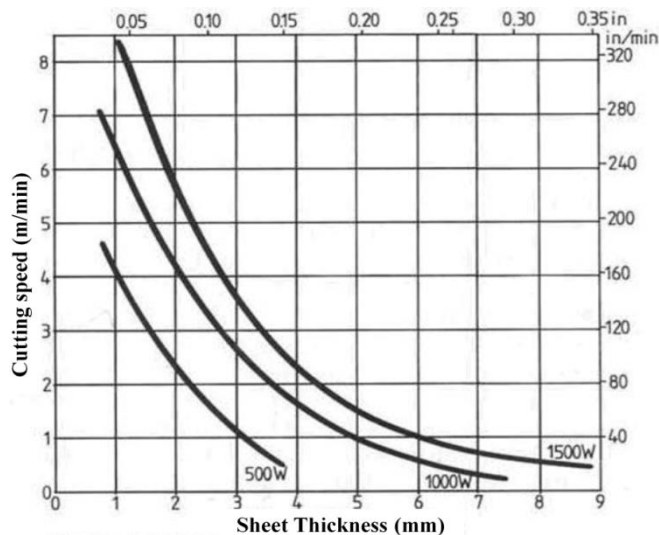


**Figure 2.28 : Effect of laser cutting speed on sheet thickness(John Powell, 1993).**

However, increase in cutting speeds causes the energy density to decrease and less heat conducted to the bulk workpiece resulting in reduction in thickness of HAZ layers if no re-solidified material is attached to the cut edge (Shanjin & Yang, 2006).

### 2.8.5.3 Effect of assist gas and pressure

The selection of assist gas has a great importance in the laser cutting process and its quality. Three types of assist gas are used in laser cutting are oxygen, inert gas (nitrogen, argon, helium) and air. Each of them has their own advantages and generally performs following five functions:

- (i) Removal of molten material from the cutting surface.
- (ii) If oxygen is used as an assist gas, it initiates exothermic reaction and generates additional heat in cutting process.

- (iii) Restrain the plasma while thick sections are cut with high laser power.
- (iv) Protects the focusing optics from spatter.
- (v) Cools the cut edge which minimizes the width of the HAZ.

Use of oxygen as an assist gas initiates an exothermic reaction, provides additional heat energy to the system and makes cutting process faster. Presence of oxygen causes oxidation, surface corrosion and sideway burnings. This may also eliminates the surface coatings and reduce the painting ability. Compare to oxygen, nitrogen needs a higher gas pressure which generates additional mechanical force to blown away the molten material from the cutting surface and produce a bright, oxide free smooth cutting edge. The main drawback associated with the nitrogen gas cutting is the formation of burrs at the bottom of the kerf. Figure 2.29 shows the typical cutting speeds for high pressure nitrogen cutting of stainless steel and oxygen assisted cutting of mild steel with 2 kW CO<sub>2</sub> laser. The cutting speeds and maximum material thickness cut are relatively higher for the oxygen assisted cutting than for high pressure nitrogen cutting (Wandera, 2006).

Figure 2.29: Cutting speed for a 2kW CO2 laser. Oxygen is used as cutting gas for mild steel and Nitrogen (20 bar) is used for stainless steel (Wandera, 2006)

#### 2.8.6 Advantages of laser beam machining

Laser cutting is an advanced machining technique having significant advantages which can be divided in two groups: associated with quality and associated with cutting process.

##### 2.8.6.1 Associated with quality

- (i) Laser cutting produces narrow cut kerf which saves substantial amount of material.
- (ii) Desired shape of cutting edge can be formed i.e round or square shape.
- (iii) Smooth and clean cutting edge can be formed by laser cutting, which limits further finishing/cleaning operation and processing time.
- (iv) Compare to traditional mechanical cutting technique it has very few edge burrs and dross adhesion can be limited to zero.

(v) It generates very narrow HAZ and dross free cut. Negligible distortion has taken place due to very thin ~~re~~solidified layer.

(vi) Blind cuts can be made in some ~~materials~~ such as wood or acrylic.

#### 2.8.6.2 Associated with cutting process

(i) Laser cutting is smart, automatic and ~~fast~~ cutting processes.

(ii) It is a noncontact cutting process; hence there is no chance of tool wear.

(iii) Any shape of cut can be possible by laser cutting.

(iv) It has low noise level.

(v) The process can easily be automated with good prospects for adaptive control.

(vi) The cutting process mainly associated with computer programming. Thus it has high flexibility in use.

(vii) Almost all kinds of materials such as friable, brittle, electric conductors or non conductors, hard or soft can be cut by laser cutting. There is some problem happens during cutting of highly reflective materials like aluminium, ~~copper~~ gold, but with proper beam control these can be cut pleasingly

#### 2.9 Modeling techniques of laser cutting

Laser cutting is a complex ~~thermo~~mechanical problem. Different types of models are proposed by researchers to describe this process. In general ~~these~~ models can be divided in two major groups; (i) Theoretical models and (ii) Artificial intelligence models (Parandoush & Hossain, 2014)

### **2.9.1 Theoretical models**

Theoretical models of laser cutting starts with mathematical formulation of the system, considering lasers material interaction principles and energy balanced equations. These kinds of models are able to describe different phenomena associated with laser cutting process such as material removal, thermal distribution, stress concentration, rate of material removal, heat affected zone (HAZ) estimation, kerf-width prediction, surface roughness estimation etc. Theoretical models are categorized in two sections: analytical solution based models and numerical solution based models. Analytical solution based models are developed based on some assumption and most of the time unable to describe the total system in real condition. On the other hand, numerical solution based models are capable to describe almost all kinds of laser cutting problem by dividing the workpiece into small elements and nodes. Numerical models are also divided in two groups: mesh based method (example: finite element method, boundary element method, finite difference method) and mesh free method (example: smoothed particle hydrodynamics, symmetric smoothed particle hydrodynamics etc.). Besides, combining two or more methods hybrids methods can be formed (Parandoush & Hossain, 2014).

#### **2.9.1.1 Analytical modelling**

Modest and Abakians (1986), proposed an analytical solution based model for grove depth prediction in evaporative laser cutting. Their proposed model was formulated based on heat conduction equation adopted with cutting speed and Gaussian beam distribution (M. Modest & Abakians, 1986). Di Pietro and Yao (1995) proposed another model to predict the surface roughness and kerf width in laser cutting process. The model was validated by performing experiment on mild steel sheet with CO<sub>2</sub> laser. Though the model showed good agreement with experiment, they suggested to use the model in combination with formerly proposed models due to the numerous mechanisms that subsist for creating striations, and changing the cutting condition may change the

solution process (P. Di Pietro & Y. Yao, 1995). Kou et al., (1983) formulated a 3D heat flow model by using the Fourier differential equation. The model was validated with experiment on stainless steel 316 by using continuous CO<sub>2</sub> laser beam (Kou et al., 1983). Yilbas and Kar analyzed (1998) used gas dynamics in reactive CO<sub>2</sub> laser cutting and proposed an experimentally validated model to predict the molten layer thickness (B. Yilbas & Kar, 1998). Man et al., (1998) studied on gas jet modelling of nozzle and calculate the expected pressure, momentum, gas density variation and presence of shock waves. From their analysis they recommended supersonic gas jet flow characteristics are well suited conical nozzles gas jets (Man et al., 1998). Kaebernick et al., (1999) proposed an analytical model of reactive laser cutting in pulse mode to predict the kerf width. They validated the proposed model with experiment and concluded that kerf width increase slightly with decrease of cutting speed up to critical point. After the critical point kerf width goes down with decrease of cutting speed (Kaebernick et al., 1999). Another analytical method for kerf width prediction in laser cutting was presented by Sheng et al., (1994). The model was prepared as a function of erosion front dimension and validated by experiment on three different material (stainless steel, aluminum oxide and acrylic) (P. Sheng & Chryssolouris, 1994). Jiang et al., proposed a model for prediction of groove depth during pulsed Nd:YAG laser cutting on sheet metal (Jiang et al., 1993). Cenna and Mathew proposed an analytical model for HAZ and kerf width prediction considering energy balance equation expressed as follows

$$(2.24)$$

where  $E_L$  is energy of laser beam,  $E_C$  is conduction energy and  $E_V$  is vaporization energy. They used three different materials such as composite material aramid fiber reinforced plastic (AFRP), glass fibre reinforced plastic (GFRP), PMMA

sheet for experiment (Cenna & Mathew, 2002). Yilbas (2004) proposed another model of reactive laser cutting for kerf-width prediction applying the scaling law and effect of laser parameters on kerf width was analyzed. He found that increasing cutting speed reduces the kerf-width (B. Yilbas, 2004). Besides, by using Taylor series of approximation a new thermal analytical model to predict the depth of HAZ and laser melted zone (LMZ) was proposed by Pantelis and Vanotas (1998). The experiment was conducted by using laser power 2500watt–3000watt, cutting speed 0.05 m/s - 1.5 m/s and beam diameter 3.5 mm - 6.85 mm. They use 15mm thick, 100 mm diameter circular disk of constructional steel CK60 and St-52 (DIN 1652) steel to predict the depth of HAZ and LMZ respectively (Pantelis & Vonatsos, 1998). Although, the outcome of said model was close to the experimental result before the melting point, the methodology was complex in nature.

### **2.9.1.2 Numerical modeling of laser cutting**

In numerical simulation or modelling the total workpiece is divided into small elements and nodes and analysis is run applying boundary condition close to reality. Thus, compare to analytical modelling, results of numerical modelling are exact to real solution with fewer assumption. This has motivated researchers to do research mostly on numerical modelling. Only drawback of numerical modelling is requirement of more computational power and time. But now-a-days computation power is advanced, which reduces the computational time and makes numerical modelling as a unique tool for modelling. The most common numerical methods used in laser beam machining (LBM) are finite element method (FEM), boundary element method (BEM), finite difference method (FDM) etc. In this section the application of different numerical models in LBM are discussed.

Bokota and Iskierka (1996) suggested numerical simulation is the best method to describe the laser treatment because it allows the user to control the process very well. By using numerical simulation they presented a numerical model for thermal heat distribution considering phase transformation by using Fourier-Kirchhoff equation. The proposed model was also able to predict the hardened layer and HAZ thickness. In order to proof the model efficiency experiment was conducted by using CO<sub>2</sub> laser with 1.5KW laser power and 5mm beam diameter. They used three different cutting speed 0.75m/min, 0.90 m/min and 1.00m/min respectively. The workpiece material was carbon steels having dimension of 100mm x 10mm x 10mm (Bokota & Iskierka, 1996).

Modest & Michael proposed a 3-D heat conduction model to predict the transient thermal distribution in a thick solid workpiece. The proposed model is be able to explain the thermal distribution while the grove shape was changing due to material evaporation during laser ablation. Finite volume method was used to develop the model and it showed good accuracy for CW and pulse laser cutting. As the model explained the thermal distribution inside the workpiece, it was used to predict the HAZ. By using finite difference method they proposed another numerical model to predict the transient thermal propagation in a thick slab. The model was able to explain the thermal profile during ablate or decompose of material by CW or pulsed laser (M. F. Modest, 1996).

Sheng and Joshi proposed a hybrid analytical-numerical model to determine the heat-affected zone during laser cutting. They integrated the analytical formula for the cutting-front geometry with the 2-D numerical analysis to draw thermal propagation curve in the profile plane. The HAZ could be predicted through transient numerical results of time-temperature response of the workpiece material in simulation. The simulation results showed good accuracy with the experimental results. The experiment was conducted by using CO<sub>2</sub> laser and stainless steel-304 as workpiece. Laser parameters were power, 600W - 750W, cutting speed 0.25mm/s - 2.5mm/s, 0.27mm

diameter laser beam was produced by using 127mm focal length lens. Khan and Yilbas (2004) also presented another model for laser heating of thin sheet metal by combining analytical and numerical model. They analysed the temperature field during laser heating analytically and calculated the thermal stress numerically. For numerical analysis they used finite element method (FEM). From their analysis they found that cutting speed has a great influence on temperature and thermal stress distribution in workpiece (Khan & Yilbas, 2004). Yu used ANSYS codes for 3D thermal analysis of laser cutting and drilling and considered change in phase and boundary as well as loading conditions in simulation (Yu, 1997). Di Pietro and Yao examined the dynamic nature of laser beam front/cutting front in CO<sub>2</sub> laser cutting together with the CNC axis acceleration. They proposed a 2-D numerical model to analyze the effect of different velocities on cutting front temperature. From their research it was evident that laser movement with acceleration causes significant effect on laser beam coupling (P. Di Pietro & Y. L. Yao, 1995). Pietero et al., developed a 2-D transient heat-transfer model by numerical analysis for quality optimization. They found that the laser beam front/cutting front has dynamic behaviour and in temperature distribution it has significant effect that needs to count. For quality improvement in laser cutting they suggested model based optimization is an alternative of trial-and-error based experimentation (Pietro et al., 2000). Kim and Zhang developed a 2-D FE model to analyse the rate of material removal and smoothness of cutting groove for pulsed laser beam in evaporative laser cutting. They used laser power and pulse number as variable input parameters keeping all other input parameters fixed. From the current study two threshold curves were proposed to determine the acceptance region for a quality cut pulsed laser cutting. Those can also be used in optimization of pulsed laser cutting process (Kim & Zhang, 2001). Later two numerical models with boundary element method for evaporative laser cutting were developed by Kim. The unsteady nature of

heat transfer in laser cutting was described with those models. He also compared the outcomes of groove shape and temperature with his previously stated FEM-based models and showed good agreement with each other (Kim, 2000, 2004). Prusa et al. developed a model for heat conduction during laser cutting and used to predict the cutting speed and temperature field in HAZ. The prime objective of their study was build a relationship between dimensionless rate of conduction heat loss and Peclet number known as dimension less cutting speed (PE) (Prusa et al., 1999). Kheloufi and Amara proposed a 3-D transient numerical model for laser melt cutting. They used finite volume method and considered various physical phenomena such absorption, heat propagation, molten flow, melting and solidification which are associated with laser cutting. Commercial code of Fluent 6.3 CFD was used to couple the heat transfer and flow phenomena in simulation. The main advantage of the proposed model was its ability to explain different phase of laser cutting (solid, liquid, gas and mushy). In their research they discuss about the effect of cutting speed on kerf-width at different stages of cutting process (Kheloufi & Amara, 2012). Scintillaand and Tricarico presented a 3-D numerical model for laser beam fusion cutting and estimated the HAZ. They also calculated the induced laser energy at the cut-kerf by using reverse method. Two different kinds of laser: CO<sub>2</sub> laser and disk laser were used to cut three different thicknesses of 90MnCrV8 steel: 1mm, 5mm and 8mm. It was found that CO<sub>2</sub> laser produced better edge quality than disk laser due to high conduction loss, which resulted lower viscosity with ease of ejection from cut-kerf (Scintilla & Tricarico, 2012).

Later the Finite Element Method (FEM) became popular to formulate the steady and transient 2D/3D heat flow model development for laser machining or laser assisted machining due to its simplicity and accuracy. The main advantage of FEM is that it allows researcher to use different thermo-mechanical properties of the material to obtain results thoroughly for different laser parameters. Moreover, thermo-mechanical analysis

can be done by combining both thermal and structural analysis. Anderson and Shin (2006) proposed a transient thermal model for laser assisted machining (LAM) and measured the surface temperature of austenitic stainless steel (Anderson & Shin, 2006). Germain et al., proposed a simulation model to plot the HAZ profile in AISI 52100 by using commercial FEA software Abaqus/Standard® and validated the model with experimental results (Germain et al., 2007). Sheng et al., proposed a 2-D FEM model for width of HAZ prediction and validated with experiment (P. S. Sheng & Joshi, 1995). Yilbas et al., used finite element method to simulate the stress development during cutting a hole having 15mm dia. The model was simulated by using ANSYS and considering the problem as sequentially coupled unidirectional problem. The model was validated with experiment by using CO2 laser as a source and 15mm thick mild steel as workpiece (B. S. Yilbas et al., 2009). Nyon et al., studied the effect of laser power and speed on the kerf width changes. They used CW CO2 laser having maximum power output of 2,700watts. The focal lens and beam diameter were 127 mm and 0.3428 mm respectively. The workpiece was Inconel 718 with thickness 1mm & 2mm. The model was simulated by using transient finite element method (Nyon et al., 2012). Arif, performed the laser cutting of tailored blanks from a thick mild steel sheet and measured the temperature and stress field by using finite element method (Arif et al., 2009). Later Akhtar et al., (2014) studied the different size of rectangle geometries and found that temperature and stress fields are affected by the size of the rectangular cut geometry. They used aluminium alloy as work piece and ABAQUS finite element code for FEM simulation (Akhtar et al., 2014).

Hence, it is found that finite element (FE) method is an efficient method which can describe the thermo-mechanical behaviour of laser cutting.

## 2.9.2 Artificial intelligence (AI) based modelling

Artificial intelligent (AI) is an experienced based modelling technique, where modelling outcomes come from previous knowledge. It is a well suited modelling technique for complex and nonlinear problem like laser beam machining (LBM). Because LBM is a complex problem associated with different linear thermo mechanical phenomena which are difficult to solve by mathematical modelling. Different kinds of AI based modelling techniques are used in LBM. Among them artificial neural network (ANN), FUZZY expert systems (FES), genetic algorithm (GA) are most common.

A multi-layered neural network is proposed by Youssef et al., for non linear micro machining process by prediction as a function of laser power (Youssef et al., 2003) proposed an artificial neural network (ANN) model for HAZ prediction considering experimental results of laser power, speed, assist gas pressure and focal position on HAZ. The experiments were performed by using CO<sub>2</sub> laser and considering stainless steel as workpiece. The proposed model showed good accuracy having 6.46% prediction error. Moreover, it was identified that for HAZ formation cutting speed had maximum influence, whereas influence of assist gas pressure was negligible. Tsai et al., did multiple regression analysis (MRA) and proposed an artificial neural network (ANN) considering current, frequency, cutting speed as input parameter to predict cutting depth, width of HAZ cutting line for epoxy and copper compounded epoxy. The experiments were performed on a flat non-lead (QFN) by using a diode pumped solid state laser (DPSSL). Moreover optimal parameter for HAZ was identified by using genetic algorithm (GA) (M.-J. Tsai et al., 2008)

FUZZY expert system is another intelligent modelling technique used in laser beam machining. Pandey and Dubey developed fuzzy expert system (FES) model for laser cutting based on FUZZY logic theory to predict the optimum kerf width. From their research it was identified that for laser cutting of aluminum sheet gas pressure is the most significant factor followed by laser frequency (Pandey & Dubey, 2012). Syn et al., (2011) proposed another FES model to predict the surface roughness and cross inclusion. CO<sub>2</sub> laser was used to cut alloy 800 (Syn et al., 2011)

## 2.10 Summary

Many researches from interdisciplinary areas of laser machining processes are done which describe not only machining process but also parametric optimization. Different LBM and LAM models are proposed by using mathematical, statistical, numerical, artificial intelligent methods. But most of the developed models are representing straight cutting. Very few models are developed which can simulate the complete process of cutting. Hence, a complete cut of square blanks from stainless steel sheet need to be developed. Moreover cutting of stainless steel by using fusion laser cutting is a big challenge. During cutting process rapid heating, melting, molten material removal and re-solidification are taken place. Which cause HAZ, kerf width and thermal stress along the kerf. Hence in this study a coupled thermo-mechanical finite element model has been introduced by ANSYS in order to explain the fusion laser cutting mechanism in CO<sub>2</sub> laser blanking of square samples. Stainless steel 304 sheet of different thicknesses are used to cut 10mm x 10mm square blank under different laser power and speed. The proposed simulation model is able to explain thermal distribution, kerf width, HAZ and thermal stress

## CHAPTER 3: RESEARCH METHODOLOGY

### 3.1 Introduction

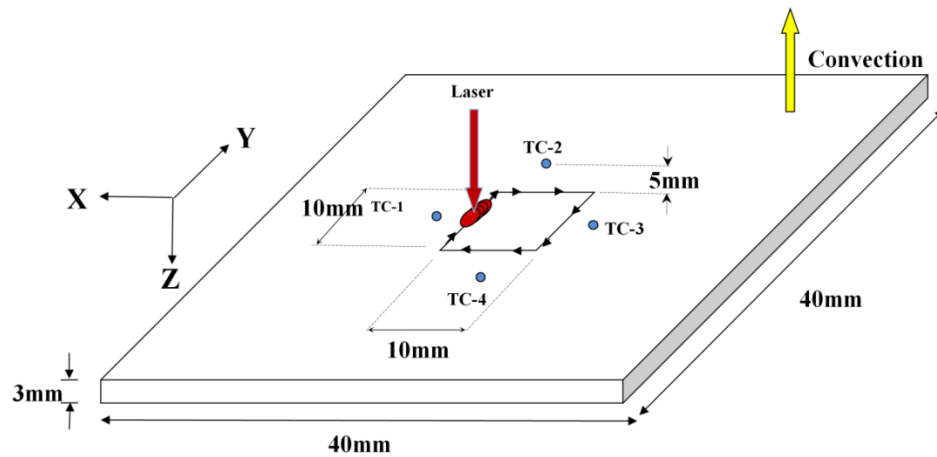
This chapter contains information about the methods and materials, which are used during the research work. The research work can be divided in two sections: Numerical analysis and Experiment & validation. In numerical analysis, finite element method (FEM) software ANSYS is used for model development, simulation and solution purpose. Whereas, experiments are conducted using laser machine, keeping identical laser parameters as in simulation. After that the outcome of simulation and experimental results are compared with each other and analyzed the parametric effect. Thus the total research activities associated in this study are listed as follows

Figure 3.1 : Activities involved in research work.

### 3.2 Model description and design of experiment:

In this research, experimental validation of the mechanical FEM simulation model has been developed and the effect of laser input parameters (laser power and cutting speed) on HAZ kerf width and thermal stress have been analyzed. The schematic diagram of experimental setup is illustrated in Figure 3.2. It is considered that

the dimension of the workpiece is 40mm x 40mm and inside it 10mm x 10mm square blank is been cut.



**Figure 3.2 : Schematic diagram of experimental set-up.**

Two different thicknesses (1mm and 3mm) of stainless steel-304 sheets are used in this study. In order to understand the parametric effect of laser input parameters (power & speed) on laser output parameters (HAZ, kerf width, thermal stress) three different laser powers and three different cutting speeds are considered. Full factorial analysis i.e. 18 experiments are done as shown in Table 3.1.

**Table 3.1 : Experimental parameters**

Exp No	Material Thickness(mm)	Laser Power(watt)	Cutting Speed(mm/sec)
1	1	2160	10
2	1	2160	15
3	1	2160	20
4	1	1800	10
5	1	1800	15
6	1	1800	20
7	1	1440	10
8	1	1440	15
9	1	1440	20
10	3	2160	10
11	3	2160	15
12	3	2160	20
13	3	1800	10
14	3	1800	15
15	3	1800	20
16	3	1440	10
17	3	1440	15
18	3	1440	20

### 3.3 Numerical Analysis

Numerical analysis provides approximate results which close to real solutions. In this research numerical analysis is done by using finite element method (FEM). It is a computational numerical method for solving different kinds of engineering problems in bodies of user-defined geometry through discretization. In this study FEM simulation software ANSYS is used for model development, simulation and extracting results. As the process of fusion laser cutting is a thermo-mechanical problem, the complete analysis is a combination of thermal and structural analysis. Hence, non-linear transient and sequential coupled field analysis technique available in ANSYS is employed in simulation. Where, thermal analysis with appropriate boundary condition is done firstly and later the outcomes of thermal analysis (nodal temperature) are considered as input in structural analysis. The flow diagram of thermo-mechanical FEM analysis is shown in Figure-3.3.

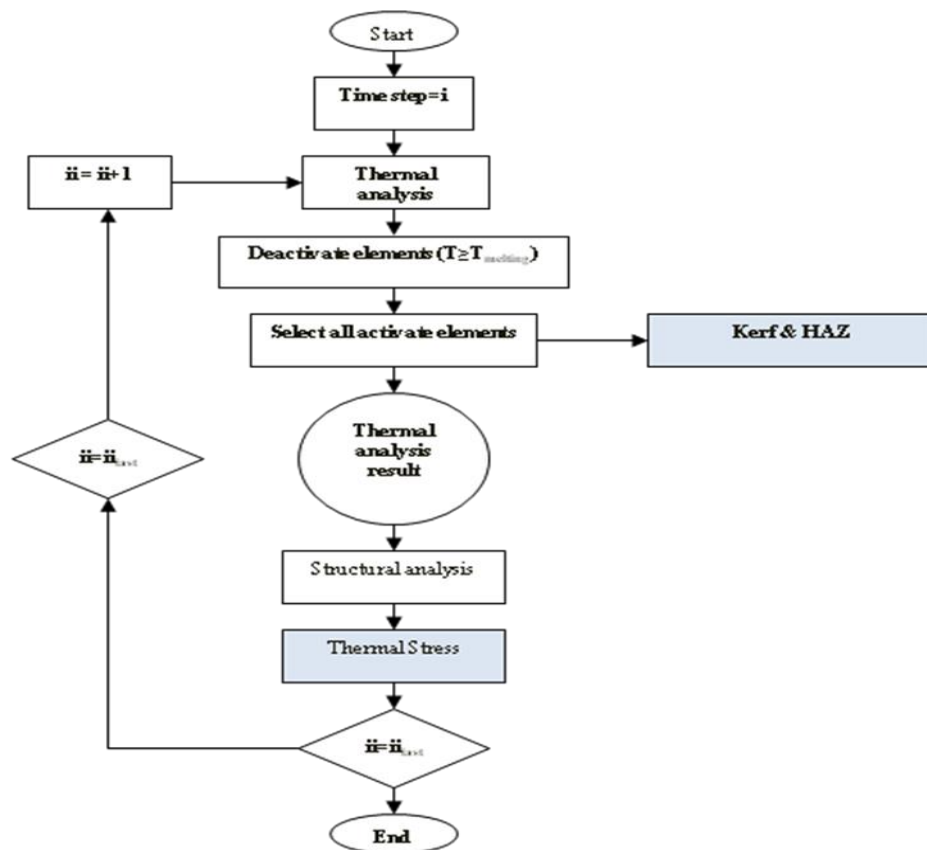
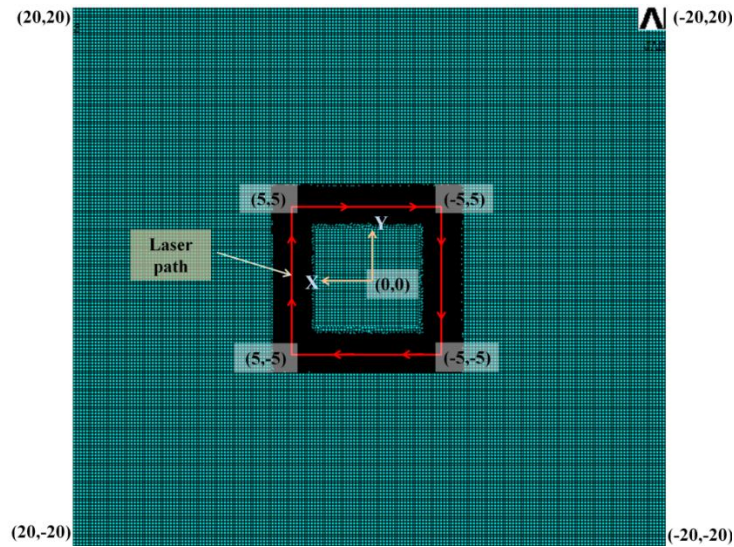


Figure 3.3 : Process flow diagram of thermo-mechanical analysis.

It is considered that the focused laser beam is Gaussian in nature. Element death methodology is used to simulate the material removal. In this methodology after each time step the elements which reach the melting temperature are selected and deactivated (the detail procedure is discussed in material removal section). These deactivated elements have negligible or no effects on the remaining load steps. In this way material removal process is simulated. In the simulation the laser beam moves along the laser path with cutting speed and simultaneously penetrates in to the workpiece by melting speed. The position and movement of laser beam is programmed by using local coordinate system, which change its origin with respect to global co-ordinate system of the model at every time step. Furthermore, the time step is calculated considering the length of laser path and cutting speed. The main focused areas of this research are analyzing the effect of laser parameters on HAZ, kerf-width and stress concentration. From thermal analysis the status or thermal distribution of model, kerf width and HAZ are calculated, whereas structural analysis gives the results of stress concentration.

### **3.3.1 Model development and element selection**

The proposed model is developed within the ANSYS environment by using related modeling tools. Identical dimensions (40mm x 40mm having 1mm and 3mm thickness) like experiment are considered in simulation model as shown in Figure 3.4.



**Figure 3.4 : Dimension of the model.**

In order to reduce the computational time, element numbers are reduced by using non-uniform mesh as shown in Figure 3.5.

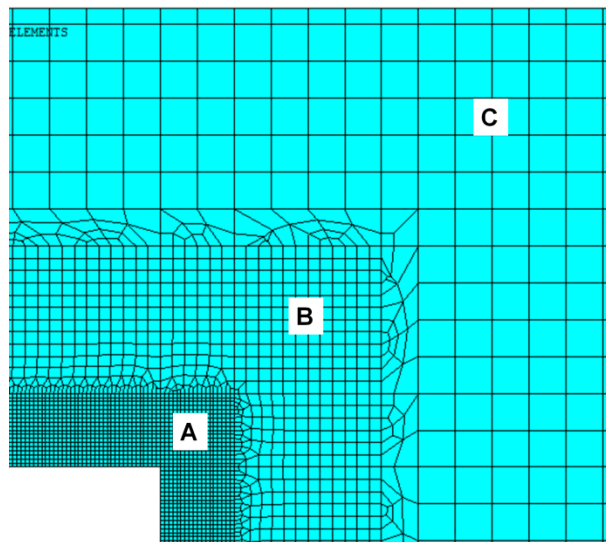


**Figure 3.5 : Non uniform mesh generation.**

As the accuracy of the model depends on refinement of mesh, some areas of the model are meshed from finer to coarser. In this study the entire model is divided into three different zones such as zone-A, zone-B, zone-C and meshed by using different size of elements. At zone-A finer mesh is considered, due to involvement of high heat flux and material removal (element deactivation). Coarser elements are created (zone-B) in the neighbouring zone. Then the coarsest elements are considered in the remaining

area (zone C) of the model. Grid density of the model is also very important and the accuracy of model mostly depends on it. For this reason appropriate mesh sizes of the model are selected by performing mesh convergence parametric studies.

The proposed model of fusion laser cutting is a thermo-mechanical FEM model i.e. it has two parts: thermal analysis and mechanical analysis. Thus two different kinds of elements are considered. For thermal analysis thermal element SOLID70 is used and in structural analysis structural element SOLID185 is considered. Both elements are equivalent 8 noded brick type element. The details of these two elements are described in Appendix B.

### 3.3.2 Thermal analysis

Non-linear transient thermal analysis is done by employing appropriate boundary conditions and thermal loading. As the workpiece is stainless-304, its thermo-mechanical properties are considered in simulation. It is assumed that the radiated laser beam is Gaussian and modeled by ANSYS Parametric Design Language (APDL) (Figure 3.6).

Figure 3.6 : Gaussian heat flux distribution.

The position of heat flux is calculated by using a table considering cutting speed. Thus desired heat flux can be modeled at different laser power and speed. Multiple time steps are used in simulation and it is assumed that after each time step the laser beam advances 0.025mm. The time step ( $T_p$ ) is calculated by following Equation:

$$T_p = \frac{D\_step}{v} \quad (3.1)$$

where  $D\_step$  is distance advances the laser beam at each time step (0.025mm) and  $v$  is cutting speed in  $ms^{-1}$ .

To cut 10mm square blank the laser beam focuses 5mm away from the centre of the square and travels along the perimeter of desired blank. Hence, the total number of load step ( $TL\_step$ ) is calculated by Equation 3.2.

$$TL\_step = \frac{4 \times L_p}{T_p} + 1 \quad (3.2)$$

where  $4 \times L_p$  is total length the laser travel during the cutting.

### 3.3.2.1 Material removal

In fusion laser cutting it is assumed that the cutting front is formed and advances through the thickness of the workpiece. Thus materials associated with that area are heated and subsequently molten material is blown away from the workpiece with the help of pressurized assist gas. Same situation is simulated in ANSYS by using element death methodology. In this methodology the elements under the heat flux are heated. After each time step the elements temperature are calculated and those elements which cross the melting temperature are selected and deactivated by using EKILL command. These deactivated elements are considered to be dead, (i.e., with insignificant effect in the subsequent time steps by setting the conductance to approximately zero). Because of

absence of customize or inbuilt menu in ANSYS Mechanical for material removal, separate subroutine need to be developed with the help of APDL coding (Appendix: A).

### 3.3.2.2 Heat affected zone (HAZ)

The area of heat affected zone (HAZ) exists near the cut kerf. In present study stainless steel-304 is considered as workpiece. It is austenitic steel, contains significant proportion of alloying elements. Thus heating and rapid cooling associated with laser cutting causes not only grain refinement but also carbide, sulphide and phosphate formation within a temperature range of 400<sup>0</sup>C to 800<sup>0</sup>C (Masumoto et al., 1990). In addition to this austenite to ferrite phase transformation also may takes place. That forms HAZ. Thus, from the temperature profile of simulation HAZ is calculated from the edge of cut kurf to nodal position of 800<sup>0</sup>C perpendicularly as shown in Figure 3.7.

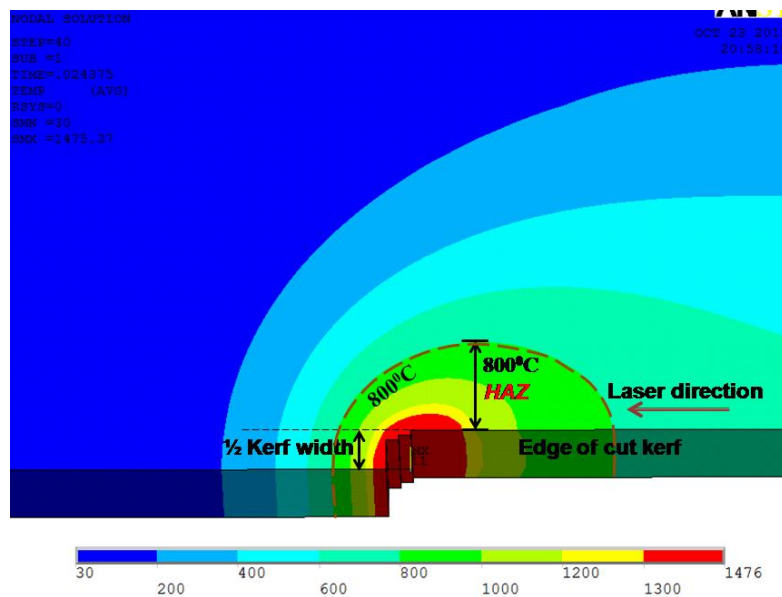


**Figure 3.7 : HAZ and kerf width form during fusion laser cutting simulation.**

### 3.3.2.3 Kerf width

The material is removed in simulation by using element death methodology as stated in section 3.2.2.1. The elements which cross the melting temperature are deactivated. Thus, the kerf width can be shown in simulation by selecting the live elements as illustrated in Figure 3.8.

Figure 3.8 : Element death and live methodology for kerf width measurement.

### 3.3.3 Thermal stress analysis

Laser cutting is taken place at room temperature (30°C) and during the cutting process, tiny area under the focused laser beam is heated up to melting temperature. Thus temporal variation has taken place which initiates thermal stress. Procedure of coupled field analysis technique (ThermalStructural) is used to simulate thermal stress as shown in Figure 3.9.

Figure 3.9 : Working flow of thermal stress analysis in ANSYS.

Keeping the same discretized modal, nodal temperatures of thermal analysis are transferred to structural analysis as body force loads by using LDREAD command. Structural properties (modulus of elasticity, thermal expansion coefficient, poisson ratio,

density) of stainless steel 304 are used as material properties and the model is well constrained by restricting the displacement at edges. The results of Vonmises stress at different locations are plotted to find the approximate residual stress.

### 3.4 Experimental work

Numerical simulation provides approximate solution of laser cutting. In order to validate the simulation or to identify the relative error experiments are conducted. Thus the experiment of fusion laser cutting is conducted by using laser machine and using stainless steel 304 as workpiece. The details procedure of experiment is illustrated in the following sections.

#### 3.4.1 Laser cutting machine

The experiment is conducted by using CO<sub>2</sub> laser machine which is continuous wave type. The brand of the machine is Amada, bearing model no: FG2412. The manufacturing year is 2004. Maximum 4.0 kW power can be produced.

Figure 3.10: (a) CO<sub>2</sub> Laser machine (b) Workpiece mounted on the table

The machine is equipped with AMNC CNC control and 2870 x 1270 x 200 axis travel. The focal length of the lens is 0.15mm and nozzle gap 0.5mm. Beam diameter 0.4mm is used for cutting. N<sub>2</sub> is used as an assist gas, because it produced brighter and smoother cut surface with smaller kerf (Chahany & Newishy, 2005). Assist gas pressure is 0.9 psi.

### 3.4.2 K-type thermo couple

The surface temperature of the workpiece is measured by using digital data logger model Tenmars TM-747DU and K-type thermo-couples. TM-747DU is a 4 channel data logging thermometer and capable to coupled with K/J/T/E/R/S/N types thermocouples. As the melting temperature of stainless steel-304 is around  $1450^{\circ}\text{C}$ , K-type thermocouple is used close to the laser scanning path. The temperature range of these thermocouples are  $-100^{\circ}\text{C} \sim 1300^{\circ}\text{C}$  (  $-148^{\circ}\text{F} \sim 2372^{\circ}\text{F}$  ) and the accuracy of TM-747DU is  $\pm (0.1\% \text{ rdg} + 0.7^{\circ}\text{C})$ .

### 3.4.3 Morphological and metallurgical analysis

The morphological and metallurgical changes in the cutting section were examined using scanning electron microscope (SEM).

### 3.4.4 Kerf width analysis

After doing experiment the kerf width is measured by using optical microscope as shown in Figure 3.11

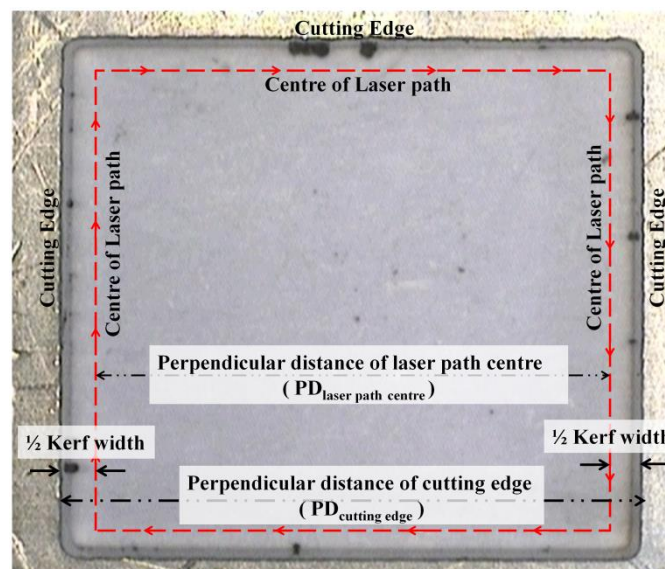


**Figure 3.11 : Procedure of kerf width measurement.**

$$Kerf\ width = PD_{cutting\ edge} - PD_{laser\ path\ centre} \quad (3.3)$$

where  $PD_{cutting\ edge}$  is perpendicular distance of cutting edge and  $PD_{laser\ path\ centre}$  is perpendicular distance of laser path centre.

### 3.5 Analysis of variance (ANOVA) study

Results of the experiments are evaluated by the analysis of variance (ANOVA) study in order to find out the contribution of the laser parameters (power, cutting speed) on quality characteristics (width of HAZ, kerf width).

The calculation of ANOVA is done on the basis of the recommendations made by the researchers (Antony, 2014; Fowlkes & Creveling, 1995) as given by Equation 3.4 to 3.13.

$$SS_F = (Exp\ No\ at\ F_1) \left( \overline{S/N_{F_1}} - \overline{S/N} \right)^2 + (Exp\ No\ at\ F_2) \left( \overline{S/N_{F_2}} - \overline{S/N} \right)^2 + \dots + (Exp\ No\ at\ F_n) \left( \overline{S/N_{F_n}} - \overline{S/N} \right)^2 \quad (3.4)$$

where,  $SS_F$  is the sum of square mean for an individual factor,  $F_1, F_2, \dots, F_n$  are the factor level number,  $\overline{S/N_{F_1}}, \overline{S/N_{F_2}}, \dots, \overline{S/N_{F_n}}$  are the mean of  $S/N$  ratio at individual level of each factor and  $\overline{S/N}$  is the mean  $S/N$  ratio of all experiments.

$$SS_T = \sum_{i=1}^N \left( S/N_i - \overline{S/N} \right)^2 \quad (3.5)$$

$$SS_{Er} = SS_T - \sum SS_F \quad (3.6)$$

where  $SS_T$  is the total sum of square,  $SS_{Er}$  is sum of square error and  $N$  is the number of experiment.

Degree of freedom for individual parameters ( $DOF_F$ ), error ( $DOF_{Er}$ ) and total experiment ( $DOF_T$ ), are explained by Equation 3.7, 3.8 and 3.9 respectively.

$$(3.7)$$

$$(3.8)$$

$$(3.9)$$

The mean square (variance) for individual process parameters ( $V_F$ ) and for error ( $V_{Er}$ ) can be obtained by using following equations

$$(3.10)$$

$$(3.11)$$

F-ratio (variance ratio) and percentage of contribution of the individual parameter on the response can be calculated by Equation 3.12 and 3.13 respectively

$$(3.12)$$

$$(3.13)$$

Moreover the mathematical and statistical methods have been used to investigate the accuracy of the simulation. Relative error ( ) of formation has been established by using the following formula:

$$(3.14)$$

Another method goodness of fit ( $R^2$ ) for the prediction capability of the system is calculated as follows:

$$(3.15)$$

where  $n$  is the total experiment number,  $x_i$  is the experimental value,  $y_i$  is simulation value and  $\bar{x}$  is the average of the experimental value.

### 3.6 Material

Both the experiment and simulation is conducted by using stainless steel sheet having 3mm thickness. Stainless steel 304 is commercially important material and widely used to fabricate food processing equipment, architectural panelling, heat exchanger and high corrosion resistance machine parts. It is an austenitic steel alloy having significant portion of carbon, manganese, phosphorus, silicon, chromium, nickel. The chemical composition of the stainless steel 304 is shown in Table 3.2.

Table 3.2 : Chemical composition of Stainless Steel 304 (Radu & Cristea, 2013)

C	Mn	P	S	Si	Cr	Ni	N	Mo	Cu
0.023	1.67	0.026	0.01	0.3	18.05	8.02	0.068	0.24	0.24

## CHAPTER 4: FEM ANALYSIS OF FUSION LASER CUTTING

### 4.1 Introduction

This chapter describes the thermo-mechanical simulation procedure of laser cutting of a square blank from stainless steel sheet with the help of finite element method. The model is developed by using APDL (ANSYS Parametric Design Language) code of finite element software ANSYS and validated by the experiments. This chapter begins with a brief description of experimental set up. Then the coupled thermo-mechanical FEM model is described. Finally, simulation results are demonstrated and discussed.

### 4.2 Physical description of model

In the present study AMADA FQ412 CQ laser machine, with AMNC CNC control is used to perform the laser blanking experiments on stainless steel sheet having thickness 1mm and 3mm. The length and width of the workpiece is 40mm x 40mm, inside that 10mm x 10mm square blank is been cut. Three different laser powers (2160watt, 1800watt, 1440watt) and cutting speeds (10mm/sec, 15mm/sec, 20mm/sec) are used to perform the through cut. The laser beam strikes on the surface of the workpiece and cutting is taken place counter clock wise from the starting point A as shown in Figure 4.1. The diameter of laser beam is 4 mm, which is formed by using 127mm focal lens. Four sets of K typed thermocouples (TC-1, TC-2, TC-3, TC-4) with data logger are placed 5mm away from the laser path to measure the surface temperature. Nitrogen is used as assist gas for clean cutting and is supplied on the workpiece from a conical nozzle at a pressure of 0.9 psi. The laser cutting is performed under atmospheric condition and heat losses are taken place from the surfaces open to atmosphere.

Figure 4.1 : Physical description of model.

### 4.3 Model development for FEM analysis

The proposed model is developed under ANSYS pre-processor environment considering same dimension as experiment i.e. length x width of the workpiece is 40mm x 40mm having two different thickness (1mm and 3mm) and laser moves to produce 10mm x 10mm square blank.

#### 4.3.1 Element selection

Appropriate element selection for finite element model is important to obtain accurate solution through the analysis. For 3D analysis brick, wedge, and tetrahedron types of elements are used. The present thermal analysis model is meshed using brick element (called SOLID70). Because SOLID70 is a lower order element and computationally more efficient than a tetrahedron element. It has eight nodes with a single degree of freedom (temperature) at each node. Heat fluxes and convections can be input as surface loads at the element faces defined by the nodes or elements. Moreover this element can be replaced by an equivalent structural element SOLID185 for structural analysis. The details of SOLID70 and SOLID185 are described in Appendix B.

#### 4.3.2 Material property

The temperature dependent mechanical properties of Stainless steel 304 in the simulation are shown in Table 4.1 and 4.2.

Table 4.1: Thermal properties of stainless steel 304 (Lee & Chen, 2011)

Temperature (°C)	Density (g cm <sup>3</sup> )	Thermal Conductivity (W m <sup>-1</sup> K <sup>-1</sup> )	Specific Heat (KJ g <sup>-1</sup> K <sup>-1</sup> )
20	7931	15.5	435
100	7896	16.2	452
200	7849	17.5	479
300	7801	18.9	499
400	7753	20.3	517
500	7704	21.8	534
600	7655	23.4	551
800	7555	26.6	585
1000	7453	29.8	622
1200	7346	33.1	663
1450	7249	36.3	865
Latent Heat of melting (Jkg <sup>-1</sup> )	2.6 x 10 <sup>5</sup> Jkg <sup>-1</sup>		
Solidus temperature (°C)	1400		
Liquidus temperature (°C)	1450		

In order to define the temperature dependent material property APDL command MPTEMP and MPDATA are used. Where MPTEMP defines the temperature and MPDATA defines corresponding material property.

Table 4.2: Mechanical properties of stainless steel 304 (Shiue et al., 2004)

Temp (°C)	Young's Modulus (GPa)	Poisson's ratio	Thermal expansion coefficient (°C <sup>-1</sup> )	Yield strength (MPa)
20	197.13	0.27	16.03	367
100	194.00	0.28	17.05	340
200	187.18	0.284	17.54	331
300	181.00	0.289	18.00	330
400	170.00	0.291	18.73	290
500	160.73	0.295	19.36	266
600	148.00	0.299	19.84	220
800	125.50	0.302	21.24	165
1000	69.20	0.305	23.49	66
1200	20.55	0.32	23.49	60
1450	8.84	0.32	23.49	60

### 4.3.3 Meshing

FEM is a computational numerical method associated with elements and nodes for solving different kinds of engineering problems. In general, more elements give better results. However, sometimes excessive number of elements may increase the computational time and round-off error. Thus, non-linear meshing technique is used and appropriate sizes of elements (fine or coarse) are selected for the relevant regions. In present study the focused areas are heat input, HAZ, kerf-width and stress development. Hence, fine mesh is considered along the laser path and its surrounding. However, coarser elements are created in the neighboring zone then the coarsest mesh is in the outer portion of the model as shown in Figure 4.2.

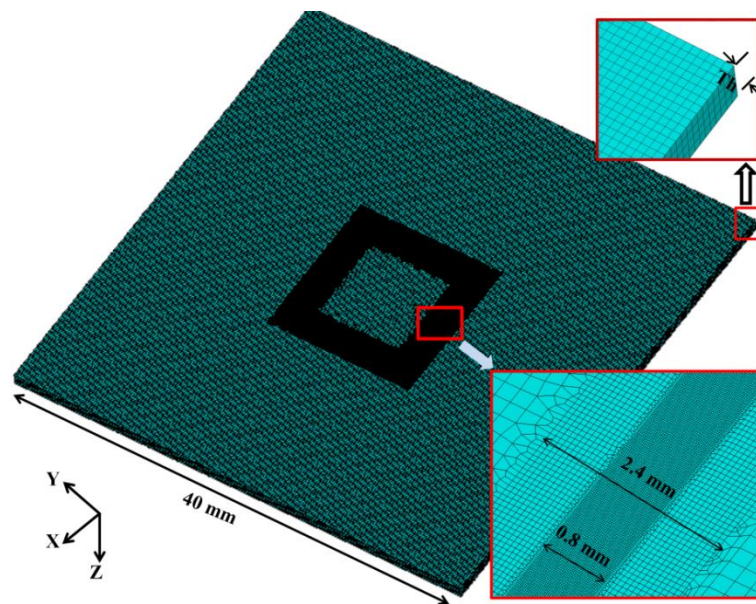
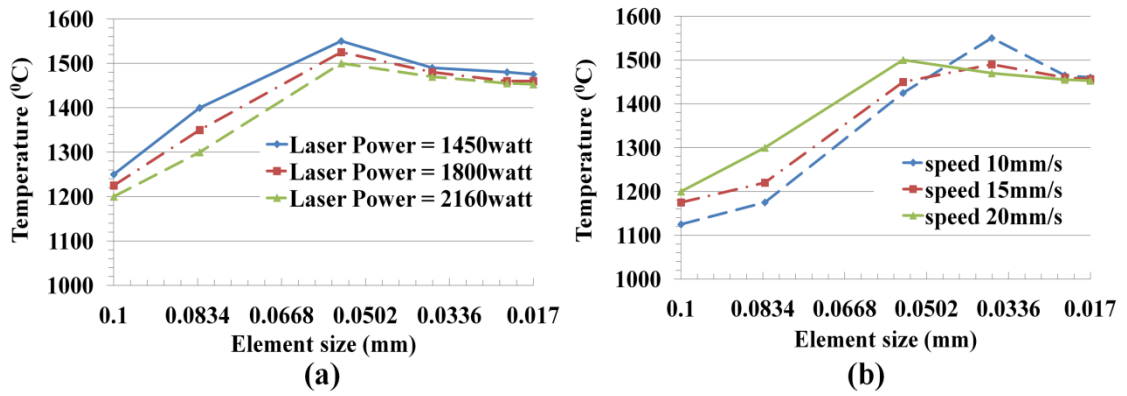


Figure 4.2 : FEM model.

### 4.3.4 Mesh density analysis

Mesh density sensitivity is investigated to select the appropriate element size. Six element densities (X-Y) are investigated; 0.1mm x 0.1mm, 0.083mm x 0.083mm, 0.055mm x 0.055mm, 0.037mm x 0.037mm, 0.022mm x 0.022mm and 0.017mm x 0.017mm for both thickness (1mm & 3mm). Each time the cutting edge temperature after the cutting is investigated and illustrated in Figure 4.3 and 4.4.



**Figure 4.3 : Mesh convergence parametric study for 1mm thickness (a) at cutting speed 20mm/s, (b) at laser power 2160watt.**

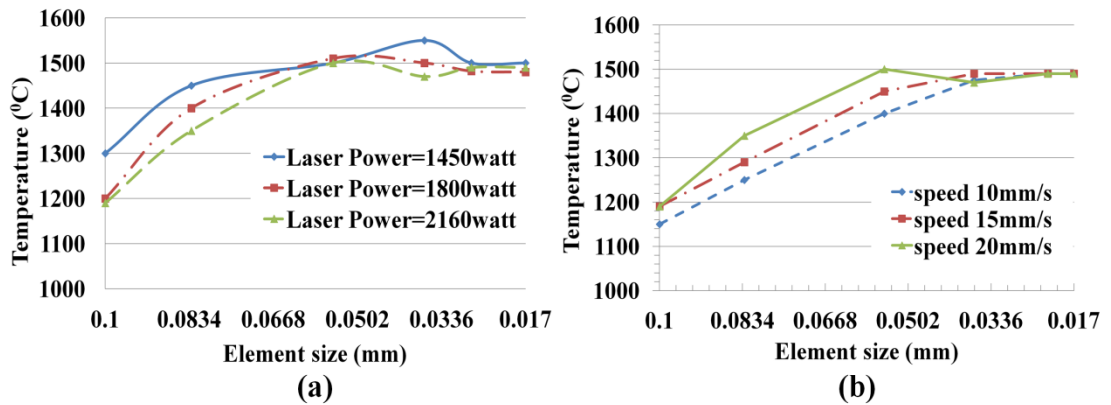


**Figure 4.4 : Mesh convergence parametric study for 3mm thickness (a) at cutting speed 20mm/s, (b) at laser power 2160watt.**

It is found that while the element size is 0.022mm x 0.022mm the model is showing reasonable accuracy at different cutting parameters. Therefore, the element size 0.022mm x 0.022mm (X-Y) is used in simulation to balance the computational time and accuracy.

In present study it is considered that the laser beam is circular and Gaussian in nature. More over the focused area of research is on laser blanking i.e the remaining part of workpiece after laser cutting. Thus half of the laser beam is considered and the proposed model is revised as shown in Figure 4.5.

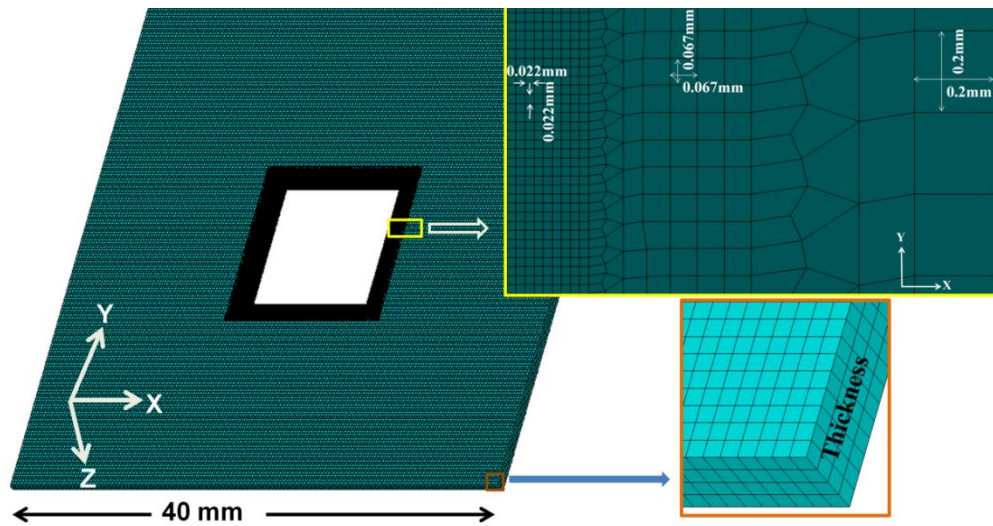


**Figure 4.5 : FEM model development and mesh management considering half of laser beam.**

This change of model result a slightly deviated temperature pattern from the model showed in Figure 4.4 by less than 1.50% (average) as shown in Figure 4.6. However, considerable amount of computational time up to two times is saved and elements number is reduced significantly. Thus model showed in Figure 4.5 is considered for further analysis, where the elements and node numbers are 4,09,740 and 4,16,240 respectively. The APDL code of proposed model is described in Appendix A.

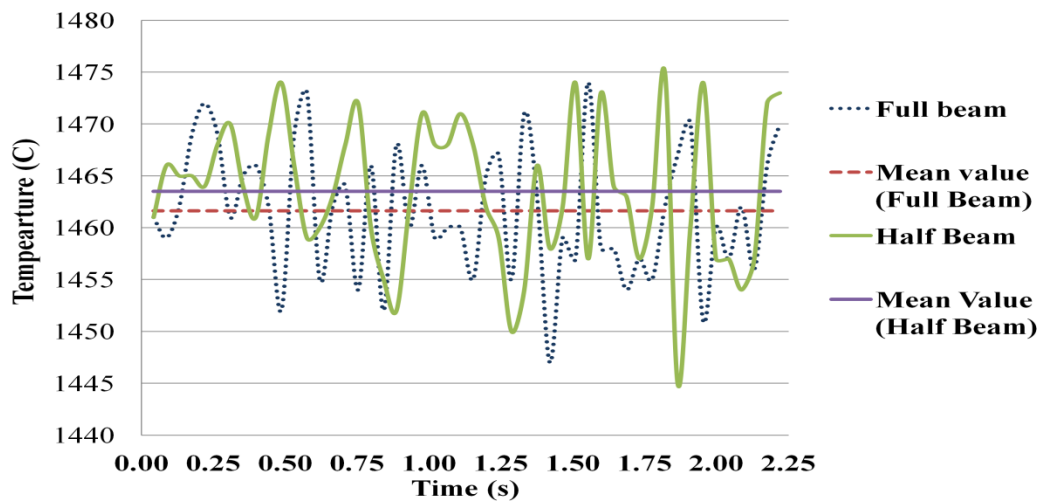


**Figure 4.6 : Maximum temperature along the cutting edge; comparison of results of full beam and half beam.**

#### 4.4 Mathematical description and boundary condition

The proposed thermo-mechanical model is a coupled analysis associated with thermal and structural physics. Where, thermal analysis with appropriate boundary condition is done firstly and later the outcomes of thermal analysis (nodal temperature) are considered as input in structural analysis.

##### 4.4.1 Thermal analysis

For thermal modeling following assumptions are considered:

- (i) The laser beam is focused perpendicularly to the material surface.
- (ii) The nature of laser beam is Gaussian.
- (iii) The plate material is homogeneous.
- (iv) With an appropriate depth of focus, the laser energy density is equal along the thickness of the workpiece.
- (v) The effect of radiation heat loss is negligible compare to conduction and convection heat transfer. Hence radiation heat transfer is not considered.
- (vi) Laser cutting is conducted at atmospheric condition
- (vii) Elements are removed or deactivated, while they reach the melting point.

)URP WKH )RXULHU¶V ODZ WKH PDWKHPDWLFDO PR  
conduction for laser cutting can be written as follows (Yang et al., 2010)

(4.1)

where  $k$ ,  $C_p$ ,  $\rho$  and  $v$  are conductivity, specific heat, density and cutting speed respectively.

The irradiated laser beam is gaussian in nature and incident laser energy is expressed by Equation 4.2.

$$(4.2)$$

where  $I_0$  is laser intensity,  $A$  is absorptivity of stainless steel 304

The value of absorptivity is so complex in nature and relates with the surface roughness, surface temperature, material properties, wavelength of laser beam, amount of incident plasma etc. Researchers found that the value of absorptivity of stainless steel 304 varies from 0.20 to 0.64 (Boyden & Zhang, 2006; C.W. Tan, 2005; Mazumder & Steen, 1988; Steen W. Met al., 2003) In this study for 3D transient FEM model development the average value of absorptivity is considered 0.45.

The experiments are conducted at the atmospheric environment and heat loss is taken place from the free surface of the workpiece by convection. Initial condition is explained by Equation 4.3.

$$T(x,y,z,0) = T_a \quad (4.3)$$

At the top surface air gas  $N_2$  strikes the surface with high pressure and heat loss is expressed by Equation 4.4.

$$(4.4)$$

where  $h$  is force heat transfer coefficient ( $3000 \text{ K}^{-1} \text{ m}^{-2}$ ) (B. Yilbas et al., 1990)

Assuming free convection to atmosphere, the boundary condition at the bottom and lateral surfaces are expressed by Equation 4.5.

$$q_{other} = h_{freeconv}(T_s - T_a) \quad (4.5)$$

where,  $h_{freeconv}$  is heat transfer coefficient at atmospheric condition (  $15\text{WK}^{-1}\text{m}^{-2}$ ) and  $T_s$  is surface temperature.

It is also assumed that any heated point on the material surface is blown away from the workpiece by assist gas as soon as its temperature reaches the melting point. Thus, the cutting is taken place avoiding further increase in temperature beyond the melting point.

#### 4.4.2 Stress analysis

The process of fusion laser cutting is a combination of heating and rapid cooling. This develops temporal variation that initiates thermal stresses. The total strain vector for laser cutting can be expressed as follows:

$$\{\varepsilon\} = \{\varepsilon^{el}\} + \{\varepsilon^{th}\} + \{\varepsilon^{pl}\} \quad (4.6)$$

where  $\{\varepsilon\}$ ,  $\{\varepsilon^{el}\}$ ,  $\{\varepsilon^{th}\}$  and  $\{\varepsilon^{pl}\}$  are total strain vector, elastic strain vector, thermal strain vector and plastic strain vector respectively.

The elastic strain vector is described by the elastic stress-strain relationship expressed as:

$$\{\sigma\} = [D]\{\varepsilon^{el}\} \quad (4.7)$$

In another expression,

$$\{\varepsilon^{el}\} = [D]^{-1}\{\sigma\} \quad (4.8)$$

The compliance matrix,  $[D]^{-1}$  is:  $[D]^{-1} = \begin{bmatrix} 1/E & -\nu/E & 0 \\ -\nu/E & 1/E & 0 \\ 0 & 0 & G \end{bmatrix}$  (4.9)

where  $\{\sigma\}$ ,  $[D]$ ,  $E$ ,  $\nu$  are stress vector, elastic stiffness matrix, Young's modulus (input) and Poisson's ratio (input) respectively.

$$G = \text{shear modulus} = \frac{E}{2(1+\nu)} \quad (4.10)$$

The thermal strain vector is expressed in the following form:

$$\{\varepsilon^{th}\} = \Delta T [\alpha^{se}(T)]^T \quad (4.11)$$

where  $[\alpha^{se}(T)]$  is temperature-dependent scant coefficient of thermal expansion (input) and thermal difference

$$\Delta T = T - T_{ref} \text{ (input)} \quad (4.12)$$

where  $T$  is current temperature at point in question and  $T_{ref}$  is reference temperature.

Plasticity is described as nonlinear stress-strain relationship which is path dependent. The simulation of plasticity is incorporated with yield criteria, flow rule and hardening rule.

The yield criterion is used to predict initial yield expressed as a function of yield stress as shown in Equation 4.13.

$$F(\{\sigma\}) = \sigma_y \quad (4.13)$$

where  $F(\{\sigma\})$  is yield function and  $\sigma_y$  is yield stress of material. In this study the von Mises yield criterion is considered as yield criterion, stated as:

$$\sigma_m = \sqrt{\frac{(\sigma_1 - \sigma_2)^2 + (\sigma_2 - \sigma_3)^2 + (\sigma_1 - \sigma_3)^2}{2}} \quad (4.14)$$

where,  $\sigma_1, \sigma_2, \sigma_3$  are the three principal stresses.

The flow rule describes the direction of plastic strain, which can be expressed by Equation 4.15

$$\{d\varepsilon^{pl}\} = \left\{ \frac{\partial Q}{\partial \sigma} \right\} d\lambda \quad (4.15)$$

where  $Q$  is plastic potential (function of stress) and  $d\lambda$  is plastic multiplier.

The hardening rule describes the shape changing phenomenon of surface due to plastic deformation. Generally two types of hardening rules are used for analysis: isotropic hardening and kinematic hardening.

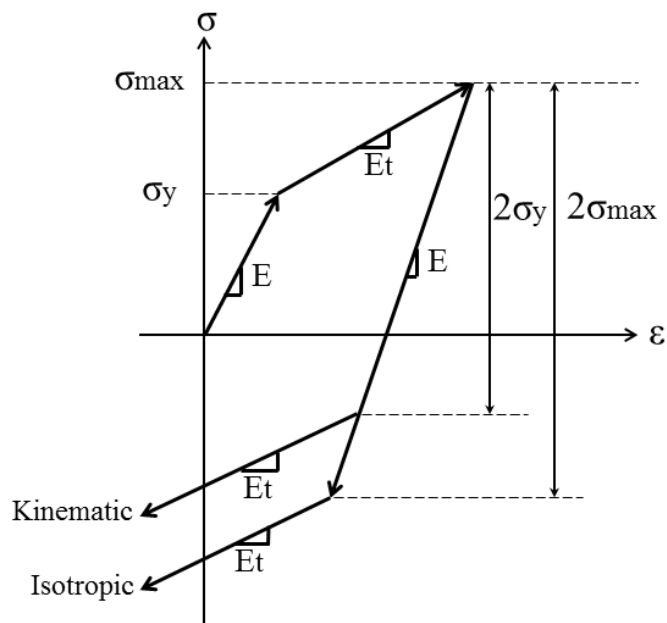


**Figure 4.7 : Kinematic and isotropic hardening rule.**

In this analysis isotropic hardening rules is considered where the elastic range is expanded from the initial value  $2\sigma_y$  to the value  $2\sigma_{max}$  after reaching  $\sigma_{max}$ .

#### 4.5 Heat flux input

Gaussian heat flux is formulated by using ANSYS APDL programming language. The intensity of heat flux is calculated by using Equation 4.2. Elements inside the laser beam are selected and heat flux is imposed on element face by using “SFE” command. The movement of the laser beam is simulated by using multiple load steps and local coordinate is used to define the laser beam. As shown in Figure 4.7, the local coordinates (for example, LS1, LS2, LS3, LS4, LS5, LS6, and LS7) are defined along the laser path as labeled steps first, then at every step the center of the laser beam is defined at the center of the local coordinate and the heat flux is imposed on the elements surface under the area of laser beam (illustrated line circle). In order to ensure convergence, the heat fluxes are imposed by small increments using \*DO loop command.

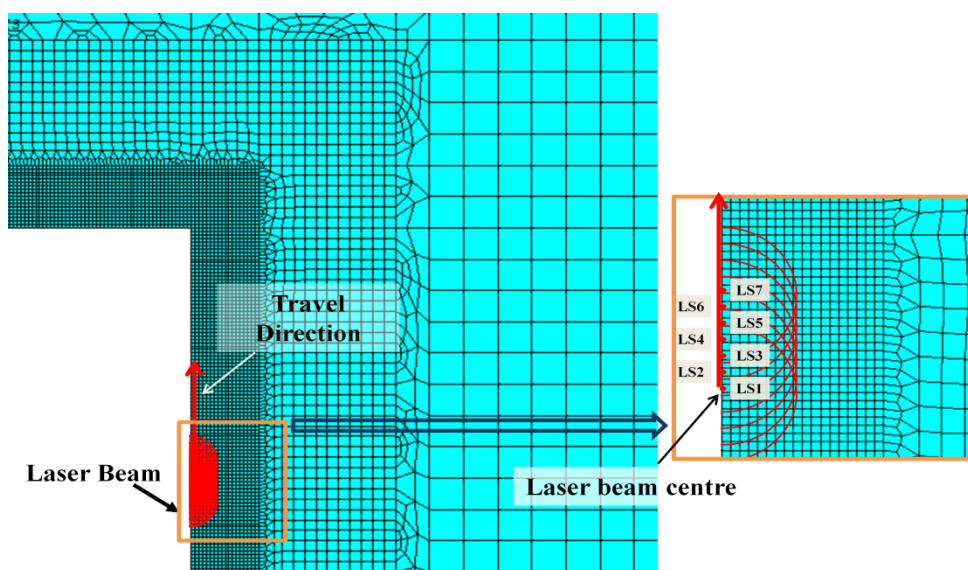


Figure 4.8 : (a) Heat flux position & (b) Local co-ordinate system.

#### 4.6 Simulation of material removal

The penetration speed of laser beam is calculated from a lumped heat capacity calculation considering energy balance of removed material (Steen W. Met al., 2003)

Figure 4.9 : (a) Cylinder with diameter  $d$ . (b) model to determine cutting speed  
(Nyon et al., 2012)

The energy required to melt a mass of a material in a cubelement (Figure 4.8) at atmospheric temperature can be expressed as (Rasovanovie, 2006)

$$(4.13)$$

where  $E_m$  is energy require for melting in Joule,  $d$  is laser beam diameter in meter,  $\rho$  is material density  $\text{kgm}^{-3}$ ,  $v_m$  is penetration speed in  $\text{ms}^{-1}$ ,  $t$  is time in second,  $C_s$  is specific heat capacity of solid in  $\text{kg}^{-1}\text{K}^{-1}$ ,  $T_m$  is melting temperature in  $^{\circ}\text{C}$ ,  $T_{\text{amb}}$  is atmospheric temperature  $^{\circ}\text{C}$  and  $L_f$  is latent heat of fusion in  $\text{kg}^{-1}$ .

Thus the required laser power to melt the material is expressed by:

$$(4.14)$$

Therefore, the volume removed per second per unit area (melting speed) is expressed by:

(4.15)

The process of material removal during laser cutting is simulated by using element death technique, existing in ANSYS. In this technique, after ending every time step the elements temperature are tested and those elements whose temperature cross the melting temperature (1450°C) are selected and deactivated by using EKILL command (i.e., making selected elements insignificant by changing the conductivity about to zero) . Hence, the cutting edge temperature is remained about to the melting point (1450) of stainless steel 304 during the cutting process.

## CHAPTER 5: RESULTS AND DISCUSSION

### 5.1 Introduction

The outcomes of the research study are discussed in this chapter. At the beginning of the chapter the results of thermal analysis of simulation model are discussed. Later effect of laser parameter (laser power, speed, thickness) on kerf width and HAZ are analyzed and validated by experiment. After that the nature of residual stress and its effect are identified. More over the percentage of contribution of laser parameters in fusion laser cutting of square blanks are measured.

### 5.2 Thermal analysis

The analyses are conducted on some significant points near the cutting edge as shown in Figure 5.1. It is considered that the cutting starts from point A and completes by following the path A→B→C→D→E→F→G→H→A. Table 5.1 shows the required time of laser beam to reach those point at different cutting speed. TC-1, TC-2, TC-3 and TC-4 are thermocouples location.

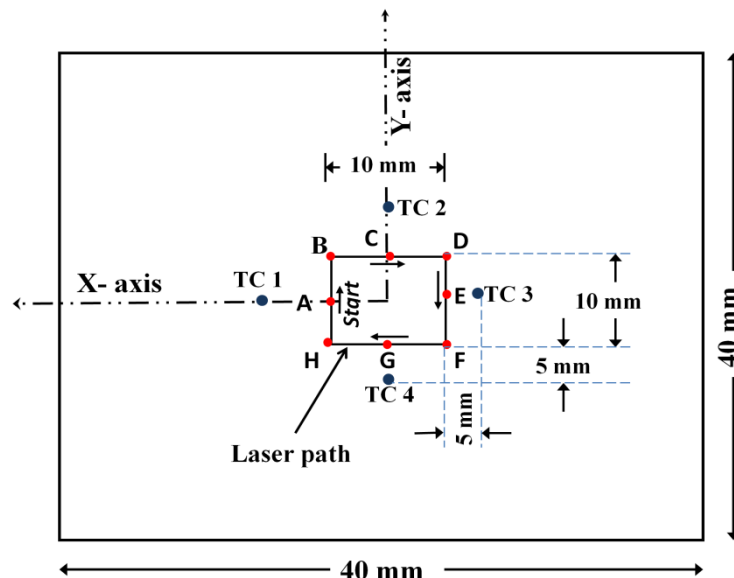


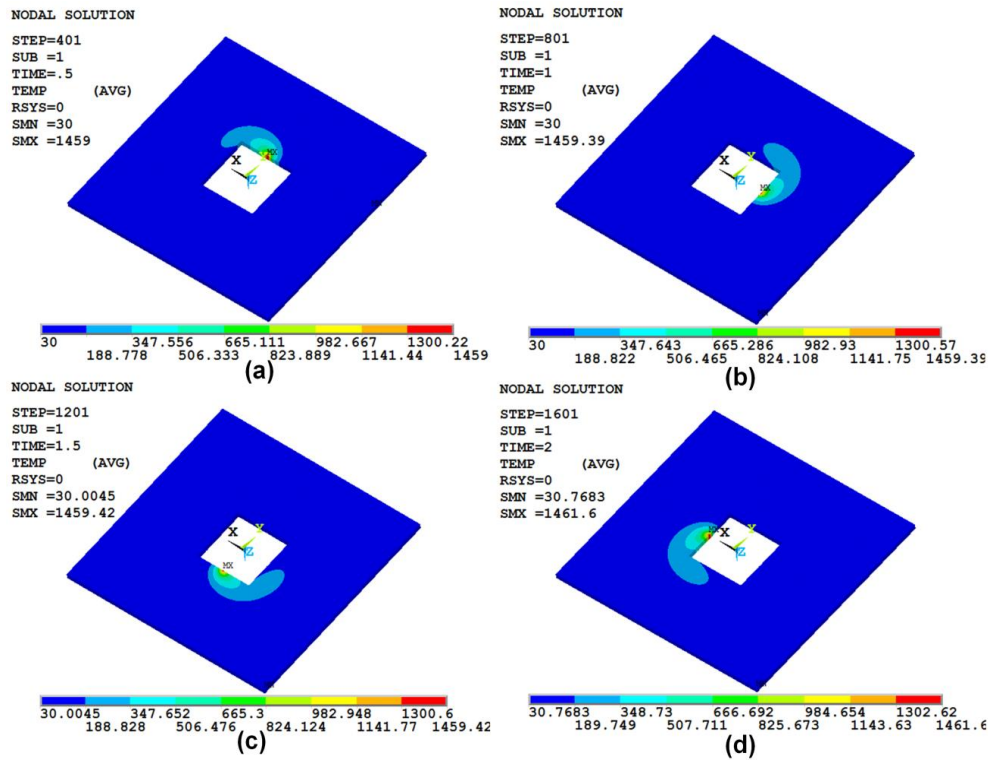
Figure 5.1 : Significant points and location in proposed model.

Table 5.1 : Required time for laser beam to reach at specific point

Cutting speed (mm/sec)	Required time for laser beam to reach the significant point (sec)							
	B	C	D	E	F	G	H	A
20	0.25	0.50	0.75	1.00	1.25	1.50	1.75	2.00
15	0.3333	0.6667	1.00	1.3333	1.6667	2.00	2.3333	2.6667
10	0.50	1.00	1.50	2.00	2.50	3.00	3.50	4.00

### 5.2.1 Thermal distribution

Maximum laser power with minimum cutting speed generates higher heat. Oppositely minimum laser power with maximum cutting speed generates lower heat. If we explain the thermal effect of higher heat and lower heat then all combination in between them can be understood. Thus in this study maximum laser power 2160 watt with minimum cutting speed 10 mm/sec and minimum laser power 1440 watt with maximum cutting speed 20 mm/sec are used to explain the thermal effects. temperature profile of simulated models is shown in Figure 5.2 and 5.3, while the laser beam moves in clockwise direction and reaches at the point A,B,C,D,E,F,G,H at different time. Both the figure shows that at any position of the laser beam maximum temperature along the cutting edge is about the melting temperature (1450) of stainless steel 304.



**Figure 5.2 : Temperature profile at different time (a) at 0.50s, (b) 1.00s , (c) 1.50s, (d) 2.00s ; laser power 1440watt, speed 20mm/s, thickness of workpiece 1mm.**

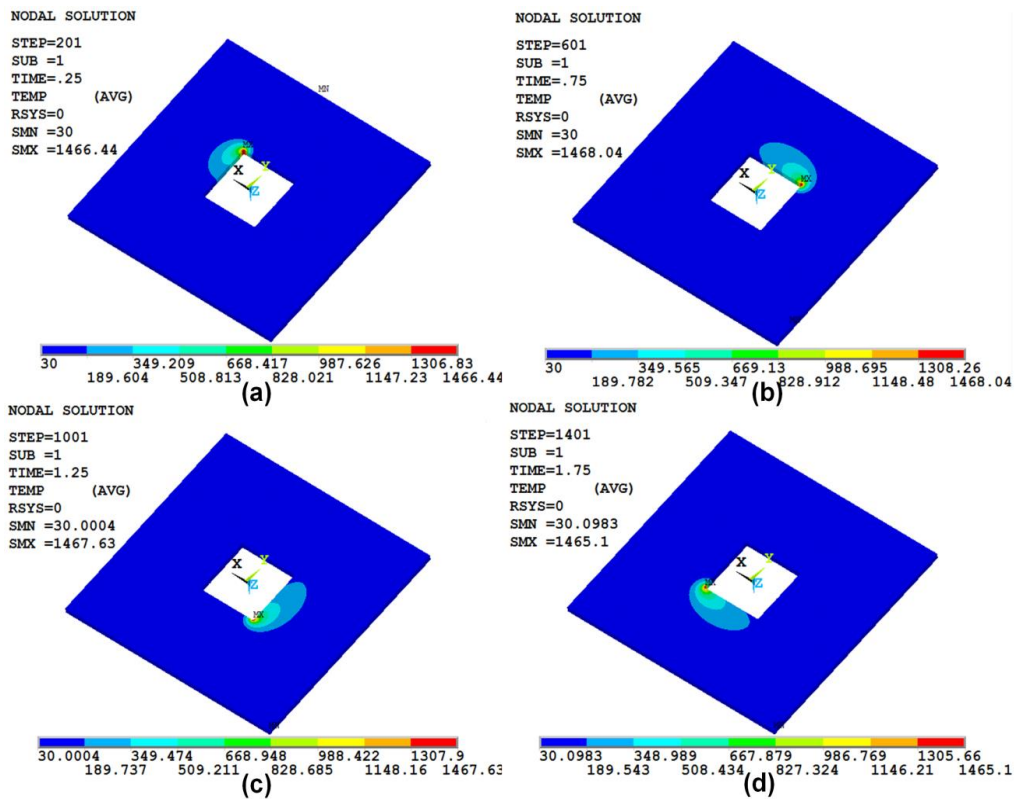


**Figure 5.3 : Temperature profile at different time (a) at 0.25 s, (b) 0.75 s , (c) 1.25 s, (d) 1.75s ; laser power 1440watt, speed 20mm/s, thickness of workpiece 1mm.**

The heat flux is focused on the selected element's surfaces located under the beam area and heated. After each time step the elements which reach the melting temperature of stainless steel-304 (1450<sup>0</sup>C) are selected and deactivated by using EKILL command. As mentioned earlier the element type of thermal analysis is SOLID70, 8 noded brick element and element temperature is average temperature of associated nodes. Thus, after material removal or element deactivation, the temperature of remaining elements (LIVE elements) along the cut kerf are found about 1450 <sup>0</sup>C. Figure 5.4 and Figure 5.5 show the change of nodal temperature with time along the cut kerf at different beam location A,B,C,D,E,F,G & H (as shown in Figure 5.1) with time. At every condition it shows that the nodal temperature at the cutting edge increases sharply first then with the laser beam forward movement it goes down rapidly first then gradually due to heat loss. Moreover, the rise and fall of temperature becomes sharper with the increase of cutting speed.

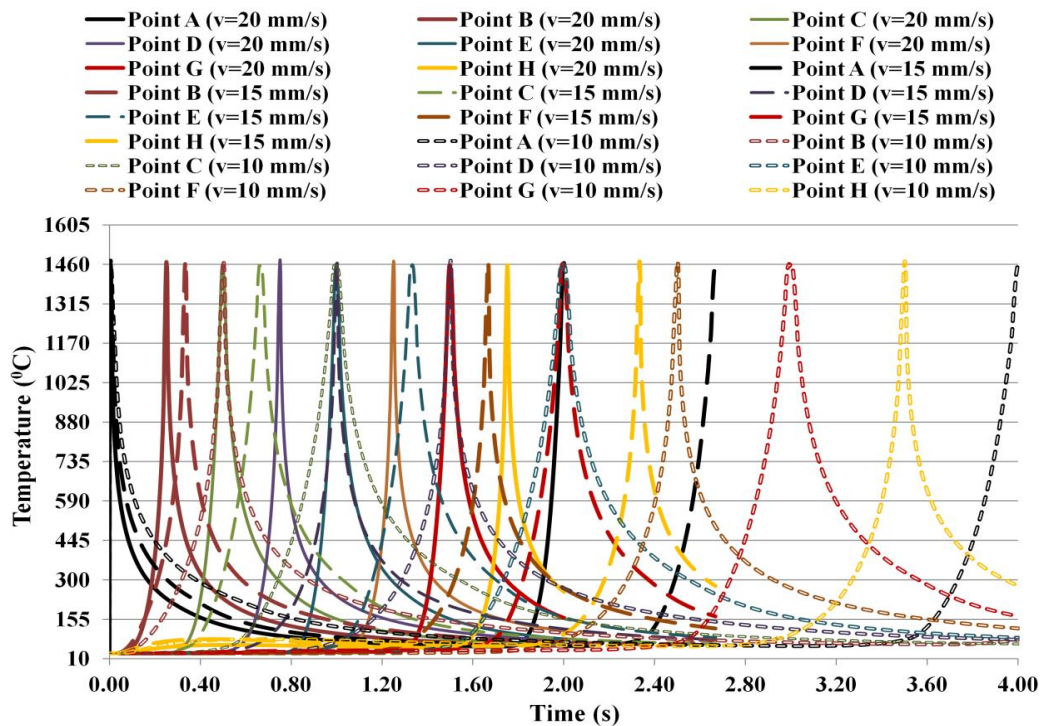


**Figure 5.4 : Time dependent temperature graph at different point along the cutting edge; laser power 2160watt; thickness 1mm.**

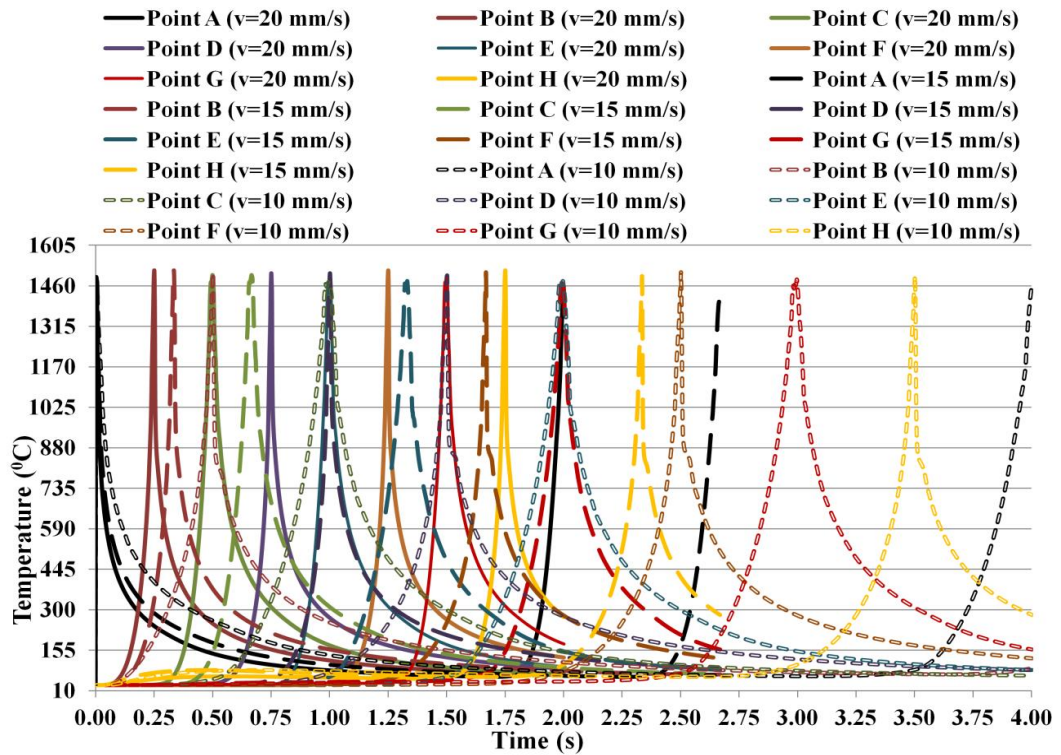


**Figure 5.5 : Time dependent temperature graph at different point along the cutting edge; laser power 2160watt; thickness 3mm.**

Figure 5.6 and 5.7 represent the temperature distribution along the X-axis and Y-axis while the laser beam is at point A, C, E and G respectively. The laser power is 2160watt having material thickness of 1mm and 3mm; cutting speeds are 10mm/sec and 20mm/sec. It shows that maximum temperature is generated at the cutting edge and it goes down rapidly first then gradually with the increase of distance from the laser center due conduction heat transfer. Same phenomenon is observed in other experiments.

Figure 5.6: (a) Temperature distribution along X-axis ; heat source at point E and A, (b) Temperature distribution along Y-axis ; heat source at point G and C; Laser power 2160watt, thickness 1mm.

Figure 5.7 : (a) Temperature distribution along X-axis ; heat source at point E and A, (b) Temperature distribution along Y-axis ; heat source at point G and C; Laser power 2160watt, thickness 3mm.

### 5.3 Heat affected zone (HAZ) analysis

Width of HAZ is measured at four specific point A, C, E and G (Figure 5.1) and average of those values are considered as width of HAZ. The details of experimental results of width of HAZ are shown in Appendix C and D.

### 5.3.1 Comparison of simulation and experimental results

The comparison of width of HAZ of simulation model and experimental outcome is represented in Figure 5.8 while the laser power is 2160watt, cutting speed is 10mm/sec and material thickness is 3mm. It is found that the experimental value of width of HAZ is little bit higher than the simulation results (1.10mm for experiment, 1.02mm for simulation) due to selection of element size. If the model is meshed by finer elements then the gap between experiment and simulation can be reduced to zero.

Figure 5.8 : Comparison of width HAZ in experiment and simulation; Laser power 2160watt, cutting speed 10mm/sec, thickness 3mm.

In this study total 18 experiments are conducted. The details of experimental and simulation outcomes of width of HAZ and their relative error are listed in Appendix C. It shows that for 1mm thick workpiece the average relative error is found 3.15% and for 3mm thickness it is 4.75%. This indicates that the outcomes of simulation have shown good agreement with experimental results. Figure 5.9 and Figure 5.10 show the graphical comparison between experimental and simulation results of width of HAZ.

Figure 5.9 : Width of HAZ for 1mm thick stainless steel304 sheet.

Figure 5.10 : Width of HAZ for 3mm thick stainless steel304 sheet.

### 5.3.2 Parametric study of width of HAZ

A parametric study is done to understand the effects of laser power and cutting speed on width of HAZ formation. It shows that the width of HAZ increases with the increase of laser power due to high beam intensity (Figure 5.11).

On the other hand with the increase of cutting speed the width of HAZ decreases (Figure 5.12). Because, laser ~~and~~ interaction time reduces with the increase of cutting speed, that narrowing the heat propagation as well as width of HAZ.

Figure 5.11 : Effect of laser power on width of HAZ; (a) for 1mm thickness, (b) for 3mm thickness.

Figure 5.12 : Effect of cutting speed on width of HAZ; (a) for 1mm thickness, (b) for 3mm thickness.

It is observed that width of HAZ becomes more at higher laser power (2160 watt), lower cutting speed (10mm/sec) and for thick workpiece (3mm). Maximum HAZ experiment and simulation are found about 1.01mm and 0.98 mm respectively. While the laser power, cutting speed and workpiece thickness are 2160 watt, 10mm/sec and 3mm respectively. On the other hand, the smallest width of HAZ in experiment and simulation are recorded 0.68mm and 0.62mm. While the laser power, cutting speed and workpiece thickness are 1440 watt, 20mm/sec and 1mm respectively. Because, laser cutting with higher laser power and lower cutting speed increases laser interaction time. Moreover, laser penetration time has been increased with material thickness. These may cause higher heat flux and more heat generation. As a result of that the grain refinement, carbide and sulphide formation in the HAZ has been increased.

#### 5.4 Kerf width results

Kerf width is measured at four specific point A, C, E and G (Figure 5.11) and average of those values are considered as kerf width. The details of experimental results of kerf width are listed in Appendix C and D.

##### 5.4.1 Comparison of simulation and experimental results

Figure 5.13 and 5.14 show the graphical comparison between experimental and simulation results of kerf width. It shows that for 1mm thick workpiece the average relative error is found 2.26% and for 3mm thickness it is 3.60%. This indicates that simulation results have good agreement with experimental results.

Figure 5.13 : Kerf -width for 1mm thick stainless steel 304 sheet.

Figure 5.14 : Kerf -width for 3mm thick stainless steel304 sheet.

#### 5.4.2 Parametric study of kerf-width

The effects of laser parameters (laser power, cutting speed) on the kerf width are determined by a parametric study. Figure 5.15 and 5.16 show the effect of laser power and cutting speed on kerf width respectively.

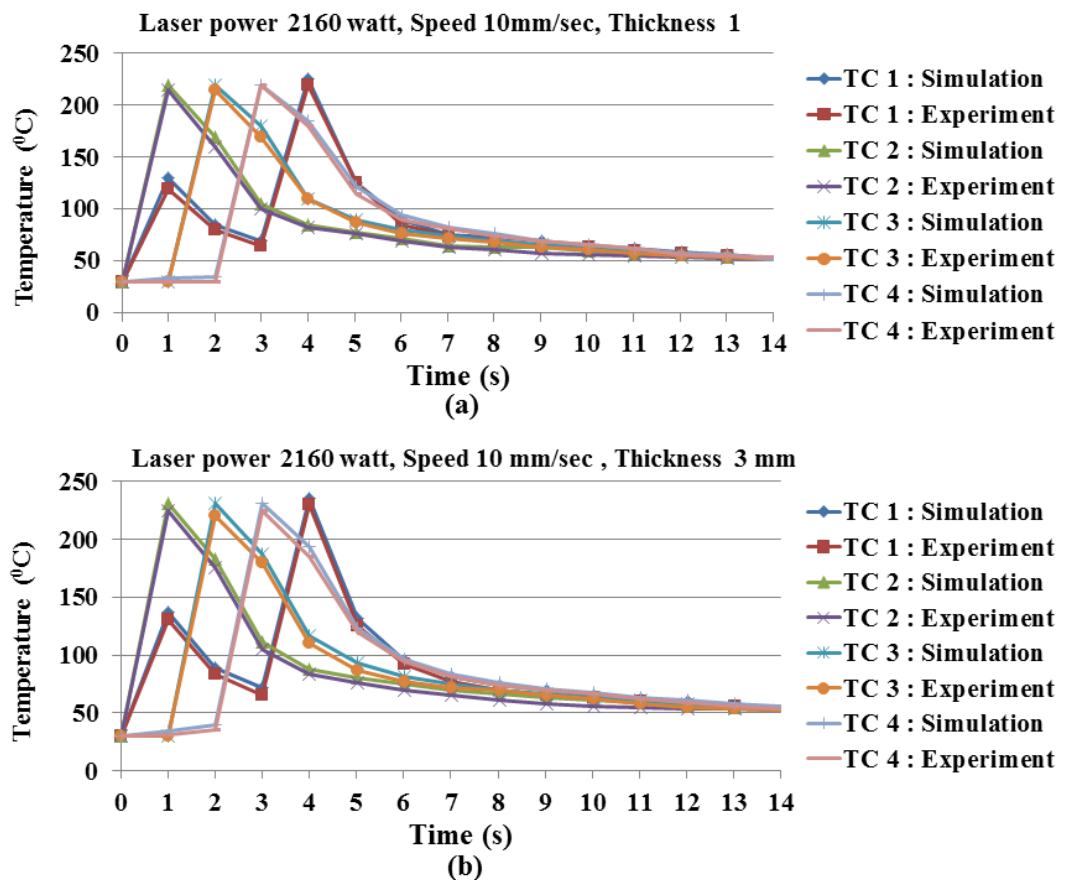
Figure 5.15: Effect of laser power on kerfwidth ; (a) for 1mm thickness, (b) for 3mm thickness.

Figure 5.16: Effect of cutting speed on kerfwidth ; (a) for 1mm thickness, (b) for 3mm thickness.

It shows that the kerf-width increases with the increase of laser power. Because, higher laser power causes higher heat flux intensity, that melts more material and cause wider cut. On the other hand with the increase of cutting speed causes narrower kerf-width.

### 5.5 Model validation for thermal analysis

The validation of the proposed model has been done by comparing the simulation results and experimental results. The surface temperature of the workpiece is recorded by four sets of thermocouples (TC-1, TC-2, TC-3, TC-4) 5mm away from laser path with a four channel data logger during the experiment as illustrated in Figure 5.1. In the simulation, nodal temperatures at the same locations (5mm away from laser path) are measured and compared with the experimental outcomes as shown in Figure 5.17.



**Figure 5.17 : Temperature at different location of thermocouple with time: comparison between the experimental and simulation outcomes.**

Both the experiment and simulation results show good agreement with each other. As the laser starts its cutting from point A, at the beginning the temperature of TC-1 point goes up a little-bit but maximum temperature pick of TC-1 is found near the end of cutting process.

Moreover, the statistical comparison of simulation and experimental results of kerf width and width of HAZ has been done as shown in Figure 5.18 and 5.19. For kerf-width the value of  $R^2$  is 0.96 and goodness of fit 0.9630. For width of HAZ the value of  $R^2$  is 0.95 and goodness of fit 0.923.

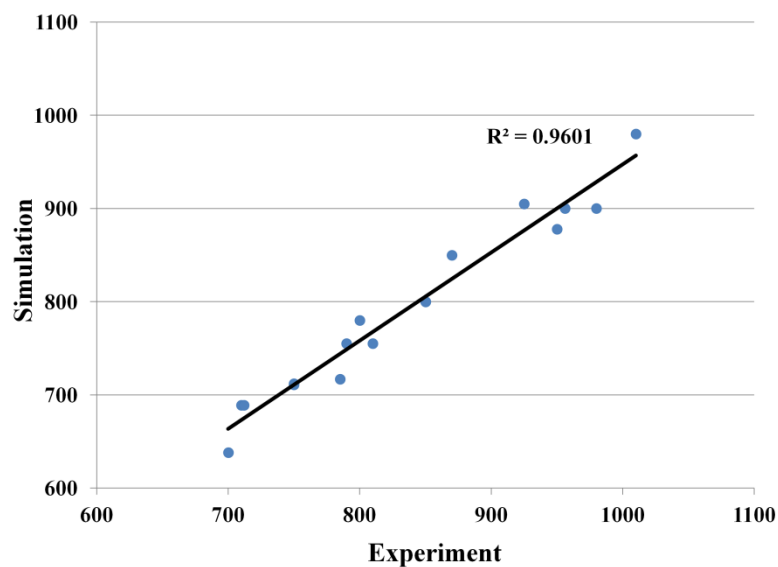


**Figure 5.18 : Correlation between experimental and simulation kerf width.**

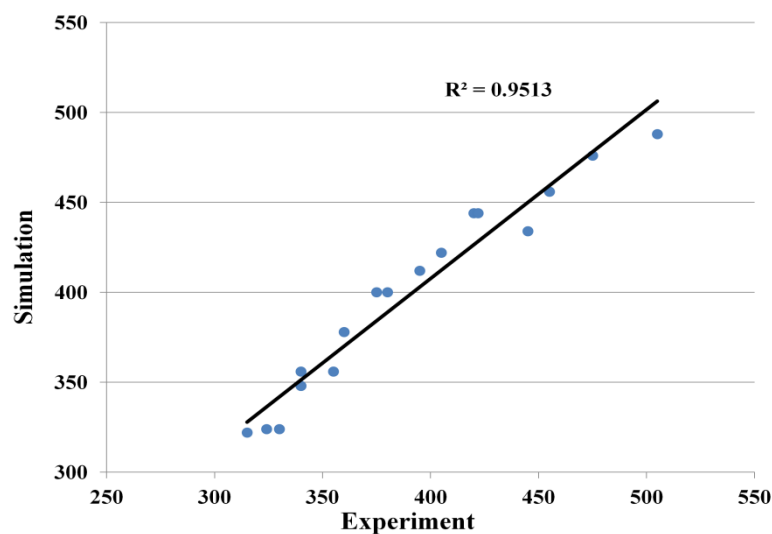


**Figure 5.19 : Correlation between experimental and simulation width of HAZ.**

## 5.6 Analysis of variance

Percentages of contribution of laser parameters (power and speed) for HAZ and kerf width formation are determined by ANOVA analysis. Calculation is done by using Equation 3.4 to 3.13 and detail of calculation is illustrated in Appendix D.

### 5.6.1 Significant parameter for width of HAZ

From the ANOVA analysis, it is observed for width HAZ, laser power is the most significant parameter (72.43% for 1mm thickness and 64.21% for 3mm thickness) as shown in Table 5.2 and 5.3.

Table 5.2 : ANOVA table for width of HAZ (workpiece thickness 1mm)

Factor	Sum of square	DOF	Variance	F ratio	Percentage of contribution
Power	132110.2	2	66055.11	689.93	72.43
Speed	43310.22	2	21655.11	226.18	23.74
Error	6989.11	73	95.74		3.83
Total	182409.60	77			

Table 5.3 : ANOVA table for width of HAZ (workpiece thickness 3mm)

Factor	Sum of square	DOF	Variance	F ratio	Percentage of contribution
Power	137688.89	2	68844.44	712.14	64.21
Speed	69688.89	2	34844.44	360.44	32.50
Error	7057.11	73	96.67		3.29
Total	214434.90	77			

### 5.6.2 Significant parameter for kerf width

ANOVA analyses for kerf width are described in Table 5.4 and 5.5. The results of ANOVA analyses indicate that laser power is the most significant parameter (52.44% for 1mm thickness, 74.67% for 3mm thickness).

Table 5.4 : ANOVA table for kerf -width (workpiece thickness 1mm)

Factor	Sum of square	DOF	Variance	F ratio	Percent of contribution
Power	6818.67	2	3409.33	330.37	52.44
Speed	5432.00	2	2716.00	263.19	41.77
Error	753.33	73	10.32		5.79
Total	13004.00	77			

**Table 5.5 : ANOVA table for kerf-width (workpiece thickness 3mm)**

Factor	Sum of square	DOF	Variance	F ratio	Percent of contribution
Power	48344.89	2	24172.44	1814.59	74.67
Speed	15424.89	2	7712.44	578.96	23.83
Error	972.44	73	13.32		1.50
Total	64742.22	77			

### 5.7 Thermal stress analysis

Figure 5.20 shows the stress distribution of workpiece at different time while the laser power is 2160watt, material thickness 3mm and cutting speed 20mm/sec.

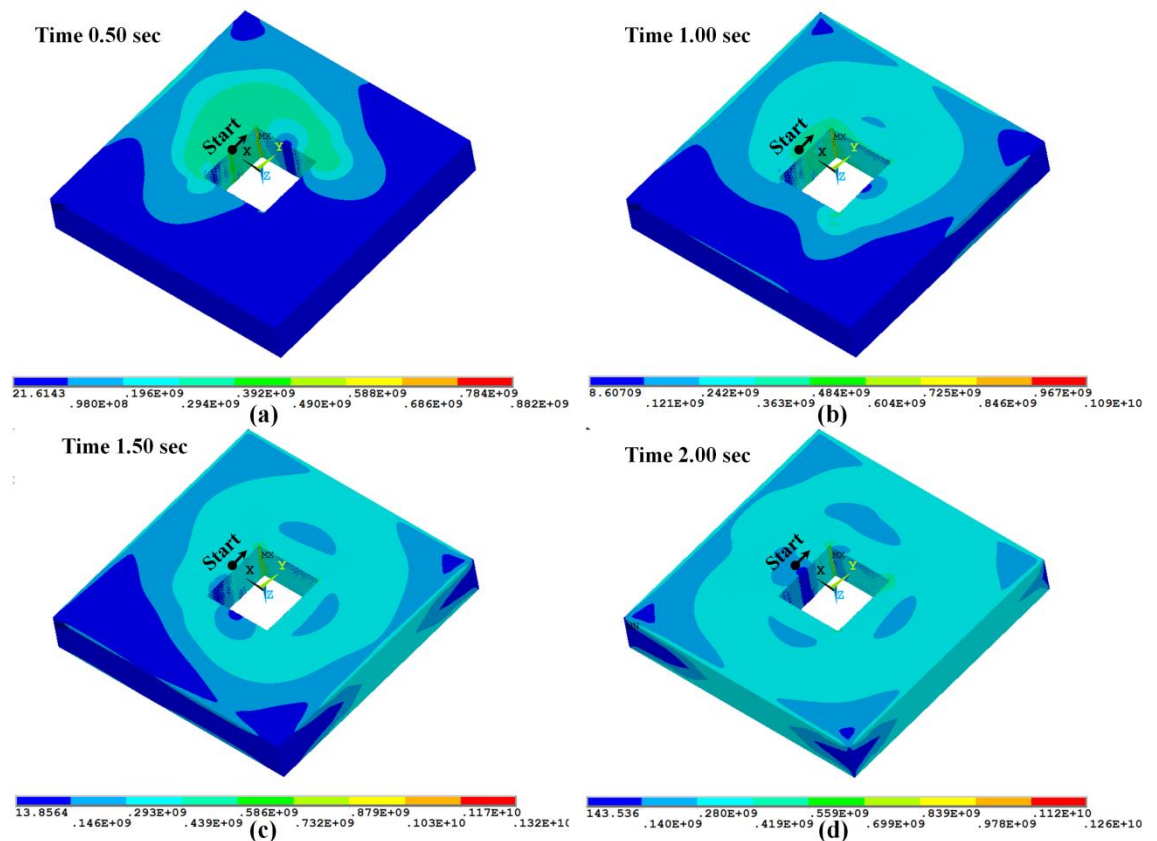


**Figure 5.20 : Von mises stress profile at different time (a) at 0.50s, (b) 1.00s, (c) 1.50s, (d) 2.00s ; laser power 2160W, speed 20mm/s, thickness of workpiece 3mm.**

Temperature distribution along the upper circumference (near the cutting edge) of square blank at the beginning and end of cooling is shown in Figure 5.21. Whereas, Figure 5.22 shows the corresponding von Mises stress distribution. It is noted that at the beginning of cooling the Von-mises stresses attain lower value. It is because of

temperature dependent young's modulus (Table 4.2) considered in simulation, which is lower at the high temperature. Furthermore, the maximum Von-mises stress is developed at the corner of the cutting edge. The reasons are the corner of the cutting edges are fixed and associated with higher temperature, which causes higher thermal expansion.

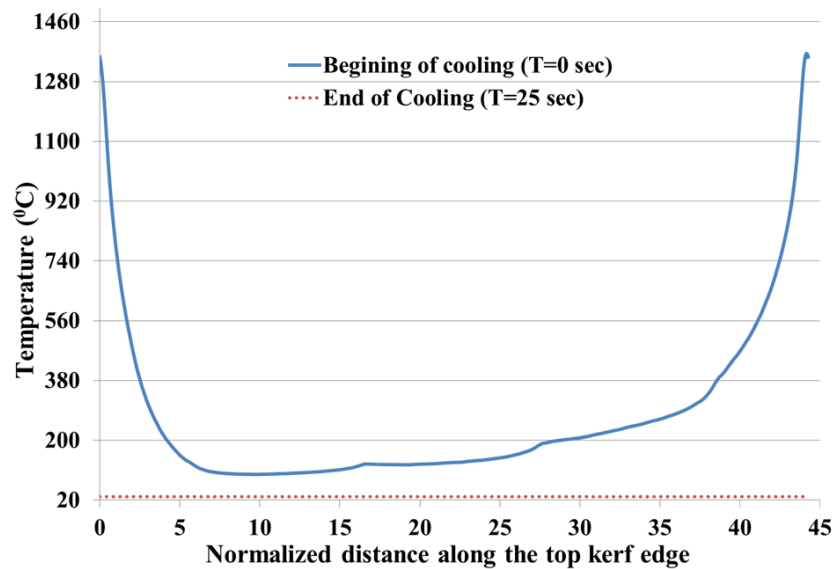


**Figure 5.21 : Temperature distribution along the upper circumference of square blanks (near the cutting edge) ; laser power 2160W, cutting speed 20mm/s, thickness 3mm.**

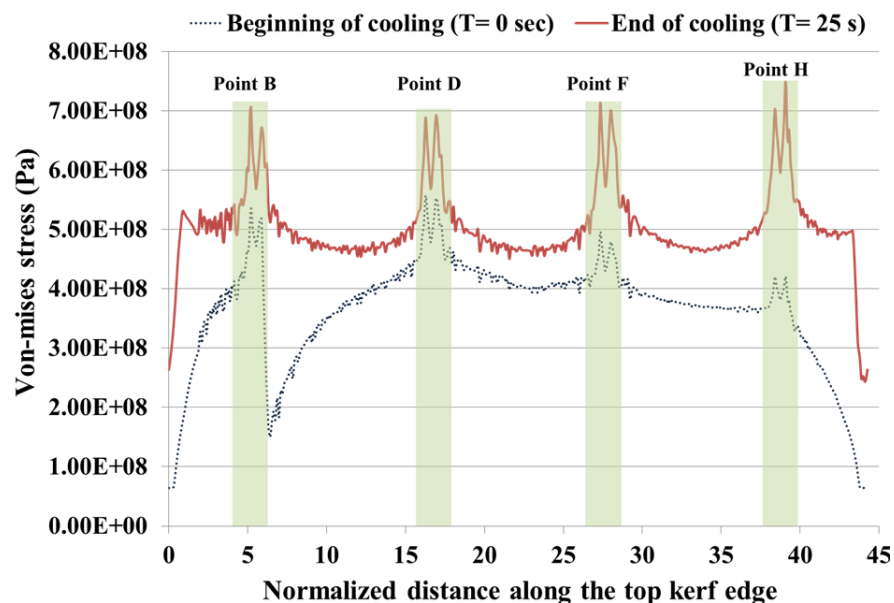


**Figure 5.22 : Von-mises stress distribution along the upper circumference of square blanks (near the cutting edge) ; laser power 2160W, cutting speed 20mm/sec, thickness 3mm.**

As maximum stress is developed at the corner of the square blank and each corner is experienced almost same amount of stress. Hence, one of the corner points (near point-D) and its neighbor points (near point-C and point-E) are considered for further analysis (Figure 5.1). Figure 5.23 and 5.24 shows the temporal variation of Von-mises stress of point C, D, E at different cutting speed.

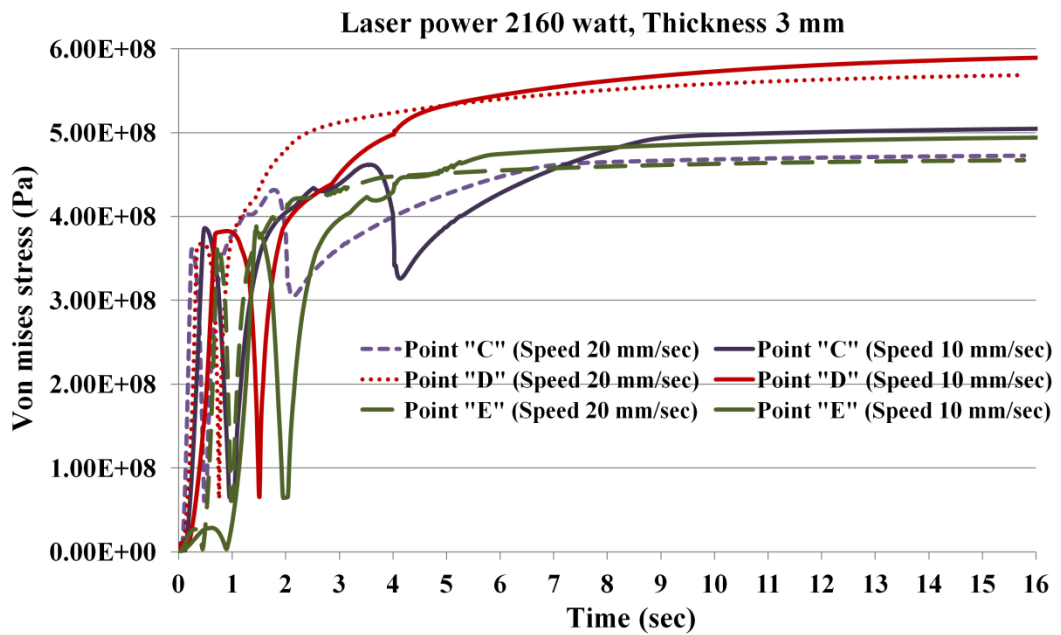


**Figure 5.23 : Temporal variation of Von-mises stress at different speed; laser power 2160W, thickness 3mm.**

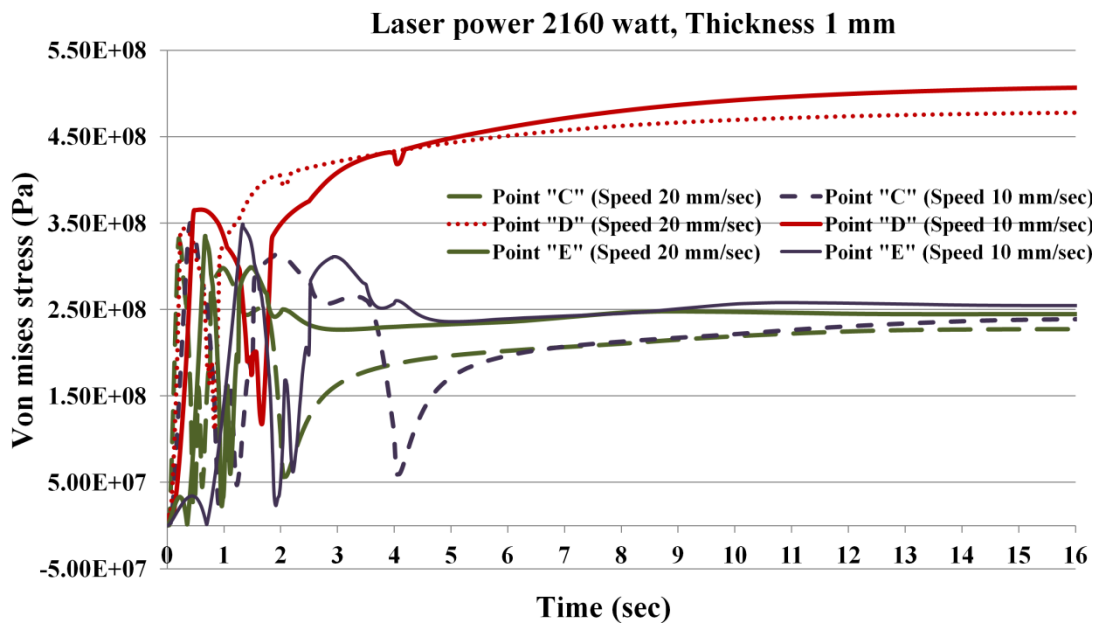


**Figure 5.24 : Temporal variation of Von-mises stress at different speed; laser power 2160W, thickness 1mm.**

It shows that during the cutting period Von-mises stress increases sharply due to rapid decay of temperature after reaching the maximum temperature (Figure 5.4, 5.5). Moreover, the increase of stress is relatively higher for the high cutting speed that corresponding to the lower cutting speed. Furthermore, once the lower temperature is achieved after cooling, the stress level becomes almost steady with time progression; which is called as residual stress. The values of residual stress at point C,D and E are shown in Table 5.6.

**Table 5.6 : Residual stress at point C,D,E**

Material thickness (mm)	Cutting speed (mm/sec)	Residual stress (MPa)			Elastic limit (MPa)
		Point -C	Point -D	Point -E	
1	10	240	510	245	360
1	20	230	480	247	360
3	10	500	590	495	360
3	20	470	565	465	360

The value of residual stress at point D of 1mm thickness workpiece and at points C,D,E are crossed the elastic limit (360MPa) of stainless steel-304. Hence cracks, surface defects are formed at those areas. This is supported by SEM results as shown in Figure 5.25.

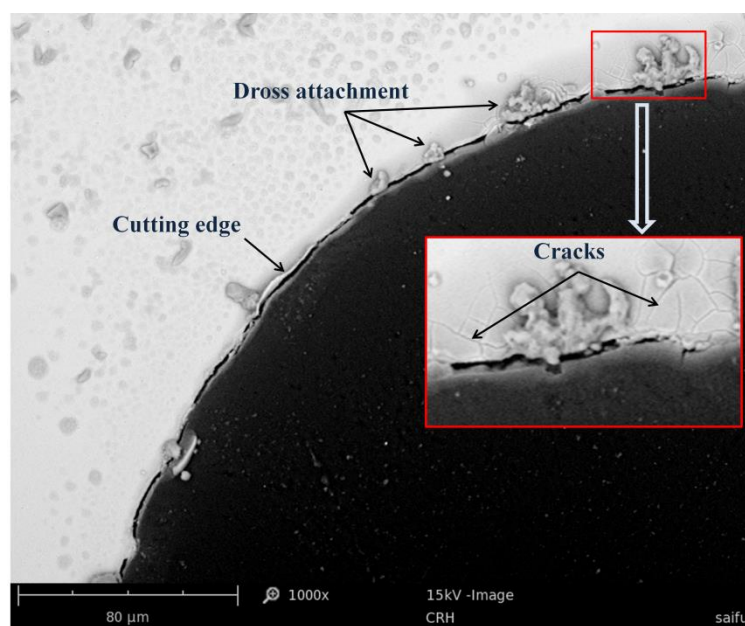


**Figure 5.25 : SEM analysis at cutting edge.**

## CHAPTER 6: CONCLUSIONS AND RECOMENDATION

### 6.1 Conclusions

In this study fusion cutting mechanism in laser blanking of stainless steel 304 is analyzed by finite element simulation with the help of ANSYS and experimentally validated the model. The moving heat source is considered as Gaussian in nature, which is simulated by using ANSYS APDL and element death methodology in ANSYS. Used to remove the molten material from the study following conclusions can be given.

- (i) The simulation and experimental results show that the kerf width increases with an increase in laser power and decreases with increase in cutting speed, which is in good agreement with the theory.
- (ii) From thermal analysis it is observed that the nodal temperature at the cutting edge increases sharply first then with the forward movement of laser beam it goes down rapidly first then gradually due to heat loss. Moreover, the rise and fall of nodal temperature becomes sharper with the increase of cutting speed.
- (iii) The proposed numerical model shows good agreement with experimental results. For kerfwidth the value of  $R^2$  is 0.96 and goodness of fit 0.9630. On the other hand for width of HAZ the value of  $R^2$  is 0.95 and goodness of fit 0.923.
- (iv) Results of ANOVA analysis showed that laser power is the most significant factor for kerfwidth (52.44% for 1mm thickness, 74.67% for 3mm thickness) and HAZ (72.43% for 1mm thickness and 64.21% for 3mm thickness).
- (v) Due to temporal variation maximum stress is developed at the corner of the square blanks, while it crosses the yield limit of stainless steel it may cause surface cracks.

## **6.2 Recommendation for future work**

The results obtained from present study demand for future work to improve the simulation and quality of laser cutting process:

1. Different laser input parameters like assist gas pressure, exothermic reaction of assist gas, molten material flow etc can be incorporated with this numerical model.
2. The effectiveness of the model can be analyzed by cutting different shapes of laser blanking.
3. The proposed model can be used for other metals and non-metals for further analysis.
4. In future mesh free models can be incorporated with FEM for better solution outcomes.

## REFERENCES

- Akhtar, S., Kardas, O. O., Keles, O., & Yilbas, B. S. (2014). Laser cutting of rectangular geometry into aluminum alloy: Effect of cut sizes on thermal stress field. *Optics and Lasers in Engineering*, *61*, 57-66.
- Anderson, M., & Shin, Y. (2006). Laser-assisted machining of an austenitic stainless steel: P550. *Proceedings of the Institution of Mechanical Engineers, Part B: Journal of Engineering Manufacture*, *220*(12), 2055-2067.
- Antony, J. (2014). *Design of experiments for engineers and scientists*: Elsevier.
- Arif, A., Yilbas, B., & Aleem, B. A. (2009). Laser cutting of thick sheet metals: residual stress analysis. *Optics & Laser Technology*, *41*(3), 224-232.
- Bokota, A., & Iskierka, S. (1996). Numerical prediction of the hardened zone in laser treatment of carbon steel. *Acta Materialia*, *44*(2), 445-450. doi: [http://dx.doi.org/10.1016/1359-6454\(95\)00225-1](http://dx.doi.org/10.1016/1359-6454(95)00225-1)
- Boyden, S., & Zhang, Y. (2006). Temperature and wavelength-dependent spectral absorptivities of metallic materials in the infrared. *Journal of thermophysics and heat transfer*, *20*(1), 9-15.
- C.W. Tan, Y. C. C., Leung, N.W. Bernard, Tsun, John, C.K. Alex. (2005). Characterization of Kovar-to-Kovar laser welded joints and its mechanical strength. *Optics and Lasers in Engineering*, *43*, 151-162.
- Cenna, A., & Mathew, P. (2002). Analysis and prediction of laser cutting parameters of fibre reinforced plastics (FRP) composite materials. *International Journal of Machine Tools and Manufacture*, *42*(1), 105-113.
- Chen, S.-L. (1999). The effects of high-pressure assistant-gas flow on high-power CO<sub>2</sub> laser cutting. *Journal of Materials Processing Technology*, *88*(1), 57-66.
- Chryssolouris, G. (1991). *Laser machining - Theory and practice*.
- Di Pietro, P., & Yao, Y. (1995). A new technique to characterize and predict laser cut striations. *International Journal of Machine Tools and Manufacture*, *35*(7), 993-1002.
- Di Pietro, P., & Yao, Y. L. (1995). A numerical investigation into cutting front mobility in CO<sub>2</sub> laser cutting. *International Journal of Machine Tools and Manufacture*, *35*(5), 673-688. doi: [http://dx.doi.org/10.1016/0890-6955\(95\)93037-7](http://dx.doi.org/10.1016/0890-6955(95)93037-7)
- Ding, H., & Shin, Y. C. (2010). Laser-assisted machining of hardened steel parts with surface integrity analysis. *International Journal of Machine Tools and Manufacture*, *50*(1), 106-114. doi: <http://dx.doi.org/10.1016/j.ijmachtools.2009.09.001>
- Duley, W. (2012). *Laser processing and analysis of materials*: Springer Science & Business Media.

- Fowlkes, W. Y., & Creveling, C. M. (1995). Engineering methods for robust product design Addison-Wesley.
- Germain, G., Morel, F., Lebrun, U., & Morel, A. (2007). Machinability and surface integrity for a bearing steel and a titanium alloy in laser assisted machining (optimisation on LAM on two materials). *Lasers in Engineering*, *15*(5), 329.
- Ghany, K. A., & Newishy, M. (2005). Cutting of 1.2 mm thick austenitic stainless steel sheet using pulsed and CW Nd: YAG laser. *Journal of Materials Processing Technology*, *163*(8), 438-447.
- Gould, R. G. (1959). The LASER, light amplification by stimulated emission of radiation. Paper presented at the The Arthur conference on optical pumping, the University of Michigan.
- Herd, R. M., Dover, J. S., & Arndt, K. A. (1997). Basic laser principles. *Dermatologic clinics*, *15*(3), 355-372.
- Higgins, T. V. (1994). Nonlinear optical effects are revolutionizing electronics. *Laser focus world*, *3*(8), 67-74.
- Hossain, A., Hossain, A., Nukman, Y., Hassan, M., Harizam, M., Sifullah, A., & Parandoush, P. (2015). A Fuzzy Logic Based Prediction Model for Kerf Width in Laser Beam Machining. *Materials and Manufacturing Processes*, *30*(1-6), 1-6.
- Huang, Z., & Kim, K.-J. (2007). Review of x-ray free electron laser theory. *Physical Review Special Topics Accelerators and Beams*, *10*(10), 034801.
- Ivarson, A., Powell, J., & Magnusson, C. (1991). The role of oxidation in laser cutting stainless and mild steel. *Journal of laser applications*, *3*(3), 41-45.
- Jamshidi Aval, H., Farzadi, A., Serajzadeh, S., & Kokabi, A. H. (2009). Theoretical and experimental study of microstructures and weld pool geometry during GTAW of 304 stainless steel. *The International Journal of Advanced Manufacturing Technology*, *42*(11-12), 1043-1051. doi: 10.1007/s00170-008-1663-6
- Jiang, C., Lau, W., Yue, T., & Chiang, L. (1993). On the maximum depth and profile of cut in pulsed Nd: YAG laser machining. *CIRP Annals/Manufacturing Technology*, *42*(1), 223-226.
- Kaebnick, H., Bicleanu, D., & Brandt, M. (1999). Theoretical and experimental investigation of pulsed laser cutting. *CIRP Annals/Manufacturing Technology*, *48*(1), 163-166.
- Kaplan, A. F. (1996). An analytical model of metal cutting with a laser beam. *Journal of Applied Physics*, *79*(5), 2198-2208.
- Khan, O. U., & Yilbas, B. (2004). Laser heating of sheet metal and thermal stress development. *Journal of Materials Processing Technology*, *156*(1-3), 45-2050.
- Kheloufi, K., & Amara, E. H. (2012). Numerical Investigation of the Effect of Some Parameters on Temperature Field and Kerf Width in Laser Cutting Process.

- Kim, M. J. (2000). Transient evaporative laser-cutting with boundary element method. *Applied Mathematical Modelling*, 25(1), 25-39. doi:  
[http://dx.doi.org/10.1016/S0307-904X\(00\)00034-2](http://dx.doi.org/10.1016/S0307-904X(00)00034-2)
- Kim, M. J. (2004). Transient evaporative laser cutting with moving laser by boundary element method. *Applied Mathematical Modelling*, 28(10), 891-910. doi:  
<http://dx.doi.org/10.1016/j.apm.2004.03.001>
- Kim, M. J., & Zhang, J. (2001). Finite element analysis of evaporative cutting with a moving high energy pulsed laser. *Applied Mathematical Modelling*, 25(3), 203-220. doi: [http://dx.doi.org/10.1016/S0307-904X\(00\)00049-4](http://dx.doi.org/10.1016/S0307-904X(00)00049-4)
- Kou, S., Sun, D., & Le, Y. (1983). A fundamental study of laser transformation hardening. *Metallurgical Transactions A*, 14(3), 643-653.
- Lamikiz, A., Lacalle, L. N. L. d., Sánchez, J. A., Pozo, D. d., Etayo, J. M., & López, J. M. (2005). CO2 laser cutting of advanced high strength steels (AHSS). *Applied Surface Science*, 242(3-4), 362-368. doi:  
<http://dx.doi.org/10.1016/j.apsusc.2004.08.039>
- Lee, H. T., & Chen, C. T. (2011). Numerical and Experimental Investigation into Effect of Temperature Field on Sensitization of AISI 304 in Butt Welds Fabricated by Gas Tungsten Arc Welding. *Materials transactions*, 52(7), 1506-1514.
- Lumley, R. (1969). Controlled separation of brittle materials using a laser. *American Ceramic Society Bulletin*, 48(9), 850-&.
- Madić, M. J., & Radovanović, M. R. (2012). Analysis of the heat affected zone in CO2 laser cutting of stainless steel. *Thermal Science*, 16(suppl. 2), 363-373.
- Mahrle, A., Lütke, M., & Beyer, E. (2010). Fibre laser cutting: beam absorption characteristics and gas-free remote cutting. *Proceedings of the Institution of Mechanical Engineers, Part C: Journal of Mechanical Engineering Science*, 224(5), 1007-1018.
- Majumdar, J. D., & Manna, I. (2003). Laser processing of materials. *Sadhana*, 28(3-4), 495-562.
- Man, H., Duan, J., & Yue, T. (1998). Dynamic characteristics of gas jets from subsonic and supersonic nozzles for high pressure gas laser cutting. *Optics & Laser Technology*, 30(8), 497-509.
- Masumoto, I., Shinoda, T., & Hirate, T. (1990). Weld Decay Recovery by Laser Beam Surfacing of Austenitic Stainless Steel Welded Joints. *Transactions of the Japan Welding Society*, 21(1), 11-17.
- Mazumder, J., & Steen, W. (1980). Heat transfer model for CW laser material processing. *Journal of Applied Physics*, 51(2), 941-947.

- Mercelis, P., & Kruth, J.P. (2006). Residual stresses in selective laser sintering and selective laser melting. *Rapid Prototyping Journal*, 12(5), 254-265.
- Modest, M., & Abakians, H. (1986). Evaporative cutting of a semi-infinite body with a moving CW laser. *Journal of Heat Transfer*, 108, 602-607.
- Modest, M. F. (1996). Three-dimensional, transient model for laser machining of ablating/decomposing materials. *International Journal of Heat and Mass Transfer*, 39(2), 221-234. doi:[http://dx.doi.org/10.1016/0017-9310\(95\)00134-J](http://dx.doi.org/10.1016/0017-9310(95)00134-J)
- Nukman, Y., Hassan, M., & Harizam, M. (2013). Optimization of Prediction Error in CO2 Laser Cutting process by Taguchi Artificial Neural Network Hybrid with Genetic algorithm. *Appl. Math*, 7(1), 363-370.
- Nyon, K., Nyeoh, C., Mokhtar, M., & Abdulrahman, R. (2012). Finite element analysis of laser inert gas cutting on Inconel 718. *The International Journal of Advanced Manufacturing Technology*, 60(12), 995-1007.
- Pandey, A. K., & Dubey, A. K. (2012). Taguchi based fuzzy logic optimization of multiple quality characteristics in laser cutting of Duralumin sheet. *Optics and Lasers in Engineering*, 50, 328-335.
- Pantelis, D., & Vonatsos, K. (1998). Development and experimental validation of analytical thermal models for the evaluation of the depth of laser-affected zones. *Applied Physics A: Materials Science & Processing*, 46, 435-439.
- Parandoush, P., & Hossain, A. (2011). A review of modeling and simulation of laser beam machining. *International Journal of Machine Tools and Manufacture*, 85, 135-145.
- Patel, C. K. N. (1964). Continuous Wave Laser Action on Vibrational Rotational Transitions of  $\text{CO}_2$ . *Physical Review*, 135(A), A1187-A1193.
- Petru, J., Zlamal, T., Cep, R., Monkova, K., & Monka, P. (2013). Influence of cutting parameters on heat-affected zone after laser cutting. *Journal of Thermal Analysis and Calorimetry*, 112, 225-230.
- Pietro, P. D., Yao, Y. L., & Jeromin, A. (2000). Quality optimisation for laser machining under transient conditions. *Journal of Materials Processing Technology*, 97(1-3), 158-167. doi: [http://dx.doi.org/10.1016/S0924-0136\(99\)00376-3](http://dx.doi.org/10.1016/S0924-0136(99)00376-3)
- Poprawe, R., & König, W. (2001). Modeling, monitoring and control in high quality laser cutting. *CIRP Annals - Manufacturing Technology*, 50, 137-140.
- Powell, J. (1993). *CO2 laser cutting* (Vol. 214): Cambridge Univ Press.
- Powell, J. (1998). *CO2 laser cutting*: Springer-Verlag, Berlin, Germany.

- Prusa, J. M., Venkitachalam, G., & Molian, P. A. (1999). Estimation of heat conduction losses in laser cutting. *International Journal of Machine Tools and Manufacture*, 39(3), 431-458. doi:http://dx.doi.org/10.1016/S0890-55(98)00044-8
- Radovanovic, M. (2006). Some possibilities for determining cutting data when using laser cutting. *Strojniski Vestnik*, 52(10), 645-652.
- Radu, M., & Cristea, I. (2013). Processing metal sheets by SPIF and analysis of parts quality. *Materials and Manufacturing Processes*, (28), 287-293. doi: 10.1080/10426914022.746702
- Ready, J. F. (1997). *Industrial applications of lasers*. Academic press.
- Schuoocker, D., & Muller, P. (1987). Dynamic effects in laser cutting and formation of periodic striations. Paper presented at the Hague International Symposium.
- Scintilla, L. D., & Tricarico, L. (2012). Estimating cutting front temperature difference in disk and CO2 laser beam fusion cutting. *Optics & Laser Technology*, (43), 1468-1479. doi:http://dx.doi.org/10.1016/j.optlastec.2011.12.016
- Shanjin, L., & Yang, W. (2006). An investigation of pulsed laser cutting of titanium alloy sheet. *Optics and Lasers in Engineering*, (44), 1067-1077.
- Sheng, P., & Chryssolouris, G. (1994). Investigation of acoustic sensing for laser machining processes Part 2: Laser grooving cutting. *Journal of Materials Processing Technology*, (2), 145-163.
- Sheng, P. S., & Joshi, V. S. (1995). Analysis of Heat-Affected Zone Formation for Laser Cutting of Stainless Steel. *Journal of Materials Processing Technology*, 53(3-4), 879-892. doi:Doi 10.1016/0924-6460(94)01764-0
- Shiue, R., Chang, C., Young, M., & Tsay, L. (2004). The effect of residual thermal stresses on the fatigue crack growth of laser surface annealed AISI 304 stainless steel: Part I: computer simulation. *Materials Science and Engineering: A*, 364(1), 101-108.
- Singh, S. C., Zeng, H., Guo, C., & Cai, W. (2012). Lasers: Fundamentals, types, and operations. *Nanomaterials: Processing and Characterization with Lasers*, 1-34.
- Steen, W. (1991). *Laser material processing*. London: Springer.
- Steen, W. M., Mazumder, J., & Watkins, K. G. (2003). *Laser material processing*. Springer.
- Syn, C. Z., Mokhtar, M., Feng, C. J., & Manurung, Y. H. (2011). Approach to prediction of laser cutting quality by employing fuzzy expert system. *Expert Systems with Applications*, 38(6), 7558-7568.
- Tsai, C.-H., & Liou, C.-S. (2001). Applying an online crack detection technique for laser cutting by controlled fracture. *The International Journal of Advanced Manufacturing Technology*, (18), 724-730.

- Tsai, C., & Chen, C. (2003). Formation of the breaking surface of alumina in laser cutting with a controlled fracture technique. *Proceedings of the Institution of Mechanical Engineers, Part B: Journal of Engineering Manufacture*, 217(4), 489-497.
- Tsai, M.-J., Li, C.-H., & Chen, C.-C. (2008). Optimal laser-cutting parameters for QFN packages by utilizing artificial neural networks and genetic algorithm. *Journal of Materials Processing Technology*, 208(1), 270-283.
- Wandera, C. (2006). *Laser cutting of austenitic stainless steel with a high quality laser beam*. LAPPEENRANTA UNIVERSITY OF TECHNOLOGY.
- Yang, J., Sun, S., Brandt, M., & Yan, W. (2010). Experimental investigation and 3D finite element prediction of the heat affected zone during laser assisted machining of Ti6Al4V alloy. *Journal of Materials Processing Technology*, 210(15), 2215-2222. doi: <http://dx.doi.org/10.1016/j.jmatprotec.2010.08.007>
- Yilbas, B. (2004). Laser cutting quality assessment and thermal efficiency analysis. *Journal of Materials Processing Technology*, 155, 2106-2115.
- Yilbas, B., Davies, R., & Yilbas, Z. (1990). Study into the measurement and prediction of penetration time during CO<sub>2</sub> laser cutting process. *Proceedings of the Institution of Mechanical Engineers, Part B: Journal of Engineering Manufacture*, 204(2), 105-113.
- Yilbas, B., & Kar, A. (1998). Thermal and efficiency analysis of CO<sub>2</sub> laser cutting process. *Optics and Lasers in Engineering*, 29(1), 17-32.
- Yilbas, B. S., Arif, A. F. M., & Aleem, B. J. A. (2009). Laser cutting of holes in thick sheet metals: Development of stress field. *Optics and Lasers in Engineering*, 47(9), 909-916. doi: <http://dx.doi.org/10.1016/j.optlaseng.2009.03.002>
- Yousef, B. F., Knopf, G. K., Bordatchev, E. V., & Nikumb, S. K. (2003). Neural network modeling and analysis of the material removal process during laser machining. *The International Journal of Advanced Manufacturing Technology*, 22(1-2), 41-53.
- Yu, L. M. (1997). Three-dimensional finite element modelling of laser cutting. *Journal of Materials Processing Technology*, 63(1-3), 637-639. doi: [http://dx.doi.org/10.1016/S0924-0136\(96\)02698-2](http://dx.doi.org/10.1016/S0924-0136(96)02698-2)
- Zhou, J., Shen, H., Pan, Y., & Ding, X. (2016). Experimental study on laser microstructures using long pulse. *Optics and Lasers in Engineering*, 78, 113-120. doi: <http://dx.doi.org/10.1016/j.optlaseng.2015.10.009>

## LIST OF PUBLICATIONS AND PAPERS PRESENTED

### Journal publication

1. A M Sifullah, Khaled I. Ahmed ,Y Nukman M A Hassan,A. Hossain "Laser cutting of square blanks in stainless steel 304 sheets :HAZ and thermal stress analysis".Sains Malaysiana(Q3, ISI).....(Accepted)

### Paper presented

1. A. M. Sifullah, Y. Nukman, M. A. Hassan. Finite Element Analysis of Fusion Laser Cutting on Stainless Steel 304. 1st International Conference on Mechanical Manufacturing and Process Plant Engineering (ICMMPPE 2015), Kuala Lumpur, Malaysia, November 22-25, 2015.

2. Sifullah, A. M., Nukman, Y., & Hassan, M. A. Heat Affected Zone during Laser Cutting of Stainless Steel 304. 6th International Conference on Mechanical and Production Processes, Pattaya Thailand, April 24-25, 2015